

New Phase Space Formulations and Quantum Dynamics Approaches

Xin He^{1,†}, Baihua Wu^{1,†}, Youhao Shang¹, Bingqi Li¹, Xiangsong Cheng¹, and Jian Liu^{1,*}

¹Beijing National Laboratory for Molecular Sciences, Institute of Theoretical and Computational Chemistry, College of Chemistry and Molecular Engineering, Peking University, Beijing 100871, China.

(Invited Contribution. Submitted on February 5th, 2022, Accepted on April 11th, 2022, Published on May 13th, 2022)

Wiley Interdisciplinary Reviews-Computational Molecular Science, e1619 (2022)

<https://doi.org/10.1002/wcms.1619>

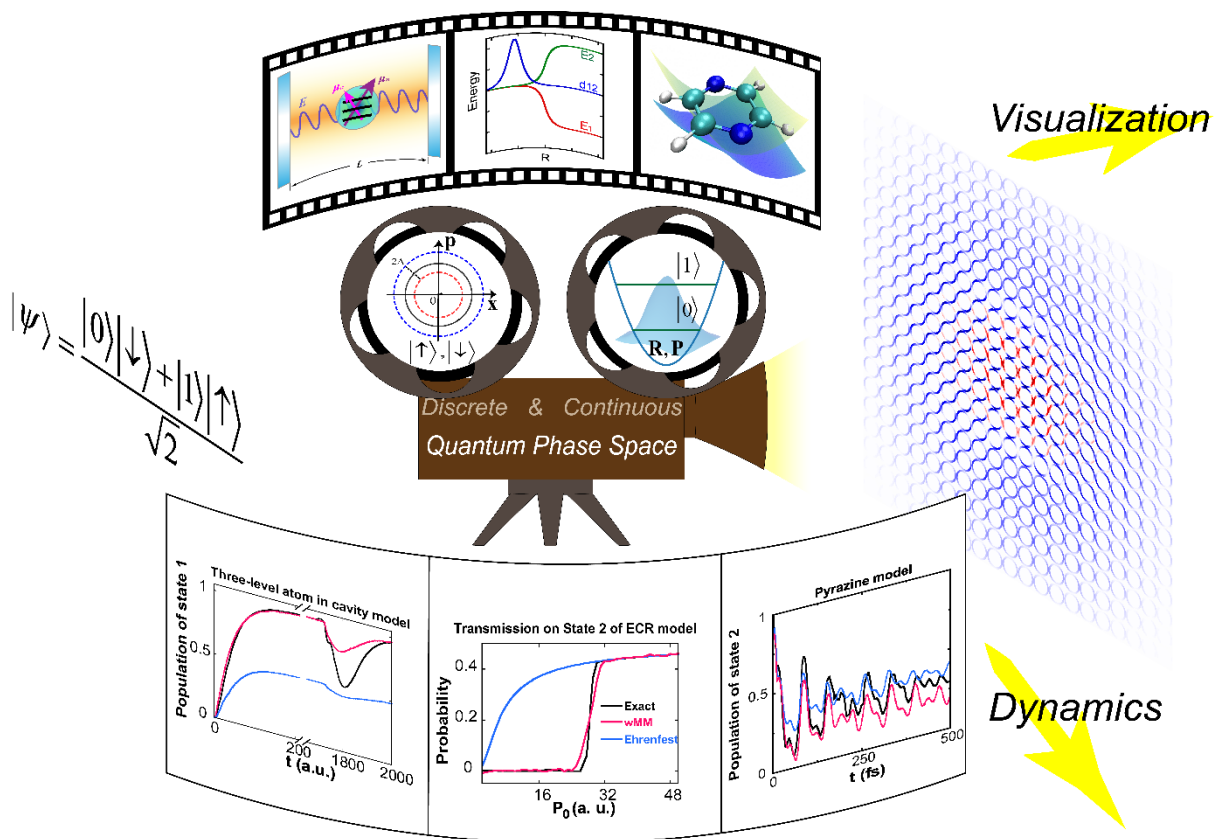
[†] X. H. and B. W. contributed equally.

* **Corresponding Author:** Email: jianliupku@pku.edu.cn

Abstract

We report recent progress on the phase space formulation of quantum mechanics with coordinate-momentum variables, focusing more on new theory of (weighted) constraint coordinate-momentum phase space for discrete-variable quantum systems. This leads to a general coordinate-momentum phase space formulation of composite quantum systems, where conventional representations on infinite phase space are employed for continuous variables. It is convenient to utilize (weighted) constraint coordinate-momentum phase space for representing the quantum state and describing nonclassical features. Various numerical tests demonstrate that new trajectory-based quantum dynamics approaches derived from the (weighted) constraint phase space representation are useful and practical for describing dynamical processes of composite quantum systems in gas phase as well as in condensed phase.

Graphical Abstract



Schematic representation of dynamics of composite quantum systems *via* phase space formulations.

1. INTRODUCTION

Phase space with coordinate-momentum variables is a fundamental concept and offers a convenient tool to describe statistics as well as dynamics in classical mechanics. In comparison to other equivalent interpretations of quantum mechanics, phase space formulations offer more insight and understanding between quantum and classical counterpart concepts, which are widely used in chemical and biological dynamics and spectroscopy¹⁻⁶⁰, quantum optics^{51, 61-70}, cryogenic physics/chemistry⁷¹⁻⁷⁵, quantum information and computation⁷⁶⁻⁸⁷, and so forth.

Phase space formulations of quantum mechanics have been developed since two important pioneering works, the Weyl transform in 1927, of which the original formulation converted a Hamiltonian on classical phase space into a quantum mechanical operator⁸⁸, and the Wigner function in 1932 that in principle depicts the inverse transform although a pure state was used for demonstration⁸⁹. The most essential element is the one-to-one correspondence mapping between quantum operators and classical functions often defined on a smooth manifold, namely, phase space. Because of the commutation relation of conjugate operators, the mapping is not unique in quantum mechanics^{90, 91}.

When infinite phase space is employed for a continuous-variable quantum system, most phase space formulations can be described by Cohen's generalized form⁹² in 1966. Quantum dynamics with phase space variables is expressed by the Moyal or Moyal-like bracket as first proposed by Groenewold⁹³ in 1946 and Moyal⁹⁴ in 1949. The Wigner and Husimi representations are most often used for the continuous-variable system. When the Moyal bracket is approximated by the Poisson bracket in the Wigner phase space expression of the quantum Liouville theorem, which was also derived as the linearized semiclassical initial value representation (LSC-IVR) or classical Wigner model^{4-8, 11, 20, 23} for the quantum correlation function, it reproduces exact quantum correlation functions even of nonlinear operators (i.e., nonlinear functions of the coordinate or momentum operator) in the harmonic or classical limit. The truncated Wigner approximation⁷⁴ with the time-dependent generalization of the Bopp representation^{90, 95} is similar to the LSC-IVR, but the former requests more demanding evaluation of the stability matrix elements along the trajectory when nonlinear operators are involved in the correlation function. Liu and Miller¹⁵ suggest a practical way to implement the imaginary time path integral treatment of the Boltzmann density operator in the LSC-IVR for general molecular systems that often contain imaginary frequencies. Its recent application illustrates that quantum dynamical effects play a critical role in reproducing the peaks in the intermediate region between the librational and bending bands, those between the bending and stretching bands, and the double-peak in the stretching band in the experimental isotropic Raman spectrum of liquid water¹⁹ (as shown in Figure 1). In addition that more advanced versions of SC-IVR⁹⁶⁻⁹⁹ are

capable of improving over the LSC-IVR, in Reference ¹¹ we first employed the quantum Liouville theorem in the phase space formulation to develop trajectory-based approaches to satisfy the two fundamental criteria: conservation of the quantum Boltzmann distribution for the thermal equilibrium system and being exact for any quantum thermal correlation functions in the classical and harmonic limits. Such trajectory-based approaches can in principle be further improved by higher order corrections of the exact series expansion of the phase space propagator as demonstrated in Reference ⁴⁴. More progress along this line can be found in References ³⁷⁻⁴⁷. (Figure 2 shows molecular vibrational spectra produced by the new phase space quantum dynamics methods.)

Phase space representations of a finite discrete F -state quantum system were first independently described by Stratonovich¹⁰⁰ in 1956, Feynman¹⁰¹ in 1987, and Wootters¹⁰² in 1987. Further developments of Stratonovich's formulation have focused on an $SU(2)$ or $SU(F)$ structure of phase space¹⁰³⁻¹¹⁷, while those on the construction of a discrete phase space are described in References ^{78, 118-126}. Other than the 2-state (or spin 1/2) system, the exact equations of motion (EOMs) of phase variables (expressed by the Moyal-like bracket) involved in these approaches for the finite discrete multi-state system are often tedious and numerically unfavourable^{109, 127-132}. (See Appendix 3 of the Supporting Information for more discussion.) Recent theoretical progress on exactly mapping the finite discrete F -state quantum system onto *constraint* coordinate-momentum phase space suggests that there exists a novel unified framework to derive comprehensive exact mapping Hamiltonians^{44, 57, 133, 134}, of which the quantum EOMs of mapping coordinate-momentum variables are simply linear^{44, 57, 133-136}.

The unified mapping formulation on coordinate-momentum phase space^{44, 57, 133-136} then offers a useful tool to treat dynamics of a composite quantum system, in which both continuous and finite discrete degrees of freedom (DOFs) are involved and coupled with one another. Because a typical molecular system has vibrational, rotational, and translational motion, it is often much more convenient to employ continuous coordinate space rather than Hilbert space with dense states to describe the nuclear DOFs. On the other hand, the energy gap between different electronic states of interest is often significantly larger such that the (adiabatic or diabatic) state representation is more useful to depict the electronic DOFs. It is evident that a general description of the molecular system leads to a composite quantum system, especially in the nonadiabatic region¹³⁷⁻¹⁵⁴. A comprehensive version of the Meyer-Miller mapping Hamiltonian model^{155, 156} can rigorously be formulated in the general coordinate-momentum phase space formulation^{44, 57, 133-136}.

In the Focus Article we focus on novel developments on the phase space formulation of quantum mechanics with coordinate-momentum variables for discrete-variable systems as well as for composite systems^{44, 57, 133-136}. In Section 2 we first review the general coordinate-momentum phase space formulation, where infinite space is

used for describing continuous variables and constraint space is employed for mapping discrete variables. We then propose a weighted constraint phase space representation that is also an exact formulation for mapping discrete-variable quantum systems. Section 3 demonstrates several examples and discusses implications of the (weighted) constraint coordinate-momentum phase space for studying and illustrating discrete-variable or composite quantum systems. When we use the weighted constraint phase space representation for mapping composite quantum systems, the mapping Hamiltonian (we use the Meyer-Miller mapping Hamiltonian for demonstration throughout the article, albeit that other mapping Hamiltonians are also available^{57, 58, 133, 134}) yields a novel trajectory-based approximate approach for composite systems. Such a new method satisfies the frozen nuclei limit [i.e., the dynamics reproduces the exact evolution when only finite discrete (electronic) DOFs are involved]. In Section 4 the performance of new trajectory-based quantum dynamics approaches on (weighted) constraint phase space is extensively tested for a few typical benchmark composite systems in gas phase as well as in condensed phase. Finally, conclusion remarks are presented in Section 5.

2. GENERAL COORDINATE-MOMENTUM PHASE SPACE FORMULATION OF QUANTUM MECHANICS

Consider a (molecular) system with N continuous (nuclear) DOFs and F discrete (electronic) states, of which the Hamiltonian reads

$$\hat{H} = \sum_{n,m=1}^F H_{nm}(\hat{\mathbf{R}}, \hat{\mathbf{P}}) |n\rangle\langle m| = \sum_{n,m=1}^F \left[\frac{1}{2} \hat{\mathbf{P}}^T \mathbf{M}^{-1} \hat{\mathbf{P}} \delta_{nm} + V_{nm}(\hat{\mathbf{R}}) \right] |n\rangle\langle m|, \quad (1)$$

where \mathbf{R} and \mathbf{P} are the nuclear coordinate and momentum variables, respectively, \mathbf{M} is the diagonal mass matrix, and the F states form an orthonormal complete basis set, that is,

$$\langle m|n\rangle = \delta_{mn}, \quad \hat{I}_{\text{ele}} = \sum_{n=1}^F |n\rangle\langle n|. \quad (2)$$

\hat{I}_{ele} and \hat{I}_{nuc} stand for the identity operator of the discrete (electronic) DOFs and that of the continuous (nuclear) DOFs. For simplicity, eq (1) employs the (electronically) diabatic representation, where the Hermitian potential matrix $\mathbf{V}(\mathbf{R})$ is a function of only the coordinate vector. (In applications $\mathbf{V}(\mathbf{R})$ is often a real symmetric matrix.) More discussion on the adiabatic representation of discrete (electronic) DOFs is available in Section-4.1.

The unified formulation of mapping phase space with coordinate-momentum variables offers a useful exact approach to describe the composite system. The trace of a product of two quantum operators is expressed as an integral of two functions on mapping phase space, that is,

$$\text{Tr}_{n,e} [\hat{A}\hat{B}] = \int d\boldsymbol{\mu}_{\text{nuc}}(\mathbf{R}, \mathbf{P}) \int_{\mathcal{S}(\mathbf{x}, \mathbf{p})} d\boldsymbol{\mu}_{\text{ele}}(\mathbf{x}, \mathbf{p}) A_C(\mathbf{R}, \mathbf{P}; \mathbf{x}, \mathbf{p}) \tilde{B}_C(\mathbf{R}, \mathbf{P}; \mathbf{x}, \mathbf{p}) \quad (3)$$

with

$$A_C(\mathbf{R}, \mathbf{P}; \mathbf{x}, \mathbf{p}) = \text{Tr}_{n,e} \left[\hat{A} \hat{K}_{\text{nuc}}(\mathbf{R}, \mathbf{P}) \otimes \hat{K}_{\text{ele}}(\mathbf{x}, \mathbf{p}) \right] \quad , \quad (4)$$

$$\tilde{B}_C(\mathbf{R}, \mathbf{P}; \mathbf{x}, \mathbf{p}) = \text{Tr}_{n,e} \left[\hat{K}_{\text{nuc}}^{-1}(\mathbf{R}, \mathbf{P}) \otimes \hat{K}_{\text{ele}}^{-1}(\mathbf{x}, \mathbf{p}) \hat{B} \right] \quad , \quad (5)$$

$d\boldsymbol{\mu}_{\text{nuc}}(\mathbf{R}, \mathbf{P}) = (2\pi\hbar)^{-N} d\mathbf{R}d\mathbf{P}$ and $d\boldsymbol{\mu}_{\text{ele}}(\mathbf{x}, \mathbf{p}) = Fd\mathbf{x}d\mathbf{p}$ as the integration measure on nuclear phase space and that on electronic phase space, respectively, and $\text{Tr}_{n,e}$ represents the trace over the corresponding nuclear and electronic Hilbert space. The integral over the mapping phase space variables for the finite discrete (electronic) DOFs in eq (3) is performed as

$$\int_{\mathcal{S}(\mathbf{x}, \mathbf{p})} Fd\mathbf{x}d\mathbf{p} g(\mathbf{x}, \mathbf{p}) = \int Fd\mathbf{x}d\mathbf{p} \frac{1}{\Omega} \mathcal{S}(\mathbf{x}, \mathbf{p}) g(\mathbf{x}, \mathbf{p}) = \int Fd\mathbf{x}d\mathbf{p} \bar{\mathcal{S}}(\mathbf{x}, \mathbf{p}) g(\mathbf{x}, \mathbf{p}) \quad , \quad (6)$$

where the area of constraint space $\mathcal{S}(\mathbf{x}, \mathbf{p})$

$$\Omega = \int d\mathbf{x}d\mathbf{p} \mathcal{S}(\mathbf{x}, \mathbf{p}) \quad (7)$$

is the normalization constant, and $\bar{\mathcal{S}}(\mathbf{x}, \mathbf{p})$ is the normalized constraint space.

The normalization of the (inverse) mapping kernel reads

$$\text{Tr}_n \left[\hat{K}_{\text{nuc}}(\mathbf{R}, \mathbf{P}) \right] = \text{Tr}_n \left[\hat{K}_{\text{nuc}}^{-1}(\mathbf{R}, \mathbf{P}) \right] = 1 \quad (8)$$

$$\text{Tr}_e \left[\hat{K}_{\text{ele}}(\mathbf{x}, \mathbf{p}) \right] = \text{Tr}_e \left[\hat{K}_{\text{ele}}^{-1}(\mathbf{x}, \mathbf{p}) \right] = 1 \quad (9)$$

and

$$\int d\boldsymbol{\mu}_{\text{nuc}}(\mathbf{R}, \mathbf{P}) \hat{K}_{\text{nuc}}(\mathbf{R}, \mathbf{P}) = \int d\boldsymbol{\mu}_{\text{nuc}}(\mathbf{R}, \mathbf{P}) \hat{K}_{\text{nuc}}^{-1}(\mathbf{R}, \mathbf{P}) = \hat{I}_{\text{nuc}} \quad (10)$$

$$\int_{\mathcal{S}(\mathbf{x}, \mathbf{p})} d\boldsymbol{\mu}_{\text{ele}}(\mathbf{x}, \mathbf{p}) \hat{K}_{\text{ele}}(\mathbf{x}, \mathbf{p}) = \int_{\mathcal{S}(\mathbf{x}, \mathbf{p})} d\boldsymbol{\mu}_{\text{ele}}(\mathbf{x}, \mathbf{p}) \hat{K}_{\text{ele}}^{-1}(\mathbf{x}, \mathbf{p}) = \hat{I}_{\text{ele}} \quad . \quad (11)$$

The one-to-one correspondence mapping from phase space function $A_C(\mathbf{R}, \mathbf{P}; \mathbf{x}, \mathbf{p})$ or $\tilde{B}_C(\mathbf{R}, \mathbf{P}; \mathbf{x}, \mathbf{p})$ of Eq (4) back to operator \hat{A} or \hat{B} is

$$\begin{aligned}\hat{A} &= \int d\boldsymbol{\mu}_{\text{nuc}}(\mathbf{R}, \mathbf{P}) \int_{S(\mathbf{x}, \mathbf{p})} d\boldsymbol{\mu}_{\text{ele}}(\mathbf{x}, \mathbf{p}) A_C(\mathbf{R}, \mathbf{P}; \mathbf{x}, \mathbf{p}) \hat{K}_{\text{nuc}}^{-1}(\mathbf{R}, \mathbf{P}) \otimes \hat{K}_{\text{ele}}^{-1}(\mathbf{x}, \mathbf{p}) \\ \hat{B} &= \int d\boldsymbol{\mu}_{\text{nuc}}(\mathbf{R}, \mathbf{P}) \int_{S(\mathbf{x}, \mathbf{p})} d\boldsymbol{\mu}_{\text{ele}}(\mathbf{x}, \mathbf{p}) \tilde{B}_C(\mathbf{R}, \mathbf{P}; \mathbf{x}, \mathbf{p}) \hat{K}_{\text{nuc}}(\mathbf{R}, \mathbf{P}) \otimes \hat{K}_{\text{ele}}(\mathbf{x}, \mathbf{p})\end{aligned}\quad (12)$$

The nuclear or electronic kernel should satisfy five criteria, namely, linearity, reality, standardization (normalization), traciality, and covariance^{93, 94, 100, 115}.

2.1 Mapping kernel for continuous (nuclear) degrees of freedom

The integrals for (\mathbf{R}, \mathbf{P}) in eqs (3), (10), and (12) are over infinite (nuclear) phase space. The mapping kernel and its inverse for the nuclear DOFs are

$$\begin{aligned}\hat{K}_{\text{nuc}}(\mathbf{R}, \mathbf{P}) &= \left(\frac{\hbar}{2\pi}\right)^N \int d\boldsymbol{\zeta} \int d\boldsymbol{\eta} e^{i\boldsymbol{\zeta} \cdot (\hat{\mathbf{R}} - \mathbf{R}) + i\boldsymbol{\eta} \cdot (\hat{\mathbf{P}} - \mathbf{P})} f(\boldsymbol{\zeta}, \boldsymbol{\eta}) \\ \hat{K}_{\text{nuc}}^{-1}(\mathbf{R}, \mathbf{P}) &= \left(\frac{\hbar}{2\pi}\right)^N \int d\boldsymbol{\zeta} \int d\boldsymbol{\eta} e^{i\boldsymbol{\zeta} \cdot (\hat{\mathbf{R}} - \mathbf{R}) + i\boldsymbol{\eta} \cdot (\hat{\mathbf{P}} - \mathbf{P})} [f(-\boldsymbol{\zeta}, -\boldsymbol{\eta})]^{-1}\end{aligned}\quad , \quad (13)$$

where $f(\boldsymbol{\zeta}, \boldsymbol{\eta})$ is a scalar function. For example, we have the Wigner function^{89, 157}

$$f(\boldsymbol{\zeta}, \boldsymbol{\eta}) = 1 \quad , \quad (14)$$

the Husimi function¹⁵⁸

$$f(\boldsymbol{\zeta}, \boldsymbol{\eta}) = \exp\left(-\frac{\boldsymbol{\zeta}^T \boldsymbol{\Gamma}^{-1} \boldsymbol{\zeta}}{4} - \frac{\hbar^2}{4} \boldsymbol{\eta}^T \boldsymbol{\Gamma} \boldsymbol{\eta}\right) \quad , \quad (15)$$

the anti-Husimi function

$$f(\boldsymbol{\zeta}, \boldsymbol{\eta}) = \exp\left(\frac{\boldsymbol{\zeta}^T \boldsymbol{\Gamma}^{-1} \boldsymbol{\zeta}}{4} + \frac{\hbar^2}{4} \boldsymbol{\eta}^T \boldsymbol{\Gamma} \boldsymbol{\eta}\right) \quad , \quad (16)$$

the Glauber-Sudarshan P function^{61, 62, 66} (with the characteristic frequency matrix $\boldsymbol{\omega}$ of the system)

$$f(\boldsymbol{\zeta}, \boldsymbol{\eta}) = \exp\left[\frac{\hbar}{4} \boldsymbol{\zeta}^T \mathbf{M}^{-1/2} \boldsymbol{\omega}^{-1} \mathbf{M}^{-1/2} \boldsymbol{\zeta} + \frac{\hbar}{4} \boldsymbol{\eta}^T \mathbf{M}^{1/2} \boldsymbol{\omega} \mathbf{M}^{1/2} \boldsymbol{\eta}\right] \quad (17)$$

and its generalized versions⁶⁶, the Glauber Q function¹⁵⁹

$$f(\zeta, \boldsymbol{\eta}) = \exp \left[-\frac{\hbar}{4} \zeta^T \mathbf{M}^{-1/2} \boldsymbol{\omega}^{-1} \mathbf{M}^{-1/2} \zeta - \frac{\hbar}{4} \boldsymbol{\eta}^T \mathbf{M}^{1/2} \boldsymbol{\omega} \mathbf{M}^{1/2} \boldsymbol{\eta} \right], \quad (18)$$

the normal-antinormal ordered function⁹¹

$$f(\zeta, \boldsymbol{\eta}) = \cosh \left[\frac{\hbar}{4} \zeta^T \mathbf{M}^{-1/2} \boldsymbol{\omega}^{-1} \mathbf{M}^{-1/2} \zeta + \frac{\hbar}{4} \boldsymbol{\eta}^T \mathbf{M}^{1/2} \boldsymbol{\omega} \mathbf{M}^{1/2} \boldsymbol{\eta} \right], \quad (19)$$

the Kirkwood antistandard-ordered function^{160, 161}

$$f(\zeta, \boldsymbol{\eta}) = e^{i\hbar \zeta^T \boldsymbol{\eta} / 2}, \quad (20)$$

the Mehta standard-ordered function¹⁶²

$$f(\zeta, \boldsymbol{\eta}) = e^{-i\hbar \zeta^T \boldsymbol{\eta} / 2}, \quad (21)$$

the Rivier function^{163, 164}

$$f(\zeta, \boldsymbol{\eta}) = \cos \left[\frac{1}{2} \hbar \zeta^T \boldsymbol{\eta} \right], \quad (22)$$

and the distribution function of Born and Jordan¹⁶⁵

$$f(\zeta, \boldsymbol{\eta}) = \frac{\sin \left[\frac{1}{2} \hbar \zeta^T \boldsymbol{\eta} \right]}{\frac{1}{2} \hbar \zeta^T \boldsymbol{\eta}}, \quad (23)$$

and so forth.

When operator \hat{A} is a function of only the nuclear DOFs, its phase space function from Eq (4) and the dual function from eq (5) become

$$A_{\text{nuc}}(\mathbf{R}, \mathbf{P}) = \text{Tr}_n \left[\hat{A} \hat{K}_{\text{nuc}}(\mathbf{R}, \mathbf{P}) \right] \quad (24)$$

and

$$\tilde{A}_{\text{nuc}}(\mathbf{R}, \mathbf{P}) = \text{Tr}_n \left[\hat{K}_{\text{nuc}}^{-1}(\mathbf{R}, \mathbf{P}) \hat{A} \right]. \quad (25)$$

When the Wigner function eq (14) is used, the mapping kernel and its inverse are the same, that is.,

$\hat{K}_{\text{nuc}}(\mathbf{x}, \mathbf{p}) = \hat{K}_{\text{nuc}}^{-1}(\mathbf{x}, \mathbf{p})$. The Wigner phase space function of operator \hat{A} (from eq (24)) is identical to its dual (from eq (25)),

$$A_{\text{nuc}}^W(\mathbf{R}, \mathbf{P}) = \tilde{A}_{\text{nuc}}^W(\mathbf{R}, \mathbf{P}) \quad . \quad (26)$$

When the Husimi phase space (eq (15)) is employed, it is straightforward to show the relation between the Wigner and Husimi phase space functions (obtained from eq (24))

$$A_{\text{nuc}}^H(\mathbf{R}, \mathbf{P}) = \exp\left[\frac{1}{4}\left(\frac{\mathbf{d}}{\mathbf{dR}}\right)^T \Gamma^{-1}\left(\frac{\mathbf{d}}{\mathbf{dR}}\right) + \frac{\hbar^2}{4}\left(\frac{\mathbf{d}}{\mathbf{dP}}\right)^T \Gamma\left(\frac{\mathbf{d}}{\mathbf{dP}}\right)\right] A_{\text{nuc}}^W(\mathbf{R}, \mathbf{P}) \quad , \quad (27)$$

and the relation between the dual function of Husimi phase space $\tilde{A}_{\text{nuc}}^H(\mathbf{R}, \mathbf{P})$ and the Wigner phase space function $A_{\text{nuc}}^W(\mathbf{R}, \mathbf{P})$

$$\tilde{A}_{\text{nuc}}^H(\mathbf{R}, \mathbf{P}) = \exp\left[-\frac{1}{4}\left(\frac{\mathbf{d}}{\mathbf{dR}}\right)^T \Gamma^{-1}\left(\frac{\mathbf{d}}{\mathbf{dR}}\right) - \frac{\hbar^2}{4}\left(\frac{\mathbf{d}}{\mathbf{dP}}\right)^T \Gamma\left(\frac{\mathbf{d}}{\mathbf{dP}}\right)\right] A_{\text{nuc}}^W(\mathbf{R}, \mathbf{P}) \quad . \quad (28)$$

Because any choice of $f(\boldsymbol{\zeta}, \boldsymbol{\eta})$ in eq (13) leads to an informationally complete representation of the continuous-variable quantum system, it is not difficult to establish the relation between different (dual) phase space functions in addition to eq (27) and eq (28).

2.2 Mapping kernel on constraint space for discrete (electronic) degrees of freedom

As derived first in Appendix A of Reference ¹³⁴ in the spirit of Reference ¹³³ and then in the Supporting Information of Reference ¹³⁶, the kernel that maps a set of F states onto constraint phase space $\mathcal{S}(\mathbf{x}, \mathbf{p})$ reads

$$\hat{K}_{\text{ele}}(\mathbf{x}, \mathbf{p}) = \sum_{n,m=1}^F \left[\frac{1}{2} (x^{(n)} + ip^{(n)})(x^{(m)} - ip^{(m)}) - \gamma \delta_{nm} \right] |n\rangle \langle m| \quad (29)$$

and the corresponding inverse kernel is

$$\hat{K}_{\text{ele}}^{-1}(\mathbf{x}, \mathbf{p}) = \sum_{n,m=1}^F \left[\frac{1+F}{2(1+F\gamma)^2} (x^{(n)} + ip^{(n)})(x^{(m)} - ip^{(m)}) - \frac{1-\gamma}{1+F\gamma} \delta_{nm} \right] |n\rangle \langle m| \quad . \quad (30)$$

As naturally required by eq (9), constraint phase space $\mathcal{S}(\mathbf{x}, \mathbf{p})$ is defined by

$$\delta\left(\sum_{n=1}^F \frac{(x^{(n)})^2 + (p^{(n)})^2}{2} - (1 + F\gamma)\right) , \quad (31)$$

of which the area is

$$\Omega(\gamma) = \int d\mathbf{x}d\mathbf{p} \delta\left(\sum_{n=1}^F \frac{(x^{(n)})^2 + (p^{(n)})^2}{2} - (1 + F\gamma)\right) . \quad (32)$$

The normalized constraint phase space is $\bar{\mathcal{S}}(\mathbf{x}, \mathbf{p}) = \mathcal{S}(\mathbf{x}, \mathbf{p})/\Omega(\gamma)$.

Equations (29)-(32) define the mapping kernel and inverse kernel as well as constraint phase space, which are the key elements of the coordinate-momentum phase space formulation of the discrete-variable quantum system that we first established in References ^{133, 134} and further developed in References ^{57, 58, 136}. As yielded from eq (4), when the Wigner function eq (14) is used for the nuclear DOFs, the mapping Hamiltonian for the quantum Hamiltonian operator eq (1) reads

$$H_C(\mathbf{R}, \mathbf{P}; \mathbf{x}, \mathbf{p}; \gamma) = \frac{1}{2} \mathbf{P}^T \mathbf{M}^{-1} \mathbf{P} + \sum_{n,m=1}^F V_{nm}(\mathbf{R}) \left[\frac{1}{2} (x^{(n)} + ip^{(n)})(x^{(m)} - ip^{(m)}) - \gamma \delta_{nm} \right] . \quad (33)$$

Because $\mathbf{V}(\mathbf{R})$ is Hermitian, the mapping Hamiltonian is real. As $\mathbf{V}(\mathbf{R})$ is often a real symmetric matrix, eq (33) becomes

$$H_C(\mathbf{R}, \mathbf{P}; \mathbf{x}, \mathbf{p}; \gamma) = \frac{1}{2} \mathbf{P}^T \mathbf{M}^{-1} \mathbf{P} + \sum_{n,m=1}^F \left[\frac{1}{2} (x^{(n)} x^{(m)} + p^{(n)} p^{(m)}) - \gamma \delta_{nm} \right] V_{nm}(\mathbf{R}) , \quad (34)$$

which is the seminal Meyer-Miller Hamiltonian¹⁵⁵ that has extensively been implemented for nonadiabatic dynamics in the literature^{4, 56, 60, 140, 156, 166-220}. In References ^{58, 133, 134} it is shown that there also exist other comprehensive mapping Hamiltonian models in the general coordinate-momentum phase space formulation of quantum mechanics. When the mapping Hamiltonian is employed to generate trajectory-based dynamics in the phase space formulation for a composite quantum system, we denote it the classical mapping model (CMM) approach. It satisfies the frozen nuclei limit. We use the Meyer-Miller Hamiltonian for demonstration throughout the Focus Article.

When Meyer and Miller proposed the conventional Meyer-Miller mapping Hamiltonian model for the nonadiabatic system in 1979, they did not invoke the phase space formulation. In 1997 Stock and Thoss¹⁵⁶ utilized the Schwinger oscillator theory of angular momentum^{221, 222} to derive the Meyer-Miller mapping Hamiltonian¹⁵⁵. Its LSC-IVR approximation⁴ in principle includes *infinite* Wigner phase space for the finite set of (electronic) states. The applications, however, suggest that the LSC-IVR approximation in the framework of

References^{4, 156, 172} is not good^{174, 179, 183, 189, 197, 202, 204}. More advanced semiclassical approaches^{96, 97} improve the performance but request more computational effort^{174, 175}. The symmetric-window-function and other techniques have been introduced to practically overcome the drawbacks^{179, 183, 189, 197, 202, 204}. Recent progress along this line is briefly summarized in Reference¹⁴⁰.

Equation (31) indicates that parameter γ lies in region $(-1/F, \infty)$. It is shown that parameter γ can be either positive or negative^{133, 136} and should be interpreted as a special case of the commutator matrix^{57, 58, 133, 136} rather than the conventional zero-point-energy parameter^{155, 156}. There exist three key elements for a trajectory-based quantum dynamics method to evaluate the evolution of the expectation/ensemble average of a physical property, namely,

- 1) the EOMs of the trajectory,
- 2) the initial condition of the trajectory, and
- 3) the integral expression for the expectation/ensemble average of the physical property of interest.

In the frozen-nuclei limit, Hamilton's EOMs governed by the Meyer-Miller mapping Hamiltonian is isomorphic to exact dynamics. While it is reasonable to employ the mapping Hamiltonian to define the EOMs of the trajectory, the left two elements are also important to consider such that the trajectory-based dynamics method is consistent. The constraint coordinate-momentum phase space formulation then offers a more advanced platform to consider all the three key elements.

It is evident that eq (31) is a special choice of constraint phase space $\mathcal{S}(\mathbf{x}, \mathbf{p})$. The interpretation of parameter γ in References^{57, 58, 133, 136} hints that a more comprehensive choice of normalized constraint phase space $\bar{\mathcal{S}}(\mathbf{x}, \mathbf{p})$ is

$$\int_{-1/F}^{\infty} d\gamma w(\gamma) \frac{1}{\Omega(\gamma)} \delta \left(\sum_{n=1}^F \frac{(x^{(n)})^2 + (p^{(n)})^2}{2} - (1 + F\gamma) \right), \quad (35)$$

with the *quasi*-probability distribution function

$$\int_{-1/F}^{\infty} d\gamma w(\gamma) = 1. \quad (36)$$

Equation (6), the integral over the mapping phase space variables for the finite discrete (electronic) DOFs then becomes

$$\begin{aligned}
& \int_{\mathcal{S}(\mathbf{x}, \mathbf{p})} F d\mathbf{x} d\mathbf{p} g(\mathbf{x}, \mathbf{p}) \\
&= \int_{-1/F}^{\infty} d\gamma w(\gamma) \int F d\mathbf{x} d\mathbf{p} \frac{1}{\Omega(\gamma)} \delta\left(\sum_{n=1}^F \frac{(x^{(n)})^2 + (p^{(n)})^2}{2} - (1 + F\gamma)\right) g(\mathbf{x}, \mathbf{p}) \quad . \quad (37)
\end{aligned}$$

If we require that the kernel is the same as its inverse, that is.,

$$\hat{K}_{\text{ele}}(\mathbf{x}, \mathbf{p}) = \hat{K}_{\text{ele}}^{-1}(\mathbf{x}, \mathbf{p}) = \sum_{n,m=1}^F \left[\frac{1}{2} (x^{(n)} + ip^{(n)})(x^{(m)} - ip^{(m)}) - \gamma \delta_{nm} \right] |n\rangle \langle m| \quad , \quad (38)$$

it is then not difficult to obtain

$$\int_{-1/F}^{\infty} d\gamma w(\gamma) \chi(\gamma) = 1 \quad (39)$$

with

$$\chi(\gamma) = F\gamma^2 + 2\gamma \quad . \quad (40)$$

(See Appendix 1 of the Supporting Information for more discussion.) Equations (35)-(40) define normalized constraint phase space $\overline{\mathcal{S}}(\mathbf{x}, \mathbf{p})$, the mapping kernel and inverse kernel, and the *quasi*-probability distribution function $w(\gamma)$ of parameter γ . The weighted constraint phase space formulation for the discrete-variable quantum system is the key new theoretical result of the Focus Article. When the Wigner function eq (14) is used for the nuclear DOFs, where $\hat{K}_{\text{nuc}}(\mathbf{x}, \mathbf{p}) = \hat{K}_{\text{nuc}}^{-1}(\mathbf{x}, \mathbf{p})$, eq (4) is then identical to eq (5) when $\hat{A} = \hat{B}$. The mapping Hamiltonian for the quantum Hamiltonian operator eq (1) produced by either of eq (4) and eq (5) leads to the same expression as eq (34). When the mapping Hamiltonian is utilized to produce the trajectory-based dynamics for a composite system, it is denoted the weighted mapping model (wMM) approach. The frozen nuclei limit is satisfied in wMM.

Many choices are possible for the discrete or continuous version of the normalized quasi-probability distribution function $w(\gamma)$ in the weighted constraint phase space mapping theory. In the Focus Article we consider only the simplest cases of the discrete version. When but a single value of parameter γ is chosen in eq (39), that is, $w(\gamma) = \delta(\gamma - \gamma_1)$, we obtain

$$F\gamma^2 + 2\gamma = 1 \quad , \quad (41)$$

of which the physical solution is

$$\gamma = \frac{\sqrt{1+F} - 1}{F} \quad (42)$$

Equation (42) is a trivial result that was used in References^{57, 114, 115, 117, 199}. In this case, the weighted constraint phase space formulation is identical to the constraint phase space formulation, and wMM becomes CMM with eq (42) when trajectory-based dynamics is considered. When only two values of parameter γ are selected, that is,

$$w(\gamma) = \sum_{j=1}^2 w(\gamma_j) \delta(\gamma - \gamma_j) \quad (43)$$

eq (36) and eq (39) lead to

$$\begin{aligned} w(\gamma_1) &= \frac{1 - \chi(\gamma_2)}{\chi(\gamma_1) - \chi(\gamma_2)} \\ w(\gamma_2) &= \frac{\chi(\gamma_1) - 1}{\chi(\gamma_1) - \chi(\gamma_2)} \end{aligned} \quad (44)$$

When the values of parameter γ are close to zero or smaller than zero in region $(-1/F, \infty)$, trajectories produced by the Meyer-Miller mapping Hamiltonian eq (34) for nonadiabatic molecular dynamics are stable. For demonstration in the paper we choose

$$\gamma_1 = -\gamma_2 = \Delta \quad (45)$$

with Δ a reasonably small positive real number in region $(0, 1/F)$. Figure 3 presents the constraint coordinate-momentum phase space formulation when a single value of parameter γ is used (Figure 3a) as well as the weighted formulation when two values of parameter γ suggested by eq (45) are used (Figure 3b).

3. PHASE SPACE REPRESENTATION OF THE NONCLASSICAL FEATURE OF QUANTUM SYSTEMS

Recent advance on quantum technologies makes it possible to control and manipulate quantum states in experiment. Because the phase space formulation offers an informationally complete description of the density matrix, direct measurements of phase space of the quantum system with continuous DOFs, those of the quantum system with discrete DOFs, and those of the composite quantum system have been realized in experiment^{70, 85, 223-236}. While the celebrated Wigner phase space has long been used for illustration of the negative *quasi*-probability for continuous-variable systems^{227, 237}, Stratonovich phase space has recently been proposed for visualization and tomography of discrete-variable systems^{85, 113, 229-231, 233, 238, 239}. A combination of these two spaces has been used

for illustration of nonclassical correlations or entanglement between the discrete DOF and the continuous DOF of the composite system^{240, 241}. (In Appendix 3 of the Supporting Information, we briefly review Stratonovich phase space with an either $SU(2)$ or $SU(F)$ structure^{114, 242, 243}, as well as the relationship between Stratonovich phase space and constraint coordinate-momentum phase space as already pointed out in References^{57, 58}.)

As coordinate-momentum phase space is well-established in classical mechanics, the formulation of (weighted) constraint coordinate-momentum phase space described in Section 2 offers a potentially useful approach for describing correlations and dynamics in the discrete-variable system as well as the composite system in quantum mechanics. When (weighted) constraint coordinate-momentum phase space is used for mapping an F -state system, the phase space distribution is

$$\rho_C(\mathbf{x}, \mathbf{p}) = \sum_{m,n=1}^F \rho_{mn} K_{nm}(\mathbf{x}, \mathbf{p}), \quad (46)$$

where $\rho_{mn} = \langle m | \hat{\rho} | n \rangle$ and $K_{nm}(\mathbf{x}, \mathbf{p}) = \langle n | \hat{K}_{\text{ele}}(\mathbf{x}, \mathbf{p}) | m \rangle$ with $\hat{K}_{\text{ele}}(\mathbf{x}, \mathbf{p})$ defined in eq (38). For the sake of visualization, it is convenient to further reduce constraint phase space variables (\mathbf{x}, \mathbf{p}) to two relevant variables, $(x^{(n)}, x^{(m)})$ or $(x^{(n)}, p^{(m)})$ for describing the correlation on arbitrary two states $|n\rangle$ and $|m\rangle$.

We define the marginal function, $\mathcal{K}_{(n,m)}(x^{(n)}, x^{(m)})$, on constraint coordinate-momentum phase space (Figure 4),

$$\mathcal{K}_{(n,m)}(x^{(n)}, x^{(m)}) = \int F d\mathbf{x}_{\perp} d\mathbf{p} \frac{1}{\Omega(\gamma)} \delta \left(\sum_{j=1}^F \frac{(x^{(j)})^2 + (p^{(j)})^2}{2} - (1 + F\gamma) \right) K_{nm}(\mathbf{x}, \mathbf{p}; \gamma), \quad (47)$$

where \mathbf{x}_{\perp} represents all $x^{(i)}$ other than $\{x^{(n)}, x^{(m)}\}$, and that on weighted constraint phase space,

$$\mathcal{K}_{(n,m)}(x^{(n)}, x^{(m)}) = \int_{-1/F}^{\infty} d\gamma w(\gamma) \frac{1}{\Omega(\gamma)} \int F d\mathbf{x}_{\perp} d\mathbf{p} \delta \left(\sum_{j=1}^F \frac{(x^{(j)})^2 + (p^{(j)})^2}{2} - (1 + F\gamma) \right) K_{nm}(\mathbf{x}, \mathbf{p}; \gamma). \quad (48)$$

Figure 5 demonstrates the case of eq (48) when the quasi-probability distribution function $w(\gamma)$ is defined by eqs (43)-(45) where two symmetrical values of parameter γ are used. Similar definitions are also applied for $\mathcal{K}_{(n,m)}(x^{(n)}, p^{(m)})$. The explicit formula of these marginal functions can be derived by using the integral techniques (where we use Wick's theorem^{244, 245}) in Appendix 1 of the Supporting Information.

Figures 4-5 demonstrate a composite system that consists of a discrete DOF for spin-1/2 and a continuous DOF for a harmonic oscillator. The marginal joint distribution function of the composite system reads

$$\rho_C^{(n,m)}(\mathbf{R}, \mathbf{P}; x^{(n)}, x^{(m)}) = \text{Tr}_{n,e} \left[\hat{\rho} \hat{K}_{nuc}(\mathbf{R}, \mathbf{P}) \otimes |n\rangle\langle m| \mathcal{K}_{(n,m)}(x^{(n)}, x^{(m)}) \right]. \quad (49)$$

The marginal quasi-probability distribution functions of the continuous variable for both the pure state and the mixed state are presented in Figure 4a, where infinite Wigner phase space is employed. The marginal functions of the discrete variables (based on eq (47)) of the spin-1/2 system read

$$\begin{aligned} & \begin{pmatrix} \mathcal{K}_{\uparrow\uparrow}(x^{(1)}, x^{(2)}) & \mathcal{K}_{\uparrow\downarrow}(x^{(1)}, x^{(2)}) \\ \mathcal{K}_{\downarrow\uparrow}(x^{(1)}, x^{(2)}) & \mathcal{K}_{\downarrow\downarrow}(x^{(1)}, x^{(2)}) \end{pmatrix} \\ &= \frac{1}{2\pi(1+2\gamma)} \begin{pmatrix} 1 + \frac{1}{2}(x^{(1)})^2 - \frac{1}{2}(x^{(2)})^2 & x^{(1)}x^{(2)} \\ x^{(1)}x^{(2)} & 1 - \frac{1}{2}(x^{(1)})^2 + \frac{1}{2}(x^{(2)})^2 \end{pmatrix}, \end{aligned} \quad (50)$$

where notations \uparrow, \downarrow are used to represent the two discrete states.

The marginal functions for the discrete variable are demonstrated on constraint coordinate-momentum phase space in Figure 4b and on weighted constraint space in Figure 5b. More interestingly, the identical angular behaviour and the radial cancellation behaviour of two weighted components lead to a hollow ring structure on weighted constraint phase space (Figure 5a, also see Appendix 4 of the Supporting Information). The difference between the Schrodinger cat state and the mixed state is distinct in either Figure 4b on constraint space or Figure 5b on weighted constraint space.

The marginal joint function of a pure Bell entangled state, $(|0\rangle|\downarrow\rangle + |1\rangle|\uparrow\rangle)/2$, of the composite system is demonstrated in Figure 4c (by adopting the similar strategy of References^{240, 241}), where constraint coordinate-momentum phase space is used for the discrete DOF at each grid, as well as in Figure 5c where weighted constraint space is employed for the discrete DOF at each grid. The two-dimensional grids represent variables (R, P) of infinite Wigner phase space for the continuous DOF in either of Figure 4c and Figure 5c. When the pure Bell entangled state is studied, both Figure 4c and Figure 5c clearly demonstrate a Gaussian decay of the joint marginal function against Wigner phase space variables (R, P) of the continuous DOF. Either Figure 4c or Figure 5c also shows the pattern of the correlation between the continuous DOF and the discrete DOF. It is convenient to distinguish the pure Bell entangled state, $(|0\rangle|\downarrow\rangle + |1\rangle|\uparrow\rangle)/2$, from the direct product of the Schrodinger cat states, $(|0\rangle + |1\rangle) \otimes (|\uparrow\rangle + |\downarrow\rangle)/2$, when the hybrid representation of the general coordinate-momentum phase space is used.

4. DYNAMICS OF COMPOSITE QUANTUM SYSTEMS

The quantum Liouville theorem can be expressed as a generalized Moyal bracket on hybrid coordinate-momentum phase space. When the Poisson bracket for classical Hamilton's EOMs governed by the mapping Hamiltonian, eq (34), is used to approximate the generalized Moyal bracket on phase space^{57, 58}, we have CMM when constraint space is used, and wMM when weighted constraint space is employed. (Please see Appendices 2, 3, and 5 of the Supporting Information for more discussion.) We compare the new wMM and CMM approaches to Ehrenfest dynamics^{246, 247} as well as the fewest-switches surface hopping (FSSH) method²⁴⁸⁻²⁵⁰, two prevailing trajectory-based dynamics methods for a few typical composite quantum systems. (In this section we set $\hbar = 1$ for simplicity if it is not specifically stated).

4.1 Equations of motion governed by the mapping Hamiltonian

In eq (1), the 'complete' set of diabatic states $\{|n\rangle\}$ is independent of nuclear coordinate/configuration \mathbf{R} . The mapping variables for discrete (electronic) DOFs, (\mathbf{x}, \mathbf{p}) , are independent of \mathbf{R} . Define $\mathbf{g} = \mathbf{x} + i\mathbf{p}$. The EOMs governed by eq (33), the mapping Hamiltonian of eq (1), then read,

$$\dot{\mathbf{g}} = -i\mathbf{V}(\mathbf{R})\mathbf{g} \quad . \quad (51)$$

$$\dot{\mathbf{R}} = \mathbf{M}^{-1}\mathbf{P} \quad (52)$$

$$\dot{\mathbf{P}} = -\sum_{n,m=1}^F (\nabla_{\mathbf{R}} V_{mn}(\mathbf{R})) \left(\frac{1}{2} (x^{(n)} + ip^{(n)}) (x^{(m)} - ip^{(m)}) - \gamma \delta_{nm} \right) \quad . \quad (53)$$

Diabatic potential matrix $\mathbf{V}(\mathbf{R})$ is Hermitian, so is the force matrix, $\{\nabla_{\mathbf{R}} V_{mn}(\mathbf{R})\}$. It is trivial to verify that the mean force of the right-hand side (RHS) of eq (53) is always real. When $\mathbf{V}(\mathbf{R})$ is a real symmetric matrix, the EOMs become

$$\begin{aligned} \dot{\mathbf{x}} &= \mathbf{V}(\mathbf{R})\mathbf{p} \\ \dot{\mathbf{p}} &= -\mathbf{V}(\mathbf{R})\mathbf{x} \\ \dot{\mathbf{R}} &= \mathbf{M}^{-1}\mathbf{P} \\ \dot{\mathbf{P}} &= -\sum_{n,m=1}^F (\nabla_{\mathbf{R}} V_{mn}(\mathbf{R})) \left[\frac{1}{2} (x^{(n)} x^{(m)} + p^{(n)} p^{(m)}) - \gamma \delta_{nm} \right] \end{aligned} \quad . \quad (54)$$

Consider the full Hamiltonian of nuclei and electrons of the molecular system,

$$\hat{H} = \frac{1}{2} \hat{\mathbf{P}}^T \mathbf{M}^{-1} \hat{\mathbf{P}} + \hat{H}_{el}(\hat{\mathbf{R}}) \quad , \quad (55)$$

where $\hat{H}_{el}(\hat{\mathbf{R}})$ is the electronic Hamiltonian. Its representation in the diabatic basis reads

$$\hat{H}_{el}(\mathbf{R}) = \sum_{n,m} V_{nm}(\mathbf{R}) |n\rangle \langle m| \quad (56)$$

and that in the adiabatic basis is

$$\hat{H}_{el}(\mathbf{R}) = \sum_k E_k(\mathbf{R}) |\phi_k(\mathbf{R})\rangle \langle \phi_k(\mathbf{R})| \quad , \quad (57)$$

where $E_k(\mathbf{R})$ denotes the adiabatic potential energy surface of the k -th adiabatic electronic state. Assume that the unitary transformation between a set of diabatic basis states, $\{|m\rangle\}$, and a set of adiabatic basis states,

$\{|\phi_k(\mathbf{R})\rangle\}$, is

$$\begin{aligned} |\phi_k(\mathbf{R})\rangle &= \sum_m U_{mk}(\mathbf{R}) |m\rangle \\ |n\rangle &= \sum_k U_{nk}^*(\mathbf{R}) |\phi_k(\mathbf{R})\rangle \end{aligned} \quad , \quad (58)$$

where $U_{mk}(\mathbf{R}) = \langle m | \phi_k(\mathbf{R}) \rangle$. This states the diagonalization of the diabatic potential matrix,

$$\sum_{n,m} U_{nj}^*(\mathbf{R}) V_{nm}(\mathbf{R}) U_{mk}(\mathbf{R}) = E_k(\mathbf{R}) \delta_{kj} \quad , \quad (59)$$

or equivalently,

$$V_{mn}(\mathbf{R}) = \sum_k U_{mk}(\mathbf{R}) E_k(\mathbf{R}) U_{nk}^*(\mathbf{R}) \quad . \quad (60)$$

Define the nonadiabatic coupling vector,

$$\mathbf{d}_{mn}(\mathbf{R}) = \left\langle \phi_m(\mathbf{R}) \left| \frac{\partial \phi_n(\mathbf{R})}{\partial \mathbf{R}} \right. \right\rangle \quad . \quad (61)$$

It is trivial to show

$$\mathbf{d}_{mn}(\mathbf{R}) = -\mathbf{d}_{nm}^*(\mathbf{R}) \quad (62)$$

because of the orthonormality of the basis set, that is, $\langle \phi_m(\mathbf{R}) | \phi_n(\mathbf{R}) \rangle = \delta_{mn}$. We then obtain

$$\begin{aligned} \nabla_{\mathbf{R}} U_{mk}^*(\mathbf{R}) &= \langle \nabla_{\mathbf{R}} \phi_k(\mathbf{R}) | m \rangle = \sum_n \langle \nabla_{\mathbf{R}} \phi_k(\mathbf{R}) | \phi_n \rangle \langle \phi_n | m \rangle \\ &= \sum_n \mathbf{d}_{nk}^*(\mathbf{R}) U_{mn}^*(\mathbf{R}) = -\sum_n \mathbf{d}_{kn}(\mathbf{R}) U_{mn}^*(\mathbf{R}) \end{aligned} \quad (63)$$

and

$$\nabla_{\mathbf{R}} U_{mk}(\mathbf{R}) = -\sum_n \mathbf{d}_{kn}^*(\mathbf{R}) U_{mn}(\mathbf{R}) = \sum_n U_{mn}(\mathbf{R}) \mathbf{d}_{nk}(\mathbf{R}) \quad . \quad (64)$$

Below we show the explicit form of the EOMs, eqs (51)-(53), under the diabatic-to-adiabatic transformation, eq (58).

The covariant transformation for mapping variables corresponding to the diabatic-to-adiabatic transformation, eq (58), reads

$$\tilde{x}^{(n)}(\mathbf{R}) + i\tilde{p}^{(n)}(\mathbf{R}) = \sum_m U_{mn}^*(\mathbf{R}) \left(x^{(m)} + ip^{(m)} \right) \quad (65)$$

or

$$x^{(n)} + ip^{(n)} = \sum_m U_{mn}(\mathbf{R}) \left(\tilde{x}^{(m)}(\mathbf{R}) + i\tilde{p}^{(m)}(\mathbf{R}) \right) \quad . \quad (66)$$

Denote $\tilde{\mathbf{g}}(\mathbf{R}) = \tilde{\mathbf{x}}(\mathbf{R}) + i\tilde{\mathbf{p}}(\mathbf{R})$. Equations (65)-(66) become

$$\begin{aligned} \tilde{\mathbf{g}}(\mathbf{R}) &= \mathbf{U}^\dagger(\mathbf{R}) \mathbf{g} \\ \mathbf{g} &= \mathbf{U}(\mathbf{R}) \tilde{\mathbf{g}}(\mathbf{R}) \end{aligned} \quad . \quad (67)$$

The electronic mapping kernel, eq (29), is

$$\hat{K}_{\text{ele}} = \sum_{n,m} \left[\frac{1}{2} \left(\tilde{x}^{(n)} + i\tilde{p}^{(n)} \right) \left(\tilde{x}^{(m)} - i\tilde{p}^{(m)} \right) - \gamma \delta_{nm} \right] |\phi_n\rangle \langle \phi_m| \quad , \quad (68)$$

under the transformation for a specific nuclear configuration, \mathbf{R} . Substitution of eq (63) into eq (65) yields

$$\nabla_{\mathbf{R}} \left(\tilde{x}^{(n)}(\mathbf{R}) + i\tilde{p}^{(n)}(\mathbf{R}) \right) = -\sum_k \mathbf{d}_{nk}(\mathbf{R}) \left(\tilde{x}^{(k)}(\mathbf{R}) + i\tilde{p}^{(k)}(\mathbf{R}) \right) \quad . \quad (69)$$

The total time derivative of $\tilde{x}^{(n)} + i\tilde{p}^{(n)}$ reads

$$\begin{aligned} \frac{d}{dt} \left(\tilde{x}^{(n)} + i\tilde{p}^{(n)} \right) &= \sum_m U_{mn}^*(\mathbf{R}) \left(\frac{d}{dt} \left(x^{(m)} + ip^{(m)} \right) \right) + \sum_m \left(\frac{d}{dt} U_{mn}^*(\mathbf{R}) \right) \left(x^{(m)} + ip^{(m)} \right) \\ &= -i \sum_k \delta_{nk} E_k(\mathbf{R}) \left(\tilde{x}^{(k)} + i\tilde{p}^{(k)} \right) - \sum_k \dot{\mathbf{R}} \cdot \mathbf{d}_{nk}(\mathbf{R}) \left(\tilde{x}^{(k)} + i\tilde{p}^{(k)} \right) \\ &= -i \sum_k \left[E_k(\mathbf{R}) \delta_{nk} - i \dot{\mathbf{R}} \cdot \mathbf{d}_{nk}(\mathbf{R}) \right] \left(\tilde{x}^{(k)} + i\tilde{p}^{(k)} \right) \end{aligned} \quad (70)$$

Equation (70) is the EOMs for mapping variables of electronic DOFs in the adiabatic representation.

We then consider the EOMs of nuclear mapping variables under the transformation eq (58). Equation (52) remains invariant under the transformation. Substitution of eqs (60), (63), (64), and 69 into eq (53) produces

$$\begin{aligned}
\dot{\mathbf{P}} &= -\sum_{n,m=1}^F (\nabla_{\mathbf{R}} V_{mn}(\mathbf{R})) \left[\frac{1}{2} (x^{(n)} + ip^{(n)}) (x^{(m)} - ip^{(m)}) - \gamma \delta_{nm} \right] \\
&= -\sum_{n,m} \nabla_{\mathbf{R}} \left(\sum_k U_{mk}(\mathbf{R}) E_k(\mathbf{R}) U_{nk}^*(\mathbf{R}) \right) \left[\frac{1}{2} (x^{(n)} + ip^{(n)}) (x^{(m)} - ip^{(m)}) - \gamma \delta_{nm} \right] \\
&= \sum_{k,l} \mathbf{d}_{lk}(\mathbf{R}) (E_l(\mathbf{R}) - E_k(\mathbf{R})) \left[\frac{1}{2} (\tilde{x}^{(k)} + i\tilde{p}^{(k)}) (\tilde{x}^{(l)} - i\tilde{p}^{(l)}) - \gamma \delta_{kl} \right] \\
&\quad - \sum_{k,l} \nabla_{\mathbf{R}} E_k(\mathbf{R}) \delta_{kl} \left[\frac{1}{2} (\tilde{x}^{(k)} + i\tilde{p}^{(k)}) (\tilde{x}^{(l)} - i\tilde{p}^{(l)}) - \gamma \delta_{kl} \right]
\end{aligned} \tag{71}$$

Since force matrix $\{\mathbf{F}_{kl} = \nabla_{\mathbf{R}} E_k(\mathbf{R}) \delta_{kl} + (E_k(\mathbf{R}) - E_l(\mathbf{R})) \mathbf{d}_{lk}(\mathbf{R})\}$ is Hermitian, the mean force of the RHS of eq (71) stays real. Under the diabatic-to-adiabatic transformation, eq (58), the EOMs of nuclear phase variables (eqs (52)-(53)) are then recast into

$$\begin{aligned}
\dot{\mathbf{R}} &= \mathbf{M}^{-1} \mathbf{P} \\
\dot{\mathbf{P}} &= -\sum_{k,l} \left[\nabla_{\mathbf{R}} E_k(\mathbf{R}) \delta_{kl} + (E_k(\mathbf{R}) - E_l(\mathbf{R})) \mathbf{d}_{lk}(\mathbf{R}) \right] \left[\frac{1}{2} (\tilde{x}^{(k)} + i\tilde{p}^{(k)}) (\tilde{x}^{(l)} - i\tilde{p}^{(l)}) - \gamma \delta_{kl} \right].
\end{aligned} \tag{72}$$

Define the effective potential matrix, $\mathbf{V}^{(\text{eff})}$, whose element is a function of the nuclear phase variables,

$$V_{nk}^{(\text{eff})}(\mathbf{R}, \mathbf{P}) = E_n(\mathbf{R}) \delta_{nk} - i \dot{\mathbf{R}} \cdot \mathbf{d}_{nk}(\mathbf{R}) = E_n(\mathbf{R}) \delta_{nk} - i \mathbf{M}^{-1} \mathbf{P} \cdot \mathbf{d}_{nk}(\mathbf{R}) \quad . \tag{73}$$

A more compact form of eq (70) for the electronic phase variables becomes

$$\dot{\tilde{\mathbf{g}}} = -i \mathbf{V}^{(\text{eff})}(\mathbf{R}, \mathbf{P}) \tilde{\mathbf{g}} \quad . \tag{74}$$

Equations (72) and (74) are the final EOMs under the covariant transformation eq (65).

When the electronic wavefunction of the basis set is always real, that is, $\langle r | \phi_n(\mathbf{R}) \rangle$ is real for any n , which is often the case for molecular systems, eq (62) leads to

$$\mathbf{d}_{mn}(\mathbf{R}) = -\mathbf{d}_{nm}(\mathbf{R}) \quad . \tag{75}$$

Equation (72) is simplified to

$$\begin{aligned}
\dot{\mathbf{R}} &= \mathbf{M}^{-1} \mathbf{P} \\
\dot{\mathbf{P}} &= -\sum_{k,l} \left[\nabla_{\mathbf{R}} E_k(\mathbf{R}) \delta_{kl} + (E_k(\mathbf{R}) - E_l(\mathbf{R})) \mathbf{d}_{lk}(\mathbf{R}) \right] \left[\frac{1}{2} (\tilde{x}^{(k)} \tilde{x}^{(l)} + \tilde{p}^{(k)} \tilde{p}^{(l)}) - \gamma \delta_{kl} \right].
\end{aligned} \tag{76}$$

Note that the mapping Hamiltonian of eq (33) (obtained in the diabatic representation) becomes

$$H_C(\mathbf{R}, \mathbf{P}, \mathbf{x}(\tilde{\mathbf{x}}, \tilde{\mathbf{p}}), \mathbf{p}(\tilde{\mathbf{x}}, \tilde{\mathbf{p}})) = \frac{1}{2} \mathbf{P}^T \mathbf{M}^{-1} \mathbf{P} + \sum_{n=1}^F E_n(\mathbf{R}) \left(\frac{1}{2} \left((\tilde{x}^{(n)}(\mathbf{R}))^2 + (\tilde{p}^{(n)}(\mathbf{R}))^2 \right) - \gamma \right) \tag{77}$$

under the transformation defined by eq (60) and eq (65). The new EOMs, eq (72) and eq (74), conserve the mapping Hamiltonian of eq (77). The diabatic-to-adiabatic transformation depends on nuclear coordinate \mathbf{R} , which is also a time-dependent variable of the evolution. The time-dependent canonical transformation for the Hamiltonian system yields a new set of EOMs by the chain rule²⁵¹.

In eqs (71)-(74) and eqs (76)-(77) \mathbf{P} corresponds to the mapping momentum in the diabatic representation, but *not* the canonical momentum in the adiabatic representation because eq (71) is *not* generated from Hamilton's equations of motion. Equations (74) and (76) share a similar form to the EOMs proposed by Cotton *et al*¹⁸⁶ and discussed in the Supporting Information of Reference⁵⁷. Define the covariant transformation for nuclear phase variables,

$$\begin{aligned}\tilde{\mathbf{R}} &= \mathbf{R} \\ \tilde{\mathbf{P}} &= \mathbf{P} + i \sum_{m,n} \left[\frac{1}{2} (\tilde{x}^{(n)} + i\tilde{p}^{(n)}) (\tilde{x}^{(m)} - i\tilde{p}^{(m)}) - \gamma \delta_{nm} \right] \mathbf{d}_{mn}(\mathbf{R})\end{aligned}\quad (78)$$

The Hamiltonian of eq (77) becomes

$$\begin{aligned}H_c(\tilde{\mathbf{R}}, \tilde{\mathbf{P}}, \tilde{\mathbf{x}}, \tilde{\mathbf{p}}) &= \frac{1}{2} \mathbf{P}(\tilde{\mathbf{P}}, \tilde{\mathbf{x}}, \tilde{\mathbf{p}}, \tilde{\mathbf{R}})^T \mathbf{M}^{-1} \mathbf{P}(\tilde{\mathbf{P}}, \tilde{\mathbf{x}}, \tilde{\mathbf{p}}, \tilde{\mathbf{R}}) \\ &+ \sum_{n=1}^F E_n(\tilde{\mathbf{R}}) \left(\frac{1}{2} \left((\tilde{x}^{(n)}(\tilde{\mathbf{R}}))^2 + (\tilde{p}^{(n)}(\tilde{\mathbf{R}}))^2 \right) - \gamma \right),\end{aligned}\quad (79)$$

of which the canonical variables are $\{\tilde{\mathbf{R}}, \tilde{\mathbf{P}}, \tilde{\mathbf{x}}, \tilde{\mathbf{p}}\}$ instead of $\{\mathbf{R}, \mathbf{P}, \tilde{\mathbf{x}}, \tilde{\mathbf{p}}\}$. (See more discussions in Appendix 2 of the Supporting Information). The mapping diabatic momentum, \mathbf{P} , is related to the kinematic momentum of the adiabatic representation. Although we can directly use Hamilton's EOMs for $\{\tilde{\mathbf{R}}, \tilde{\mathbf{P}}, \tilde{\mathbf{x}}, \tilde{\mathbf{p}}\}$, it is more convenient to employ the EOMs for $\{\mathbf{R}, \mathbf{P}, \tilde{\mathbf{x}}, \tilde{\mathbf{p}}\}$ instead to avoid the derivative of nonadiabatic coupling terms. This is indeed the strategy suggested by Cotton *et al*¹⁸⁶. When the initial condition does not involve nonadiabatic coupling terms, the sampling of \mathbf{P} in the diabatic representation is the same for that of $\tilde{\mathbf{P}}$ in the adiabatic representation. This is the case in the following applications, where FSSH has to be used in the adiabatic representation. By applying the covariance relation under the diabatic-to-adiabatic transformation, the EOMs on mapping phase space are independent of the representation of the (electronic) basis set, which is also the merit of Ehrenfest dynamics.

We note that either eq (51) or eq (74) can analytically be solved by a symplectic approach that employs an exact propagator on electronic phase space at each nuclear phase point. For example, for eq (74) we use

$$\tilde{\mathbf{U}}(\mathbf{R}, \mathbf{P}; \Delta t) = \exp[-i\Delta t \mathbf{V}^{(\text{eff})}] \quad (80)$$

such that the evolution of electronic phase variables follows $\tilde{\mathbf{g}}(t + \Delta t) = \tilde{\mathbf{U}}(\mathbf{R}, \mathbf{P}; \Delta t)\tilde{\mathbf{g}}(t)$.

We then test a range of benchmark systems, including two-site dissipative models, Tully's scattering models, atomic systems in cavity interacted with a number of field modes, and linear vibronic coupling model systems that involve the conical intersection^{137, 252-254}. They are typical composite quantum systems in chemistry, physics, condensed matter science, quantum optics, and quantum information.

4.2 Spin-boson models at low-temperature in condensed phase

The first model illustrated is the spin-boson model, which describes a two-site system interacted with an environmental bath in condense phase. It is also a simplified model for electron transfer and energy transfer in chemical and biological reactions. Several numerically exact benchmark methods for solving the spin-boson model include quasi-adiabatic propagator path integral (QuAPI)²⁵⁵⁻²⁵⁸ and more efficient small matrix PI (SMatPI)^{259, 260}, hierarchy equations of motion (HEOM)²⁶¹⁻²⁶⁹, and (multi-layer) multi-configuration time-dependent Hartree [(ML-)MCTDH]²⁷⁰⁻²⁷⁶. Quantum dynamics of the spin-boson model exhibits interesting dissipative characters, of which the asymptotic behaviours are often missed by either of Ehrenfest dynamics and FSSH in the low temperature regime⁵⁸. Spin-boson models with strong coupling in the low temperature regime presents challenging tests for trajectory-based dynamics methods.

The Hamiltonian of the spin-boson model is divided to three parts, $\hat{H} = \hat{H}_s + \hat{H}_b + \hat{H}_{sb}$. Here $\hat{H}_s = \varepsilon \hat{\sigma}_z + \Delta_c \hat{\sigma}_x$ describes a two-site system with the bias, ε , and tunneling Δ_c , while the bath part of the Hamiltonian is discretized into a combination of a number of quantum harmonic oscillators $\hat{H}_b = \sum_{j=1}^{N_b} (\hat{P}_j^2 + \omega_j^2 \hat{R}_j^2) / 2$. The system-bath coupling adopts a bilinear interaction, $\hat{H}_{sb} = -\sum_{j=1}^{N_b} c_j \hat{R}_j \hat{\sigma}_z$. Here we use an Ohmic bath spectral density $J(\omega) = (\pi/2)\alpha\omega e^{-\omega/\omega_c}$, where α is the Kondo parameter and ω_c is the cut-off frequency. Its discrete frequencies and coupling strengths $\{\omega_j, c_j\}$ are sampled²⁷⁷⁻²⁷⁹ from

$$\begin{cases} \omega_j = -\omega_c \ln[1 - j / (1 + N_b)] \\ c_j = \omega_j \sqrt{\alpha \omega_c / (1 + N_b)} \end{cases}, \quad j = 1, \dots, N_b \quad (81)$$

The initial density is set as $|1\rangle_s \langle 1|_s \otimes \hat{\rho}_b$, where the system is in excited state $|1\rangle_s$ while all bath modes are at thermal equilibrium with $\hat{\rho}_b = e^{-\beta \hat{H}_b} / Z_b$. Initial nuclear DOFs are sampled from the Wigner distribution of $\hat{\rho}_b$, while initial electronic DOFs are sampled from (weighted) constraint coordinate-momentum phase space $\mathcal{S}(\mathbf{x}, \mathbf{p})$. The continuous spectral density is discretized into $N_b = 300$ effective bath modes to guarantee numerical convergence in simulations.

In Figure 6, we demonstrate results produced by wMM with parameter $\Delta = 0.05$, by wMM with $\Delta = 0.1$, and by CMM with $\gamma = (\sqrt{F+1}-1)/F = 0.366$ that is a special case of CMM of Reference¹³⁶. Numerically exact results, as well as results yielded by Ehrenfest dynamics and FSSH, are also shown for comparison. Figure 6 indicates that wMM, as well as CMM, outperforms both Ehrenfest dynamics and FSSH dynamics, either for short-time coherences or for long-time dissipations.

4.3 Tully's gas phase scattering models

Tully's scattering models²⁴⁸ mimic different intersection types of molecular systems, which have widely been tested for various nonadiabatic dynamics methods. They describe a two-state Hamiltonian with a central coupling area and asymptotic plateau regions where diabatic potential function $V_{mn}(R \rightarrow \pm\infty)$ is flat. All the three models, including the single avoided crossing (SAC), dual avoided crossing (DAC), and extended coupling region (ECR) problems, are used in our numerical tests.

Atomic units are used in the simulations of the Tully models. The SAC model (Panel a1 of Figure 7) describes the simplest but essential surface crossing in molecular systems. In the diabatic representation, its diagonal potential energy surfaces (PESEs) are $V_{11} = -V_{22} = A(1 - e^{-B|R|})\text{sgn}(R)$ and off-diagonal coupling terms are $V_{12} = V_{21} = Ce^{-DR^2}$. Here, the parameters are $A = 0.01$, $B = 1.6$, $C = 0.005$, and $D = 1.0$. The DAC model (Panel b1 of Figure 7) includes two crossing points, thus different (electronic) paths are interfered with the dependence on the initial momentum. Its diagonal PESEs are $V_{11} = 0$ and $V_{22} = -Ae^{-BR^2} + E_0$, and off-diagonal coupling terms are $V_{12} = V_{21} = Ce^{-DR^2}$ in the diabatic representation with parameters $A = 0.10$, $B = 0.28$, $E_0 = 0.05$, $C = 0.015$ and $D = 0.06$. The ECR model in the diabatic representation (Panel c1 of Figure 7) has diagonal PESEs $V_{11} = -V_{22} = E_0$ and coupling terms $V_{12} = V_{21} = C[e^{BR}\Theta(-R) + (2 - e^{-BR})\Theta(R)]$, with $E_0 = -0.0006$, $B = 0.9$, $C = 0.1$. Here

$\Theta(R)$ is the Heaviside function of coordinate R . The adiabatic PESes and nonadiabatic coupling vector of the ECR model are also illustrated in Panel c2 of Figure 7.

We investigate the transmission and reflection coefficients of each state. In the simulations, the initial condition is a nuclear wavepacket, $\Psi(R; t=0) \propto \exp[-\alpha(R-R_0)^2/2 + i(R-R_0)P_0]$ (here we adopt $\hbar=1$), occupied in state 1, where $\alpha=1$ is the Gaussian width parameter, and R_0 and P_0 are the initial average coordinate and momentum. The initial average coordinate is set at $R_0 = -3.8$, -10 , and -13 for the SAC, DAC and ECR models, respectively. The initial Wigner distribution for the nuclear DOF is then $\rho_W^{\text{nuc}}(R, P) \propto \exp[-\alpha(R-R_0)^2 - (P-P_0)^2/\alpha]$.

Figure 7a shows that all methods are capable of quantitatively describing transmission coefficients in (diabatic) state 1 and state 2 of the SAC model. Figure 7b demonstrates that either wMM or CMM outperforms Ehrenfest dynamics and FSSH in predicting the peak shape when the initial momentum is relatively high, for example, $P_0 \geq 15$ au. This indicates that the trajectory-based approximate dynamics approaches in the mapping phase space formulation are good for fast processes in the gas phase composite/nonadiabatic system. However, the performance of either wMM or CMM in the low initial momentum region should be improved. It is important to note that the EOMs of wMM/CMM are invariant with the representation of the electronic state, as described in the Supporting Information of Reference ⁵⁷. (More discussion is also available in Appendix 2 of the Supporting Information.) That is, both the diabatic and adiabatic representations produce the same results for wMM or CMM, which is often not satisfied in FSSH and other nonadiabatic dynamics approaches.

For the ECR model of Figure 7c, the numerically exact DVR solution indicates an energy threshold for a bifurcation. Ehrenfest dynamics totally misses the step-like behaviours for the transmission coefficient in state 1, and for the reflection coefficient in either state 1 or state 2. CMM greatly improves over Ehrenfest dynamics. It is more encouraging that wMM is capable of faithfully describing such step-like behaviours. Tully's original FSSH algorithm is not able to well describe the ECR model²⁴⁸, but a modified version for treating frustrated hopping of FSSH (e.g., see Reference ²⁵⁰) is capable of qualitatively capturing the step-like behaviours. As shown in Figure 7c, in comparison to the traditional FSSH approach^{248, 250}, the overall performance of wMM for the ECR model is better.

4.4 Atom/molecule-in-cavity models of quantum electrodynamic light-matter systems

The cavity quantum electrodynamics (cQED) focuses on studying the interaction between light and a multi-level system (e.g., an atom or a molecule) in an optical cavity, which has many applications in the field of quantum

information and quantum computation. There exist many interesting and important phenomena in cQED, for example, the Purcell effect when the coupling is weak and the vacuum Rabi splitting when the coupling becomes strong²⁸⁰⁻²⁹⁴. When the general atomic/molecular system is coupled to multi-cavity modes, it is often intractable to solve the exact evolution in real time due to the curse of dimensionality. We test wMM for two typical models that describe an imprisoned multi-level atom coupled with a series of optical modes in a one-dimensional lossless cavity^{57, 206, 295-298}.

The total Hamiltonian consists of three parts. The optical field is depicted by N effective modes

$$\hat{H}_p = \sum_{j=1}^N \frac{1}{2} (\hat{P}_j^2 + \omega_j^2 \hat{R}_j^2) , \quad (82)$$

where $\{\hat{R}_j, \hat{P}_j\}$ denote the canonical coordinate-momentum variables of j -th optical field mode with the corresponding photonic frequency ω_j . The atomic system is described by $\hat{H}_a = \sum_{n=1}^F \varepsilon_n |n\rangle\langle n|$ with ε_n representing the n -th atomic energy level. Employing the dipole approximation, one can formulate the interaction between atom and optical field as

$$\hat{H}_c = \sum_{n \neq m}^F \left(\sum_{j=1}^N \omega_j \lambda_j(r_0) \hat{R}_j \right) \mu_{nm} |n\rangle\langle m| . \quad (83)$$

Here μ_{nm} denotes the transitional dipole moment between the n -th and m -th atomic levels, and the coupling between the j -th mode and the atom is

$$\lambda_j(r_0) = \sqrt{\frac{2}{\varepsilon_0 L}} \sin\left(\frac{j\pi r_0}{L}\right) , \quad (84)$$

where L is the volume length of cavity, ε_0 denotes the vacuum permittivity, and r_0 represents the location of the atom. In the simulation, the volume length of the cavity is set to 236200 au and the atom is frozen at the central location, that is, $r_0 = L/2$. The optical field is depicted by 400 standing-wave modes in cavity, of which the j -th frequency is $\omega_j = j\pi c/L$ with c the light speed in vacuum. We use two benchmark models for studying cQED processes, a three-level model with $\varepsilon_1 = -0.6738$, $\varepsilon_2 = -0.2798$, $\varepsilon_3 = -0.1547$, $\mu_{12} = -1.034$, $\mu_{23} = -2.536$ (all in atomic units), and a reduced two-level model where only the two lowest atomic levels are employed.

The highest atomic level of each model is initially occupied with no photon in cavity, that is, all cavity modes are in the corresponding vacuum state. The spontaneous emission occurs at the beginning, the released photon evolves in the cavity, and the re-absorption and re-emission happen later when the photon is reflected to meet the atom. Figure 8 shows the population transfer of each atomic level of the two models. The wMM results are compared with CMM, Ehrenfest dynamics, FSSH, and exact results^{296, 297}. Results of Ehrenfest dynamics and of FSSH significantly deviate from exact results even since very short time, while CMM and wMM yield much more reasonable descriptions for all energy levels, including the transfer behaviour at short time and the revival at around $t = 1800$ au. The wMM approach shows overall better performance than CMM in most of the cases. Figure 8 implies that the trajectory-based methods in the general coordinate-momentum phase space formulation will be useful for studying cQED phenomena in the field of quantum optics and quantum information.

4.5 Linear vibronic coupling model for the molecular system involving the conical intersection

The conical intersection widely exists in molecular systems and plays a central role in many photophysical and photochemical phenomena^{137, 141, 216, 252, 253, 299-302}. The linear vibronic coupling model (LVCM) is the simplest but effective model widely used to describe dynamic properties around the conical intersection region, of which Hamiltonian in the diabatic representation is

$$\hat{H} = \hat{H}_0 + \hat{H}_l + \hat{H}_c \quad . \quad (85)$$

Here, $\hat{H}_0 = \sum_{k=1}^N \omega_k (\hat{P}_k^2 + \hat{R}_k^2) / 2$ is the zeroth-order harmonic oscillator Hamiltonian in normal-mode space of the electronic ground state, where \hat{P}_k, \hat{R}_k ($k = 1, \dots, N$) denote the k -th effective weighted normal-mode variables with frequency ω_k (i.e., $P_k = p_k / \sqrt{\omega_k}$, $R_k = \sqrt{\omega_k} r_k$, where p_k, r_k are the canonical momentum, and canonical coordinate of k -th normal-mode). In eq (85), $\hat{H}_l = \sum_{n=1}^F (E_n + \sum_{k=1}^N \kappa_k^{(n)} \hat{R}_k) |n\rangle \langle n|$ contains the vertical excitation energy, E_n ($n = 1, \dots, F$) of F electronic states, and the linear coupling term $\kappa_k^{(n)}$ of each nuclear DOF for diagonal Hamiltonian elements, while $\hat{H}_c = \sum_{n \neq m}^F \left(\sum_{k=1}^N \lambda_k^{(nm)} \hat{R}_k \right) |n\rangle \langle m|$ includes linear coupling $\lambda_k^{(nm)}$ for each normal-mode between two different electronic states, $|n\rangle$ and $|m\rangle$.

A typical two-level 3-mode LVCM describes the S1/S2 conical intersection of the pyrazine molecule. The parameters of this model are fitted from semi-empirical electronic structure calculations by Schneiders and

Domcke in Reference ³⁰³. The excitation energies for the two electronic states are $E_1 = 3.94$ eV and $E_2 = 4.84$ eV. The diagonal linear coupling terms of first two modes $\{\hat{R}_1, \hat{R}_2\}$ are $\kappa_1^{(1)} = 0.037$ eV, $\kappa_2^{(1)} = -0.105$ eV for the first electronic state, and $\kappa_1^{(2)} = -0.254$ eV, $\kappa_2^{(2)} = 0.149$ eV for the second electronic state, respectively. The off-diagonal linear coupling of third mode \hat{R}_3 is $\lambda_3^{(12)} = \lambda_3^{(21)} = 0.262$ eV. The normal-mode vibronic frequency of each mode is $\omega_1 = 0.126$ eV, $\omega_2 = 0.074$ eV, and $\omega_3 = 0.118$ eV, respectively. Initial conditions of nuclear DOFs are sampled from the corresponding Wigner function of the vibronic ground state while the second electronic state is occupied. All simulations employ $\sim 10^5$ trajectories and time stepsize $\Delta t = 0.01$ fs for fully converged results. Numerically exact result of this model calculated by ML-MCTDH are available in Reference ²¹⁴.

Figure 9 shows population dynamics of state 2 yielded by wMM, CMM, Ehrenfest dynamics, FSSH and ML-MCTDH. It is evident that Ehrenfest dynamics performs poorly even for the short-time behaviour (before 100 fs). In comparison, wMM, CMM, and FSSH more reasonably describe the radiationless energy transfer process at short time. Interestingly, wMM describes the oscillating behaviours in the long-time region (after 300 fs) better than other approximate methods. Such oscillating behaviour in population dynamics indicates the molecular system passes through the “slopped” conical intersection region³⁰³.

Figures 6-9 demonstrate that the overall performance of wMM is better than CMM, especially in the gas phase scattering case of Figure 7c and the quantum electrodynamic light-matter systems of Figure 8. Both wMM and CMM approaches are able to outperform Ehrenfest dynamics as well as FSSH for condensed phase systems (e.g., in Figure 6 and Figure 8).

5. CONCLUSION REMARKS

The phase space formulation of quantum mechanics not only presents a type of convenient interpretation to describe quantum-classical correspondences as well as nonclassical correlations/entanglement, but also sets the insightful scene for developing practical and useful trajectory-based quantum dynamics approaches.

In the Focus Article we show that the constraint coordinate-momentum phase space formulation for the discrete-variable system which we have recently developed, and the weighted representation that we propose in the Focus Article are useful approaches for illustration of nonclassical features of quantum systems. The novel formulation is expected to have potential use for illustration of nonclassical features of quantum states, as well as for future phase point measurement experiment^{70, 85, 223-236}.

It is straightforward to show the relation between the $SU(F)/U(F-1)$ Stratonovich phase space¹¹⁴ and constraint coordinate-momentum phase space, which is diffeomorphic to $U(F)/U(F-1)$. When $F > 2$, it is inevitable to meet singularities in dynamics for discrete-variable systems when Stratonovich phase space is used (based on the symplectic structure of the phase space³⁰⁴). In comparison, (weighted) constraint coordinate-momentum phase space does not cause any singularities in trajectory-based exact dynamics, which is much more numerically favourable. (See more discussion in Appendix 3 of the Supporting Information).

When the general Moyal bracket of the quantum Liouville theorem is approximated by the corresponding Poisson bracket^{57, 58} on (weighted) constraint phase space, it reproduces the correct frozen-nuclei limit of composite/nonadiabatic systems. Such trajectory-based EOMs on (weighted) constraint coordinate-momentum phase space do not rely on the choice of representation of electronic states and are straightforward to obtain the form under covariant transformations. Because second-order nonadiabatic coupling terms are avoided in the EOMs of the adiabatic representation, it is especially useful for applications to realistic molecular systems. (In addition to Section 4.1, more discussion on the EOMs is presented in Appendices 2 and 5 of the Supporting Information.) Various benchmark model tests of from gas phase to condensed phase quantum systems. (as shown in Figures 6-9) indicate that wMM, the new trajectory-based approximate approach with the weighted constraint coordinate-momentum phase space representation, demonstrates overall better performance than FSSH as well as Ehrenfest dynamics. It is expected that more investigations on the (weighted) constraint phase space formulation will shed light on more numerically favourable dynamics approaches with the Meyer-Miller mapping Hamiltonian or other mapping Hamiltonians (e.g., those of Reference¹³³ and discussed in Reference⁵⁸).

We note that the (weighted) constraint coordinate-momentum phase space formulation is established for any systems with a finite set of states, not only limited to discrete electronic states, but also for finite discrete nuclear states. The weighted phase space strategy that we propose can also be applied to other types of phase space formulations of the discrete-variable system, such as Stratonovich phase space, and Wootters phase space, albeit that the general coordinate-momentum phase space formulation presented in the Focus Article will be more convenient, for experimental measurements, tomography, or characterizations of fidelity, coherence, inequalities, displaced parity, atomic/molecular/optical Schrodinger cat states, and entanglement in quantum information and computation^{70, 85, 223-236, 305, 306} as well as for studying dynamic processes of composite systems in physics, chemistry, materials, biology, and environmental science.

Figures and Tables

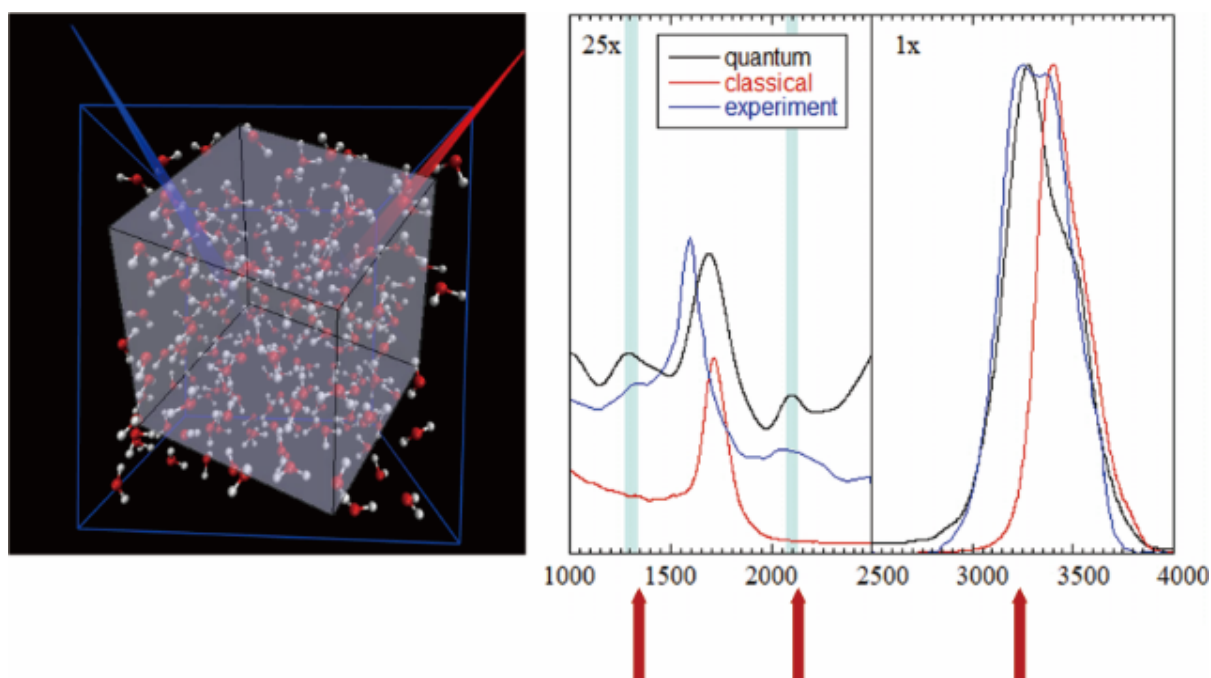


Figure 1. Quantum dynamical effects are decisive in reproducing the experimental isotropic Raman spectrum of liquid water at room temperature, as illustrated by the LSC-IVR simulation where infinite (Wigner) phase space for nuclear DOFs is used. Converged results were obtained with 216 water molecules in a box with periodic boundary conditions. (Reprinted with permission from Reference ¹⁹. Copyright 2018 Taylor & Francis.)

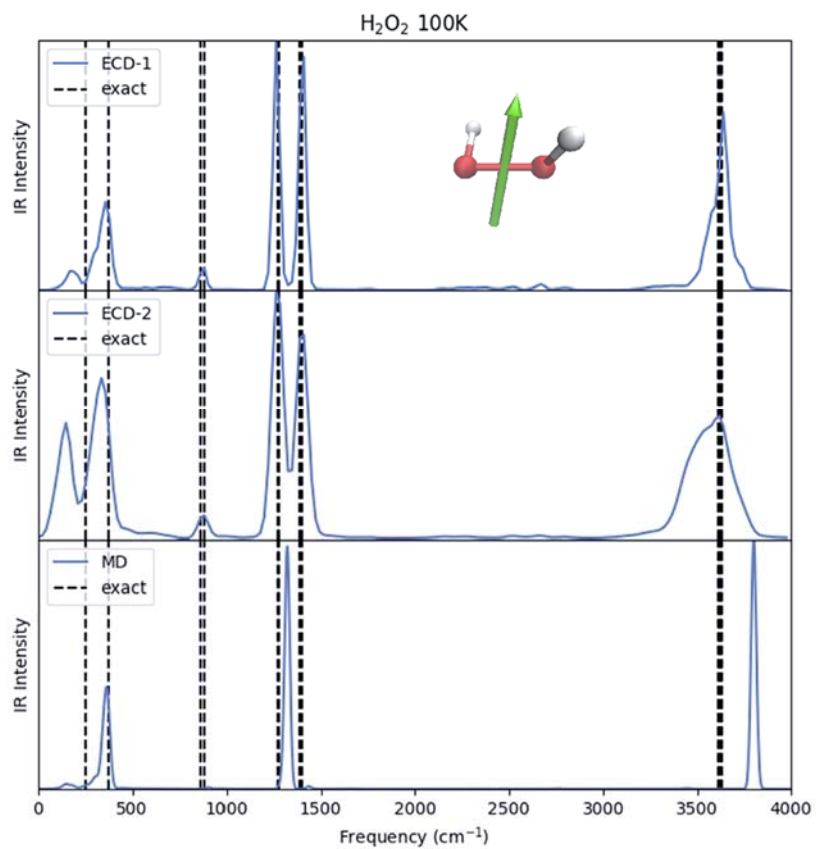
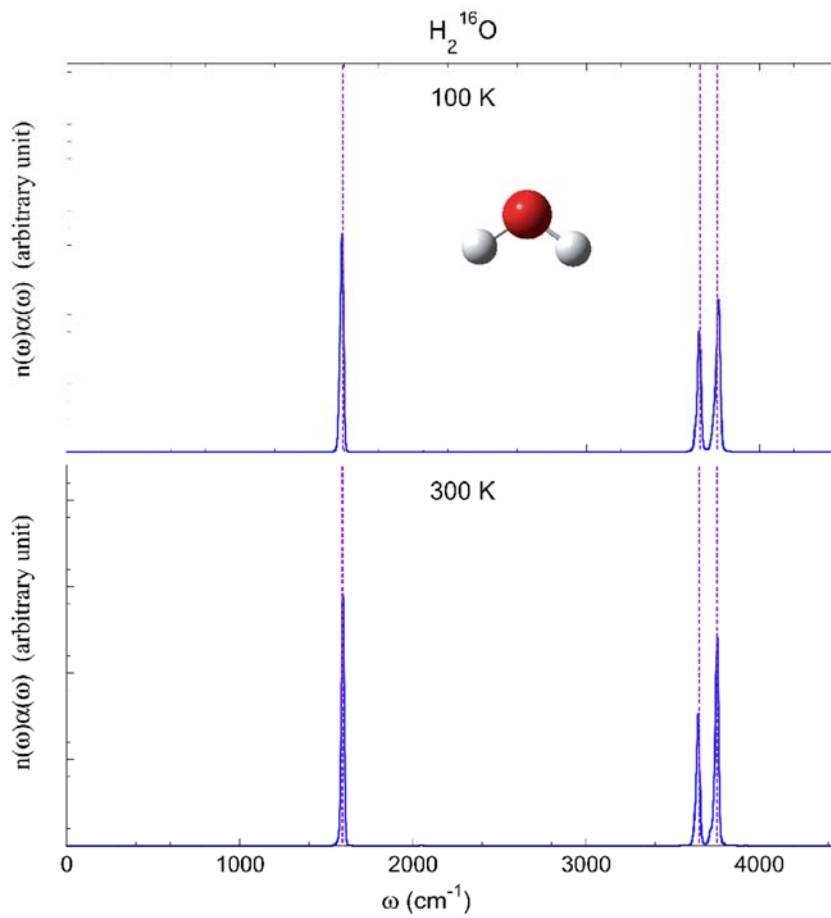


Figure 2. Molecular vibrational spectra produced by more advanced trajectory-based dynamics methods with infinite (Wigner) phase space used for nuclear DOFs, which satisfy the two fundamental criteria: conservation of the quantum Boltzmann distribution for the thermal equilibrium system and being exact for any quantum thermal correlation functions in the classical and harmonic limits. (a) Vibrational spectrum of the H_2O molecule at 100K and that at 300K. Adapted with permission from Reference ⁴¹. Copyright 2016 American Institute of Physics Publishing. (b) Vibrational spectrum of the H_2O_2 molecule at 100K. Adapted with permission from Reference ⁴⁴. Copyright 2021 American Institute of Physics Publishing.

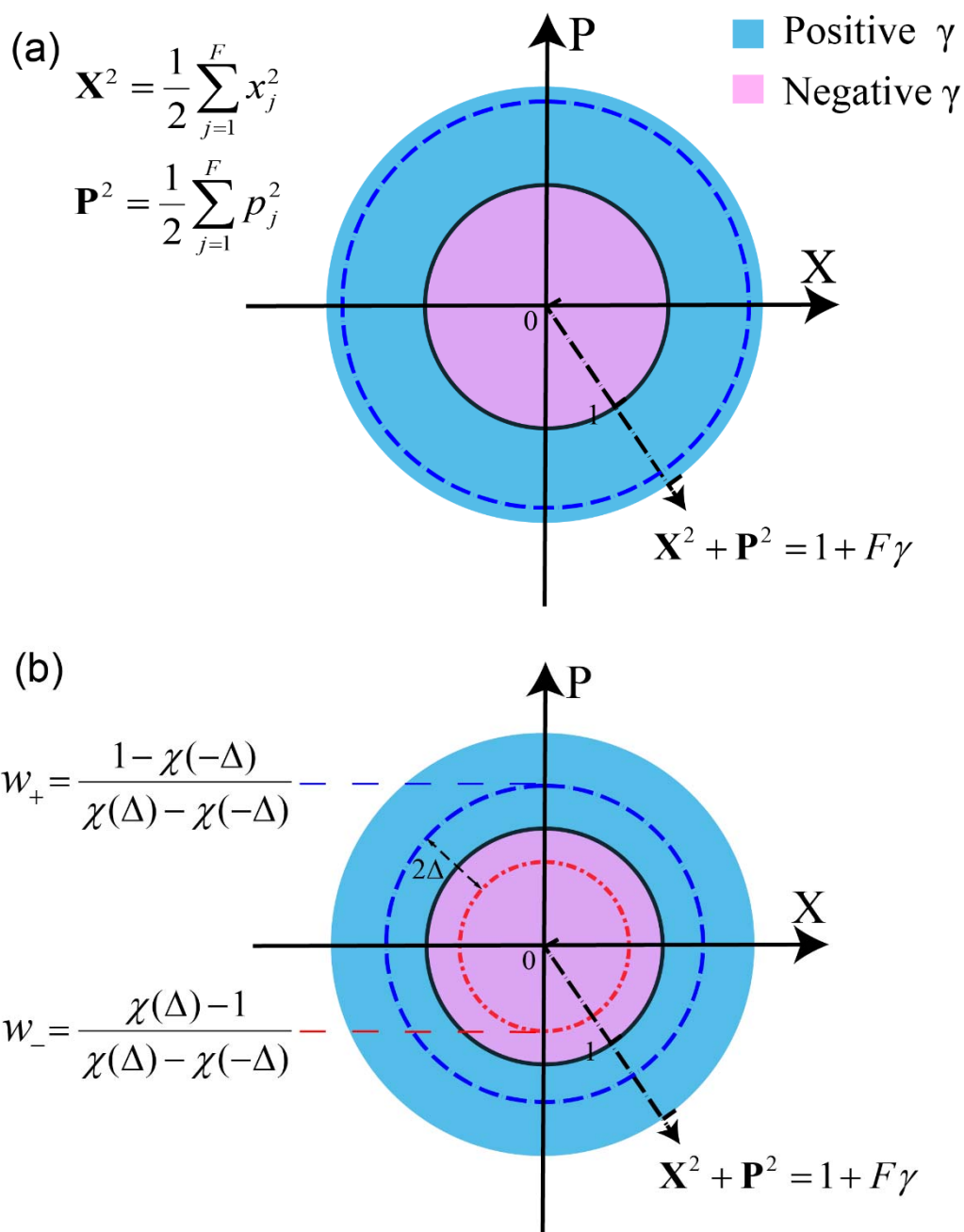


Figure 3: Illustration of the exact mapping formulation with constraint coordinate-momentum phase space. Panel (a) presents constraint phase space with only a single value of parameter γ . Panel (b) demonstrates weighted constraint phase space with two values of parameter γ , where the quasi-probability distribution function is $w(\gamma) = w_+ \delta(\gamma - \Delta) + w_- \delta(\gamma + \Delta)$. Constraint phase space with the positive weight is blue-dashed, while that with the negative weight is red dot-dashed. (Panel (a) is adapted with permission from Reference ¹³⁶. Copyright 2021 American Chemical Society.)

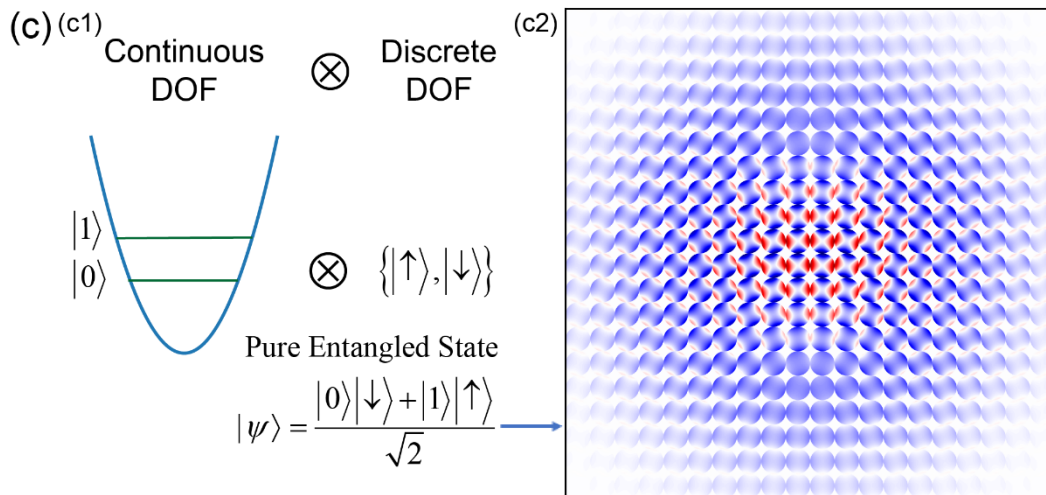
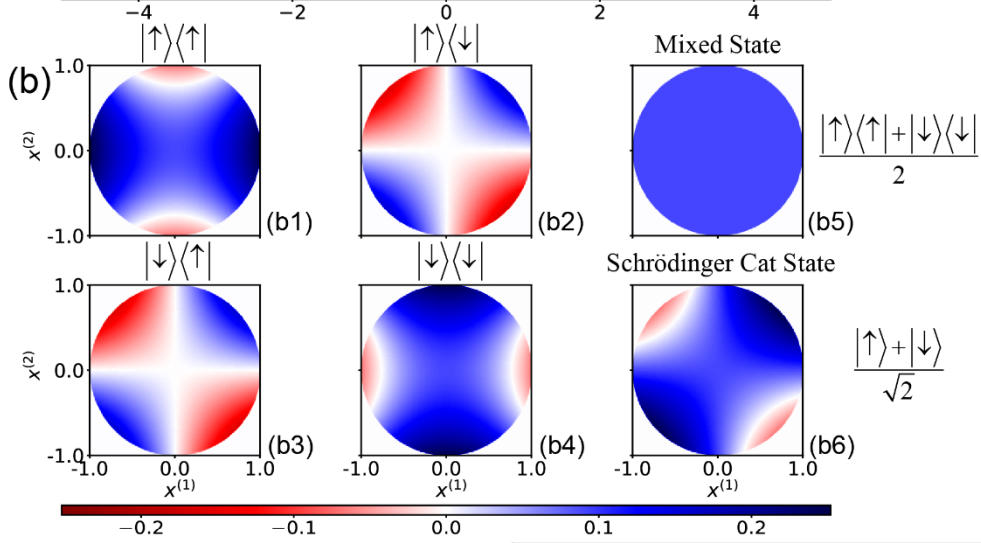
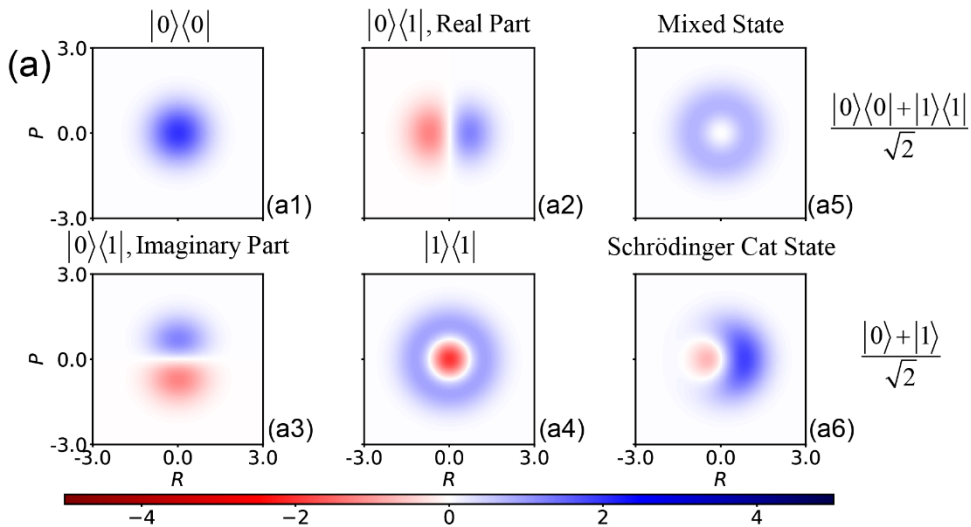


Figure 4: Illustrations of (a) Wigner representation of a continuous-variable system, (b) constraint phase space representation of a discrete-variable system, and (c) hybrid coordinate-momentum phase space representation of a composite system with both discrete and continuous DOFs.

- (a) Wigner distribution for $|0\rangle\langle 0|$ (Panel a1), that for $|1\rangle\langle 1|$ (Panel a4), real part (Panel a2) and imaginary part (Panel a3) of the Wigner distribution for $|0\rangle\langle 1|$, Wigner distribution for mixed state $(|0\rangle\langle 0| + |1\rangle\langle 1|)/2$ (Panel a5), and that for Schrödinger cat state $(|0\rangle + |1\rangle)/\sqrt{2}$ (Panel a6). Here, $|0\rangle$ and $|1\rangle$ are two energy levels of a continuous-variable system.
- (b) Marginal distribution of constraint phase space coordinates $(x^{(1)}, x^{(2)})$ for $|\uparrow\rangle\langle\uparrow|$ (Panel b1), $|\downarrow\rangle\langle\downarrow|$ (Panel b4), that for $|\uparrow\rangle\langle\downarrow|$ (Panel b2), that for $|\downarrow\rangle\langle\uparrow|$ (Panel b3), that for mixed state $(|\uparrow\rangle\langle\uparrow| + |\downarrow\rangle\langle\downarrow|)/2$ (Panel b5), and that for Schrödinger cat state $(|\uparrow\rangle + |\downarrow\rangle)/\sqrt{2}$ (Panel b6). Here, $|\uparrow\rangle$ and $|\downarrow\rangle$ represent two discrete states of a discrete-variable system.
- (c) Panel c1: Schematic representaton of the composite system and the pure entangled state $(|0\rangle|\downarrow\rangle + |1\rangle|\uparrow\rangle)/2$; Panel c2: hybrid coordinate-momentum phase space representation of the entangled state. The grid is on the Wigner phase space (R, P) for the continous DOF, and each circle of a grid stands for the local marginal distribution function of constraint phase space variables $(x^{(1)}, x^{(2)})$. The notations are identical to those in Panels (a)-(b).

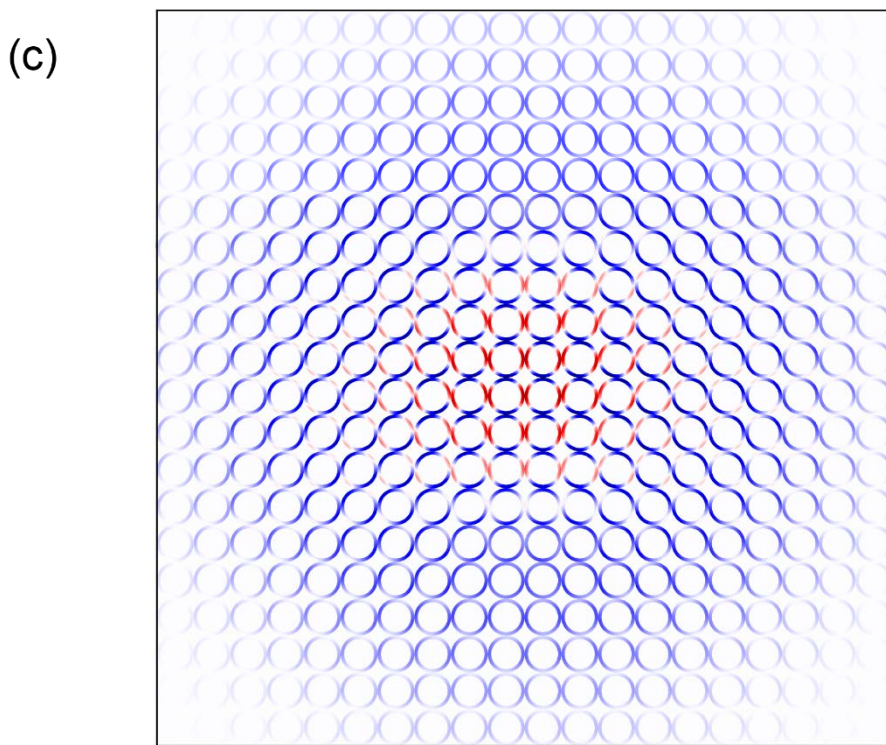
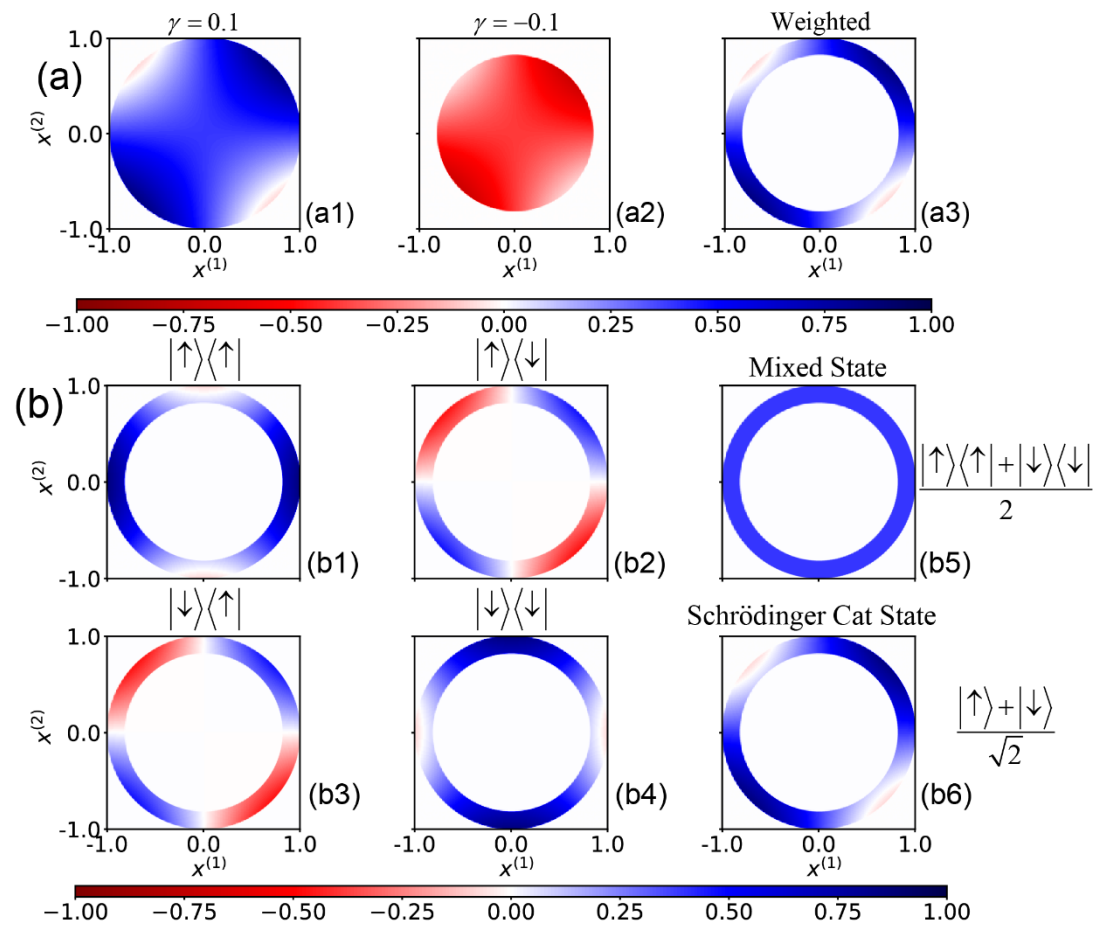


Figure 5: Illustrations of (a) components and (b) marginal distribution functions of the weighted constraint phase space representation of a discrete-variable system, and (c) weighted hybrid representation of the same composite system as that of Figure 4(c).

(a) Marginal distribution of constraint phase space coordinates $(x^{(1)}, x^{(2)})$ for Schrödinger cat state

$(|\uparrow\rangle + |\downarrow\rangle) / \sqrt{2}$ with $\gamma = \Delta$ weighted by w_+ (Panel a1), with $\gamma = -\Delta$ weighted by w_- (Panel

a2). The sum of the two components yields the marginal distribution of constraint phase space coordinates

(x_1, x_2) of the weighted representation with two values of parameter γ for the Schrödinger cat state

(Panel a3). Coordinates are scaled by the larger radius $\sqrt{2(1+2\Delta)}$.

(b) Weighted marginal distribution of constraint phase space coordinates $(x^{(1)}, x^{(2)})$ for the same properties as those in Figure 4(b).

(c) Same as Figure 4(c), but using weighted marginal distribution for the discrete DOF.

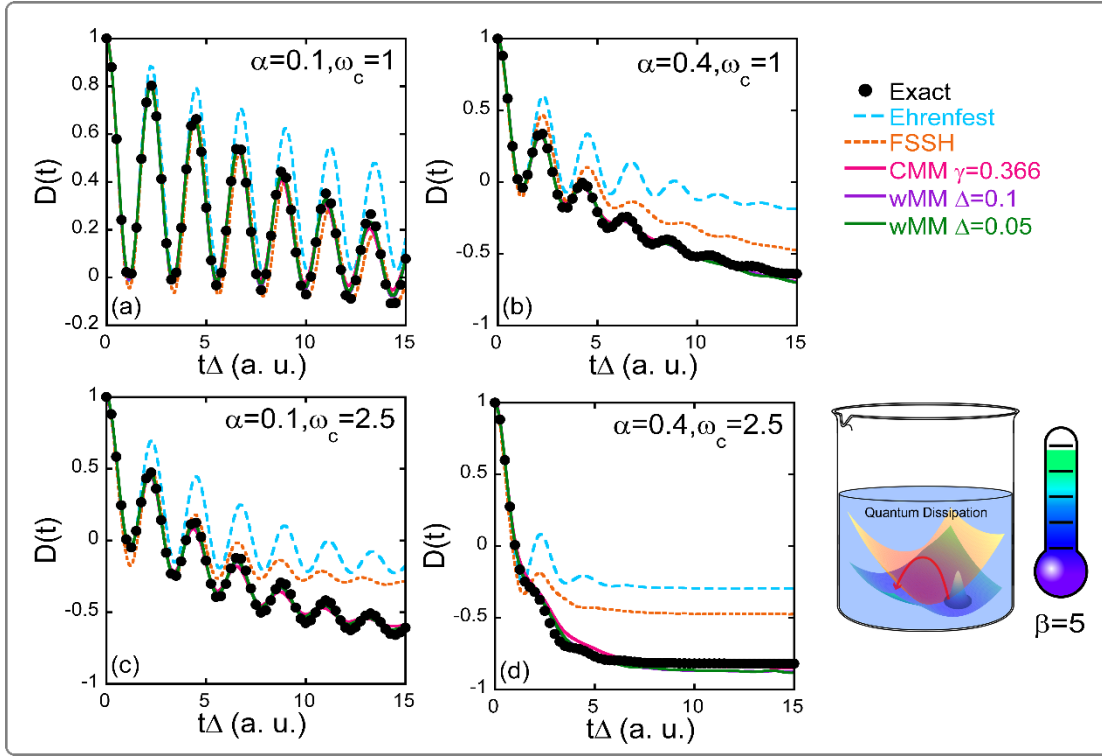


Figure 6: Results of population difference $D(t) = P_1(t) - P_0(t)$ between two states for the spin-boson model at low-temperature ($\beta = 1/(k_B T) = 5$) with the Ohmic bath. Panel (a) reports the population dynamics of the spin-boson model with parameters $\varepsilon = \Delta_c = 1$, $\beta = 5$, $\omega_c = 1$, $\alpha = 0.1$ in Panel (a). Solid circles: Exact results produced by eHEOM reported in Reference ¹³⁶. Cyan dashed lines: Ehrenfest dynamics. Orange dashed lines: FSSH. Magenta solid lines: CMM with $\gamma = 0.366$. Purple and green solid lines: wMM with $\Delta = 0.1$ and 0.05 , respectively. Panel (b) is similar to Panel (a) but for $\alpha = 0.4$; Panel (c) is similar to Panel (a) but for $\omega_c = 2.5$; Panel (d) is similar to Panel (a) but for $\omega_c = 2.5$, $\alpha = 0.4$. In each model 300 continuous DOFs (i.e., effective bath modes) are used.

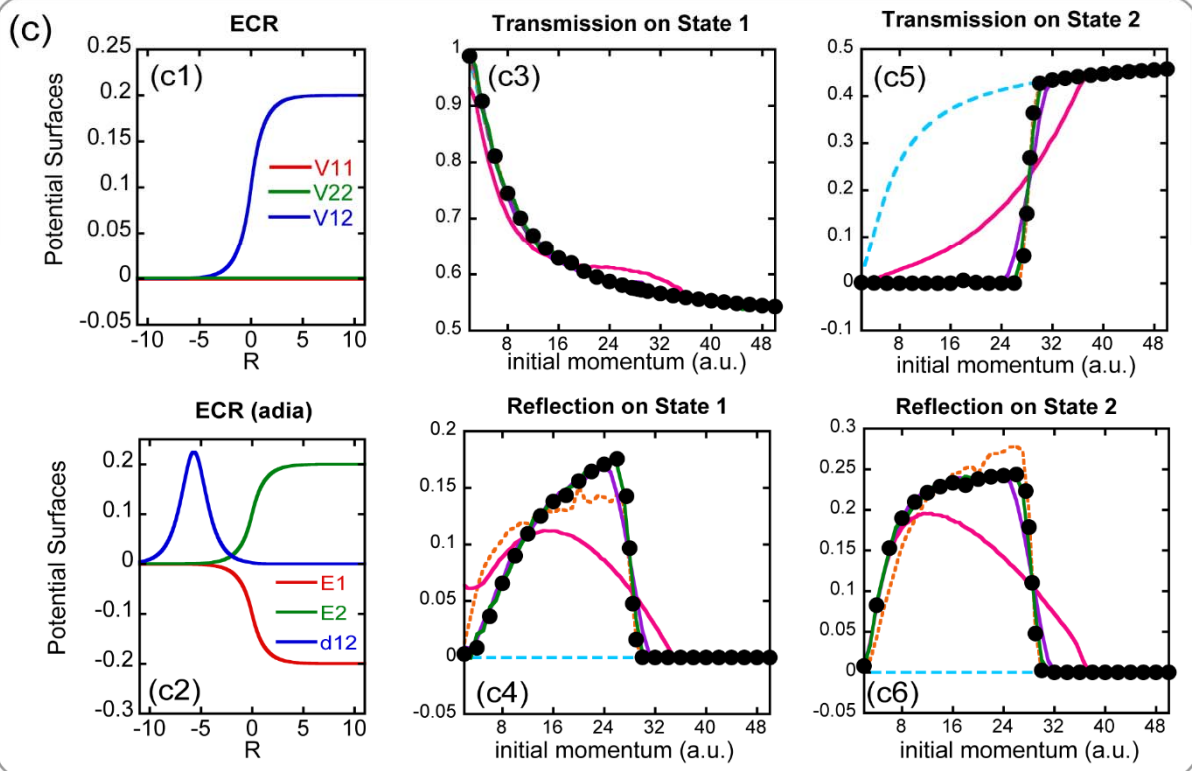
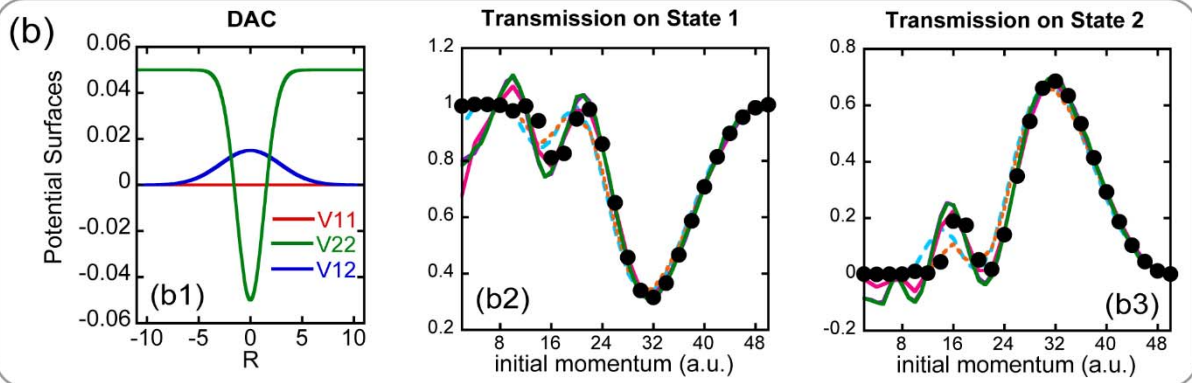
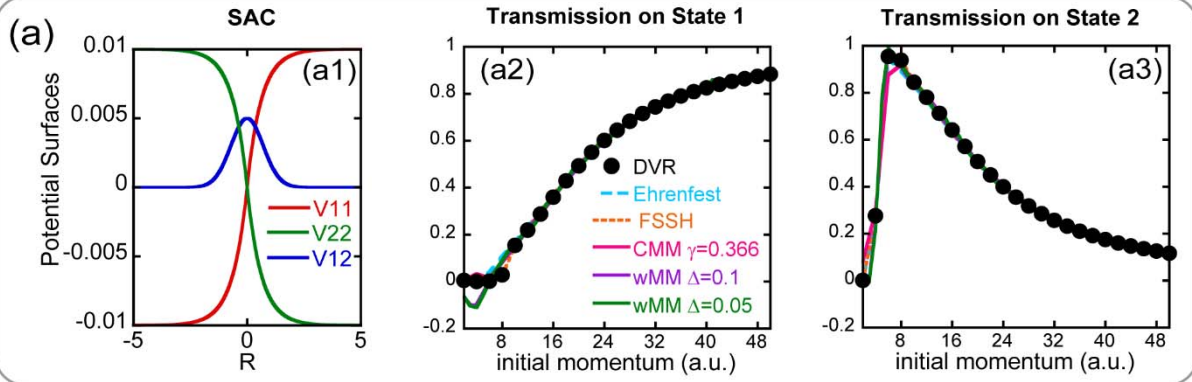


Figure 7: Illustration of three Tully models and simulation results. Panel (a1) denotes diabatic PESes $V_{11}(R)$ and $V_{22}(R)$, as well as coupling term $V_{12}(R)$ for the SAC model; Panel (b1) does so for the DAC model; Panel (c1) does so for the ECR model. Panel (c2) demonstrates adiabatic PESes $E_1(R)$ and $E_2(R)$, as well as nonadiabatic coupling vector $d_{12}(R)$.

Panels (a2)-(a3): transmission coefficients on diabatic state 1, and those on diabatic state 2 of the SAC model, respectively. Panels (b2)-(b3): similar to Panels (a2)-(a3), but for the DAC model. Panels (c3) and (c4): transmission/reflection coefficients on adiabatic state 1 of the ECR model; Panels (c5) and (c6): those on adiabatic state 2.

In Panels (a2)-(a3), (b2)-(b3), and (c3)-(c6), magenta, purple and green lines stand for transmission coefficients results for CMM with $\gamma = 0.366$, wMM with $\Delta = 0.1$, and wMM with $\Delta = 0.05$, respectively. Long-dashed blue lines: Ehrenfest dynamics; Short-dashed orange lines: FSSH; Black points: exact DVR benchmarks.

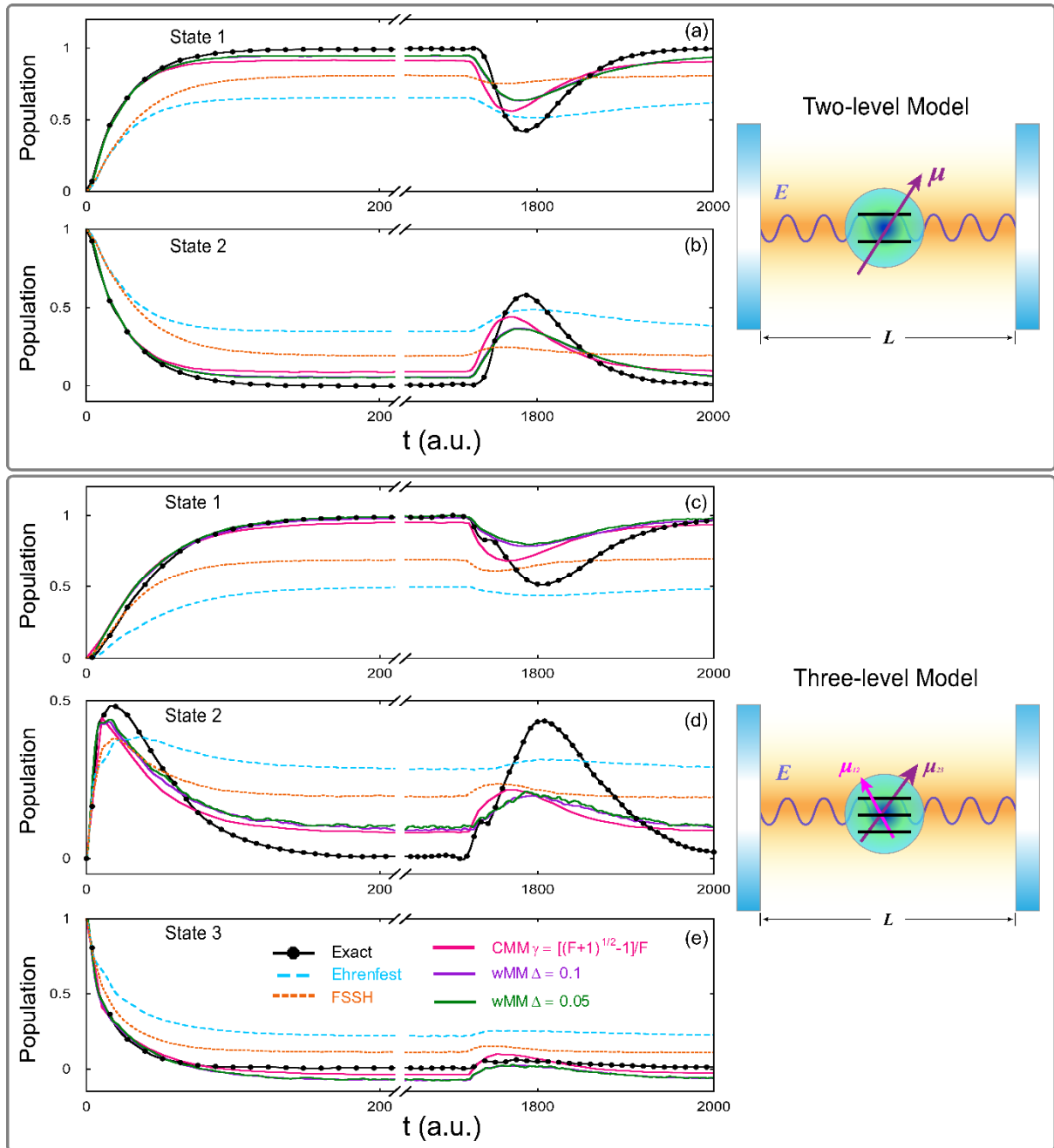


Figure 8: Results of population dynamics for the atom-in-cavity models. Panels (a)-(b) represent data of the first and second states of the two-level model, respectively. Panels (c)-(e) denote data of the first, second and third states of the three-level model, respectively. Magenta solid lines: CMM with $\gamma = (\sqrt{F+1}-1)/F$; Purple solid lines: wMM with $\Delta = 0.1$; Green solid lines: wMM with $\Delta = 0.05$; Cyan long-dashed lines: Ehrenfest dynamics; Orange short-dashed lines: FSSH; Black solid-dotted lines: exact results from References^{296, 297}. In each model 400 continuous DOFs (i.e., standing-wave modes) are involved.

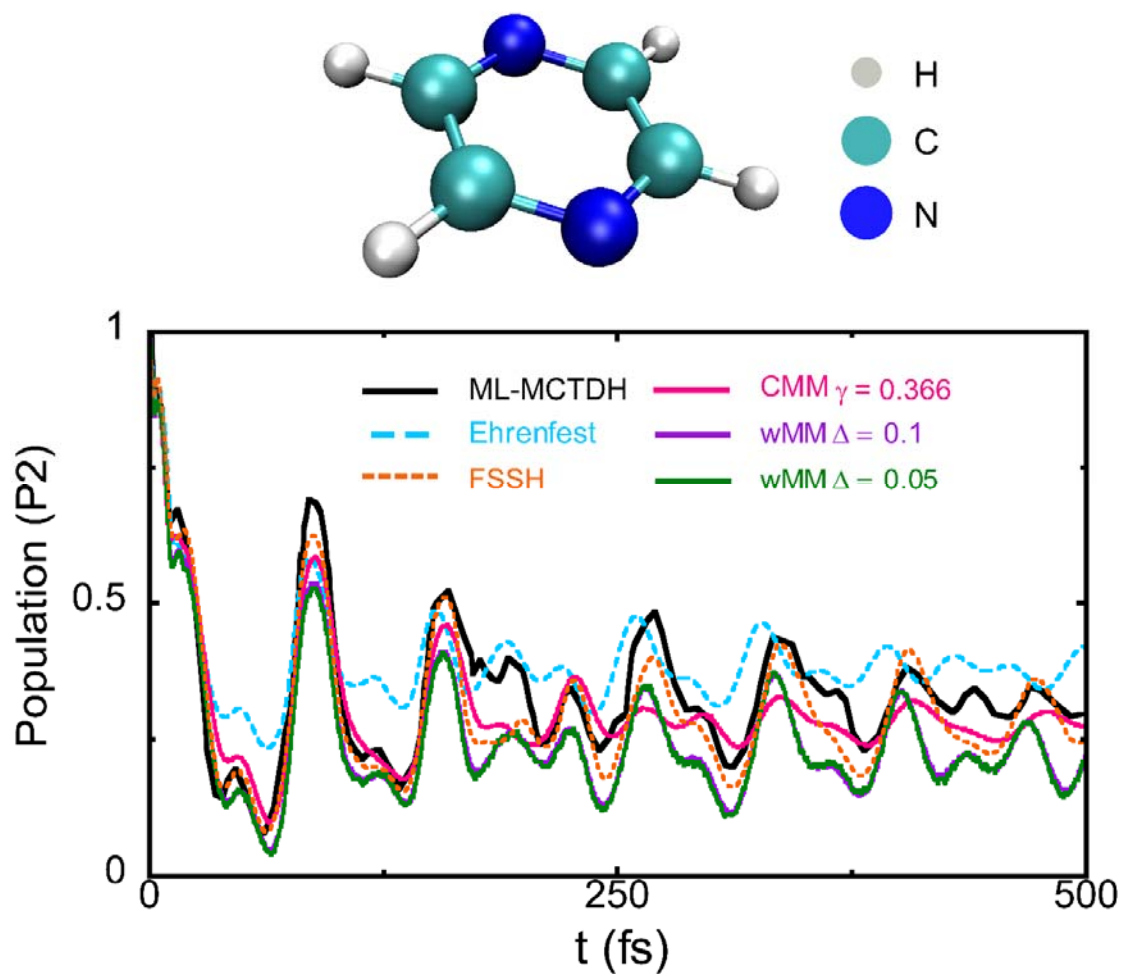


Figure 9: Results of population dynamics of the second electronic state of the 2-level 3-mode pyrazine model.

Magenta solid lines: CMM with $\gamma = (\sqrt{F+1}-1)/F \approx 0.366$; Purple solid lines: wMM with $\Delta = 0.1$;

Green solid lines: wMM with $\Delta = 0.05$. Cyan dashed lines: Ehrenfest dynamics; Orange short-dashed lines:

FSSH; Black solid lines: ML-MCTDH results of Reference ²¹⁴.

Funding Information

National Natural Science Foundation of China (NSFC) Grant No. 21961142017; Ministry of Science and Technology of China (MOST) Grant No. 2017YFA0204901

Research Resources

High-performance Computing Platform of Peking University, Beijing PARATERA Tech CO., Ltd., and Guangzhou supercomputer center

Acknowledgments

This work was supported by the National Natural Science Foundation of China (NSFC) Grant No. 21961142017, and by the Ministry of Science and Technology of China (MOST) Grant No. 2017YFA0204901. We acknowledge the High-performance Computing Platform of Peking University, Beijing PARATERA Tech CO., Ltd., and Guangzhou supercomputer center for providing computational resources.

Notes

The authors declare no competing financial interest.

Supporting Information

Appendix 1. Derivation of the formulation of (weighted) constraint coordinate-momentum phase space.

In this appendix, we introduce the techniques for performing integrals on constraint coordinate-momentum phase space, and show the brief derivation of the formulation of (weighted) constraint coordinate-momentum phase space. Such techniques have been expressed in Appendix A of ref ¹³⁴ as well as in Section S1 of the Supporting Information of ref ¹³⁶.

Consider the expectation of any function $f(X_1, X_2, \dots, X_L)$ under the L -dimensional independent standard normal distribution (i.e., $\{X_i\} \sim N^{(L)}(0,1)$). It is closely related to that under the uniform distribution on the $(L-1)$ -dimensional constraint space, i.e.,

$$\begin{aligned}
\langle f \rangle_{N^{(L)}(0,1)} &= \frac{1}{(2\pi)^{L/2}} \int dX_1 dX_2 \cdots dX_L e^{-\frac{1}{2} \sum_{k=1}^L X_k^2} f(X_1, X_2, \dots, X_L) \\
&= \frac{1}{(2\pi)^{L/2}} \int_0^\infty d\xi \int dX_1 dX_2 \cdots dX_L e^{-\xi} \delta\left(\frac{1}{2} \sum_{k=1}^L X_k^2 - \xi\right) f(X_1, X_2, \dots, X_L) \quad . (86) \\
&= \frac{1}{(2\pi)^{L/2}} \int_0^\infty d\xi e^{-\xi} S_{L-1}(\sqrt{\xi}) \langle f \rangle_{S_{L-1}(\sqrt{\xi})}
\end{aligned}$$

Here,

$$S_{L-1}(R) = \int dX_1 dX_2 \cdots dX_L \delta\left(\frac{1}{2} \sum_{k=1}^L X_k^2 - R^2\right) \quad (87)$$

denotes the area of the constraint space with radius R , and the expectation under the uniform distribution on the $(L-1)$ -dimensional constraint space, $\langle \cdots \rangle_{S_{L-1}(R)}$, is given by

$$\langle f \rangle_{S_{L-1}(R)} = \frac{1}{S_{L-1}(R)} \int dX_1 dX_2 \cdots dX_L \delta\left(\frac{1}{2} \sum_{k=1}^L X_k^2 - R^2\right) f(X_1, X_2, \dots, X_L) \quad . \quad (88)$$

(Note that the constraint space with radius R defined in eq (87) is slightly different from the $(L-1)$ -sphere in mathematics.) It is trivial to verify that $S_{L-1}(R) = R^{L-2} S_{L-1}(1)$ is the scaling relation of $S_{L-1}(R)$. We can calculate $S_{L-1}(1)$ by setting $f(X_1, X_2, \dots, X_L) \equiv 1$ in eq (86), i.e.,

$$1 = \frac{1}{(2\pi)^{L/2}} \int_0^\infty d\xi e^{-\xi} S_{L-1}(\sqrt{\xi}) = \frac{1}{(2\pi)^{L/2}} S_{L-1}(1) \int_0^\infty d\xi e^{-\xi} \xi^{\frac{L-2}{2}} \quad . \quad (89)$$

Equation (89) yields

$$S_{L-1}(1) = \frac{(2\pi)^{L/2}}{\Gamma(L/2)} \quad (90)$$

after we use the equality $\int_0^\infty dx e^{-x} x^\alpha = \Gamma(\alpha+1)$ for $\alpha > -1$, where the Gamma function is defined by

$$\Gamma(s) = \int_0^\infty dt e^{-t} t^{s-1} \quad (s > 0).$$

The k -th order moment of the uniform distribution on the $(L-1)$ -dimensional constraint space has the scaling relation,

$$\begin{aligned} \langle X_{n_1} X_{n_2} \cdots X_{n_k} \rangle_{S_{L-1}(\sqrt{\xi})} &= \frac{1}{S_{L-1}(\sqrt{\xi})} \int dX_1 dX_2 \cdots dX_L \delta\left(\frac{1}{2} \sum_{l=1}^L X_l^2 - \xi\right) X_{n_1} X_{n_2} \cdots X_{n_k} \\ &= \xi^{k/2} \langle X_{n_1} X_{n_2} \cdots X_{n_k} \rangle_{S_{L-1}(1)} \end{aligned} \quad (91)$$

Substitution of eq (91) into eq (86) produces

$$\begin{aligned} \langle X_{n_1} X_{n_2} \cdots X_{n_k} \rangle_{N^{(L)}(0,1)} &= \frac{\Gamma\left(\frac{L+k}{2}\right)}{\Gamma(L/2)} \langle X_{n_1} X_{n_2} \cdots X_{n_k} \rangle_{S_{L-1}(1)} \\ &= \frac{\Gamma\left(\frac{L+k}{2}\right)}{\xi^{k/2} \Gamma(L/2)} \langle X_{n_1} X_{n_2} \cdots X_{n_k} \rangle_{S_{L-1}(\sqrt{\xi})} \end{aligned} \quad (92)$$

The well-known Wick theorem (also called Isserlis's theorem)^{244, 245} for the independent and identical standard normal distribution reads

$$\langle X_{n_1} X_{n_2} \cdots X_{n_k} \rangle_{N^{(L)}(0,1)} = \begin{cases} 0, & k \text{ is odd} \\ \sum \left(\prod \langle X_{n_i} X_{n_j} \rangle_{N^{(L)}(0,1)} \right), & k \text{ is even} \end{cases} \quad (93)$$

Here, the notation $\sum(\prod \cdots)$ stands for the summation of the products over all possible pair partitions of $\{X_{n_1}, X_{n_2}, \cdots, X_{n_k}\}$. It is straightforward to obtain the second order moment and fourth order moment of $N^{(L)}(0,1)$,

$$\begin{aligned} \langle X_i X_j \rangle_{N(0,1)} &= \delta_{ij} \\ \langle X_i X_j X_k X_l \rangle_{N(0,1)} &= \delta_{ij} \delta_{kl} + \delta_{ik} \delta_{jl} + \delta_{il} \delta_{jk} \end{aligned} \quad (94)$$

Substitution of eq (94) into eq (92) leads to

$$\begin{aligned}
\langle X_i X_j \rangle_{S_{L-1}(\sqrt{\xi})} &= \frac{\xi}{L/2} \delta_{ij} \\
\langle X_i X_j X_k X_l \rangle_{S_{L-1}(\sqrt{\xi})} &= \frac{\xi^2}{\frac{L}{2} \left(\frac{L}{2} + 1 \right)} \left(\delta_{ij} \delta_{kl} + \delta_{ik} \delta_{jl} + \delta_{il} \delta_{jk} \right) .
\end{aligned} \tag{95}$$

We then set $L = 2F$ as well as $\xi = 1 + F\gamma$ and relabel the constraint space (defined by eq 31) as $\mathcal{S}_\gamma(\mathbf{x}, \mathbf{p})$ parameterized by γ . The comparison between eq 32 and eq (87) states that the area of constraint phase space is

$$\Omega(\gamma) = S_{2F-1} \left(R = \sqrt{1 + F\gamma} \right) = \frac{(2\pi)^F}{\Gamma(F)} (1 + F\gamma)^{F-1} . \tag{96}$$

We then obtain

$$\begin{aligned}
\langle g(\mathbf{x}, \mathbf{p}) \rangle_{S_{L-1}(\sqrt{\xi})} &= \int_{\mathcal{S}_\gamma(\mathbf{x}, \mathbf{p})} d\mathbf{X} g(\mathbf{x}, \mathbf{p}) \\
&= \int F d\mathbf{x} d\mathbf{p} \frac{1}{\Omega(\gamma)} \delta \left(\sum_{n=1}^F \frac{(x^{(n)})^2 + (p^{(n)})^2}{2} - (1 + F\gamma) \right) g(\mathbf{x}, \mathbf{p}) ,
\end{aligned} \tag{97}$$

where $\mathbf{X} = (\mathbf{x}, \mathbf{p})$. The second order moment and fourth order moment on the constraint space of eq 31 read

$$\begin{aligned}
\int_{\mathcal{S}_\gamma(\mathbf{x}, \mathbf{p})} d\mathbf{X} (X_i X_j) &= \frac{1 + F\gamma}{F} \delta_{ij} \\
\int_{\mathcal{S}_\gamma(\mathbf{x}, \mathbf{p})} d\mathbf{X} (X_i X_j X_k X_l) &= \frac{(1 + F\gamma)^2}{F(F+1)} (\delta_{ij} \delta_{kl} + \delta_{ik} \delta_{jl} + \delta_{il} \delta_{jk}) .
\end{aligned} \tag{98}$$

Consider $\hat{A} = |m\rangle\langle n|$ and $\hat{B} = |k\rangle\langle l|$. We have

$$\text{Tr}[\hat{A}\hat{B}] = \delta_{nk} \delta_{ml} . \tag{99}$$

The constraint phase space expression (i.e., eqs 3-5 when only discrete electronic DOFs exist) of the left-hand side (LHS) of eq (99) is equivalent to

$$\begin{aligned}
\text{Tr}[\hat{A}\hat{B}] &= F \int_{\mathcal{S}_\gamma(\mathbf{x}, \mathbf{p})} d\mathbf{X} \langle n | \hat{K}_{\text{ele}}(\mathbf{x}, \mathbf{p}) | m \rangle \langle l | K_{\text{ele}}^{-1}(\mathbf{x}, \mathbf{p}) | k \rangle \\
&= F \int_{\mathcal{S}_\gamma(\mathbf{x}, \mathbf{p})} d\mathbf{X} K_{nm}^{(\text{ele})}(\mathbf{x}, \mathbf{p}) K_{(\text{ele}), lk}^{-1}(\mathbf{x}, \mathbf{p})
\end{aligned} \tag{100}$$

In eq (100), $K_{nm}^{(\text{ele})}(\mathbf{x}, \mathbf{p})$ is the element of operator $\hat{K}_{\text{ele}}(\mathbf{x}, \mathbf{p})$, and $K_{(\text{ele}), lk}^{-1}(\mathbf{x}, \mathbf{p})$ is the element of operator $K_{\text{ele}}^{-1}(\mathbf{x}, \mathbf{p})$. When the mapping kernel is given by eq 29, it is straightforward to derive that its corresponding inverse kernel is eq 30 by employing eqs (98)-(100). Specifically, when the mapping kernel is identical to its inverse (i.e., eq 38), the element of the (inverse) kernel operator is

$$K_{nm}(\mathbf{x}, \mathbf{p}) = K_{nm}^{-1}(\mathbf{x}, \mathbf{p}) = \frac{1}{2} \left(x^{(n)} + ip^{(n)} \right) \left(x^{(m)} - ip^{(m)} \right) - \gamma \delta_{nm} \tag{101}$$

It is trivial to use eq (98) and eq (101) to achieve the equality

$$F \int_{\mathcal{S}_\gamma(\mathbf{x}, \mathbf{p})} d\mathbf{X} K_{nm}(\mathbf{x}, \mathbf{p}) K_{lk}^{-1}(\mathbf{x}, \mathbf{p}) = \frac{(1+F\gamma)^2}{(F+1)} \delta_{nk} \delta_{ml} + \left[\frac{(1+F\gamma)^2}{(F+1)} - 2\gamma - F\gamma^2 \right] \delta_{lk} \delta_{nm} \tag{102}$$

After employing eqs (99)-(100), we obtain $\gamma = (\sqrt{F+1} - 1) / F$ from eq (102) where the mapping kernel is identical to its inverse (i.e., eq 38).

Similarly, the weighting constraint phase space formulation (eqs 3-5 when only discrete electronic DOFs exist, and eq 37) leads to

$$\begin{aligned}
\text{Tr}_e[\hat{A}\hat{B}] &= \int_{\mathcal{S}(\mathbf{x}, \mathbf{p})} F d\mathbf{x} d\mathbf{p} A_C(\mathbf{x}, \mathbf{p}) \tilde{B}_C(\mathbf{x}, \mathbf{p}) \\
&= \int_{-1/F}^{\infty} d\gamma w(\gamma) \int F d\mathbf{x} d\mathbf{p} \frac{1}{\Omega(\gamma)} \delta \left(\sum_{n=1}^F \frac{(x^{(n)})^2 + (p^{(n)})^2}{2} - (1+F\gamma) \right) A_C(\mathbf{x}, \mathbf{p}) \tilde{B}_C(\mathbf{x}, \mathbf{p}) \\
&= \int_{-1/F}^{\infty} d\gamma w(\gamma) \langle A_C(\mathbf{x}, \mathbf{p}) \tilde{B}_C(\mathbf{x}, \mathbf{p}) \rangle_{\mathcal{S}_{L^{-1}(\sqrt{\xi})}}
\end{aligned} \tag{103}$$

Employing eq (99), we obtain an equation similar to eq (100)

$$F \int d\gamma w(\gamma) \int_{\mathcal{S}_\gamma(\mathbf{x}, \mathbf{p})} d\mathbf{X} K_{nm}(\mathbf{x}, \mathbf{p}) K_{lk}^{-1}(\mathbf{x}, \mathbf{p}) = \delta_{nk} \delta_{ml} \tag{104}$$

Because we request eq 38 that the mapping kernel is identical to its inverse in the weighted constraint phase space formulation, eqs (101)-(102) also hold. Substitution of eq (102) into eq (104) generates

$$\int d\gamma w(\gamma) (F\gamma^2 + 2\gamma) = \int d\gamma w(\gamma) \chi(\gamma) = 1 \quad , \quad (105)$$

which is eq 39 of the main text. When $w(\gamma)$, the quasi-probability distribution function of parameter γ , is a single Dirac delta function, the constraint coordinate-momentum phase space formulation with $\gamma = (\sqrt{F+1}-1)/F$ is a special case of eq (105), or of eq 39 of the main text. When in eq (105) or eq 39 $w(\gamma)$ is represented by a linear combination of two symmetrical delta functions (i.e., eqs 43-45), we achieve the symmetrically weighted constraint phase space formulation employed in wMM of the Focus Article. Apparently, various other choices for quasi-probability distribution function $w(\gamma)$ are also available and can be investigated in the future.

Appendix 2. More discussion on the equations of motion in the adiabatic representation

Below we will show that eq 74 and eq 76, the equations of motion (EOMs) under the diabatic-to-adiabatic transformation are intrinsically equivalent to Hamilton's EOMs generated by the Hamiltonian, eq 79, when (nuclear) canonical phase variables $(\tilde{\mathbf{R}}, \tilde{\mathbf{P}})$ are defined by eq 78. For simplicity, assume that all nonadiabatic coupling terms $\{\mathbf{d}_{mn}^{(l)}(\mathbf{R})\}$ are real. It leads to a simplified relation

$$\tilde{\mathbf{P}} = \mathbf{P} + \hbar \sum_{n,m=1}^F \tilde{x}^{(n)} \tilde{p}^{(m)} \mathbf{d}_{mn}(\mathbf{R}) \quad (106)$$

in eq 78. In the adiabatic representation, $\mathbf{P} = \tilde{\mathbf{P}} - \hbar \sum_{n,m=1}^F \tilde{x}^{(n)} \tilde{p}^{(m)} \mathbf{d}_{mn}(\tilde{\mathbf{R}})$ is denoted the kinematic momentum (e.g., in ref¹⁸⁶), which is different from canonical momentum $\tilde{\mathbf{P}}$. (Yet, $\mathbf{R} = \tilde{\mathbf{R}}$.) The Hamiltonian, eq 79, is recast into

$$H_C(\tilde{\mathbf{R}}, \tilde{\mathbf{P}}, \tilde{\mathbf{x}}, \tilde{\mathbf{p}}) = \sum_{l=1}^N \frac{\left(\tilde{P}_l - \hbar \sum_{n,m=1}^F \tilde{x}^{(n)} \tilde{p}^{(m)} d_{mn}^{(l)}(\tilde{\mathbf{R}}) \right)^2}{2M_l} + \sum_{k=1}^F E_k(\tilde{\mathbf{R}}) \left(\frac{1}{2} \left((\tilde{x}^{(k)})^2 + (\tilde{p}^{(k)})^2 \right) - \gamma \right) \quad . (107)$$

Here, $d_{mn}^{(l)}(\tilde{\mathbf{R}})$ and \tilde{P}_l are the the l -th DOF component of $\mathbf{d}_{mn}(\tilde{\mathbf{R}})$ and that of $\tilde{\mathbf{P}}$, respectively. Note that canonical variables $(\tilde{\mathbf{R}}, \tilde{\mathbf{P}}, \tilde{\mathbf{x}}, \tilde{\mathbf{p}})$ are independent of one another. Hamilton's EOMs produced by eq (107) are

$$\begin{aligned}\dot{\tilde{x}}^{(m)} &= \frac{1}{\hbar} \frac{\partial}{\partial \tilde{p}^{(m)}} H_C(\tilde{\mathbf{R}}, \tilde{\mathbf{P}}, \tilde{\mathbf{x}}, \tilde{\mathbf{p}}) \\ &= - \sum_{J=1}^N \sum_{n=1}^F \frac{\tilde{P}_J - \hbar \sum_{k,l=1}^F \tilde{x}^{(k)} \tilde{p}^{(l)} d_{lk}^{(J)}(\tilde{\mathbf{R}})}{M_J} \tilde{x}^{(n)} d_{mn}^{(J)}(\tilde{\mathbf{R}}) + \frac{1}{\hbar} E_m(\tilde{\mathbf{R}}) \tilde{p}^{(m)}\end{aligned}\quad , \quad (108)$$

$$\begin{aligned}\dot{\tilde{p}}^{(m)} &= - \frac{1}{\hbar} \frac{\partial}{\partial \tilde{x}^{(m)}} H_C(\tilde{\mathbf{R}}, \tilde{\mathbf{P}}, \tilde{\mathbf{x}}, \tilde{\mathbf{p}}) \\ &= \sum_{J=1}^N \sum_{n=1}^F \frac{\tilde{P}_J - \hbar \sum_{k,l=1}^F \tilde{x}^{(k)} \tilde{p}^{(l)} d_{lk}^{(J)}(\tilde{\mathbf{R}})}{M_J} \tilde{p}^{(n)} d_{nm}^{(J)}(\tilde{\mathbf{R}}) - \frac{1}{\hbar} E_m(\tilde{\mathbf{R}}) \tilde{x}^{(m)}\end{aligned}\quad , \quad (109)$$

$$\dot{\tilde{R}}_l = \frac{\partial}{\partial \tilde{P}_l} H_C(\tilde{\mathbf{R}}, \tilde{\mathbf{P}}, \tilde{\mathbf{x}}, \tilde{\mathbf{p}}) = \frac{\tilde{P}_l - \hbar \sum_{n,m=1}^F \tilde{x}^{(n)} \tilde{p}^{(m)} d_{mn}^{(l)}(\tilde{\mathbf{R}})}{M_l}\quad , \quad (110)$$

$$\begin{aligned}\dot{\tilde{P}}_l &= - \frac{\partial}{\partial \tilde{R}_l} H_C(\tilde{\mathbf{R}}, \tilde{\mathbf{P}}, \tilde{\mathbf{x}}, \tilde{\mathbf{p}}) \\ &= \hbar \sum_{J=1}^N \sum_{n,m=1}^F \frac{\tilde{P}_J - \hbar \sum_{k,l=1}^F \tilde{x}^{(k)} \tilde{p}^{(l)} d_{lk}^{(J)}(\tilde{\mathbf{R}})}{M_J} \tilde{x}^{(n)} \tilde{p}^{(m)} \frac{\partial d_{mn}^{(J)}(\tilde{\mathbf{R}})}{\partial \tilde{R}_l} \\ &\quad - \sum_{k=1}^F \frac{\partial E_k(\tilde{\mathbf{R}})}{\partial \tilde{R}_l} \left(\frac{1}{2} \left((\tilde{x}^{(k)})^2 + (\tilde{p}^{(k)})^2 \right) - \gamma \right)\end{aligned}\quad . \quad (111)$$

It is evident that eqs (108)-(109) are identical to eq 70 and that eq (110) is the same as the first equation of eq 76. We will then prove that eq (111) is equivalent to the second equation of eq 76.

Consider the full time-derivative of canonical momentum \tilde{P}_l ,

$$\begin{aligned}
\dot{\tilde{P}}_I &= \dot{P}_I(\tilde{\mathbf{R}}, \tilde{\mathbf{P}}, \tilde{\mathbf{x}}, \tilde{\mathbf{p}}) + \hbar \frac{d}{dt} \sum_{n,m=1}^F \tilde{x}^{(m)} \tilde{p}^{(n)} d_{nm}^{(I)}(\tilde{\mathbf{R}}) \\
&= \dot{P}_I + \hbar \sum_{n,m=1}^F \dot{\tilde{x}}^{(m)} \tilde{p}^{(n)} d_{nm}^{(I)}(\tilde{\mathbf{R}}) + \hbar \sum_{n,m=1}^F \tilde{x}^{(m)} \dot{\tilde{p}}^{(n)} d_{nm}^{(I)}(\tilde{\mathbf{R}}) + \hbar \sum_{n,m=1}^F \tilde{x}^{(m)} \tilde{p}^{(n)} \sum_{J=1}^N \frac{\partial d_{nm}^{(I)}(\tilde{\mathbf{R}})}{\partial \tilde{R}_J} \dot{\tilde{R}}_J
\end{aligned} \tag{112}$$

Substitution of eqs (108)-(111) into eq (112) yields,

$$\begin{aligned}
\dot{P}_I(\tilde{\mathbf{R}}, \tilde{\mathbf{P}}, \tilde{\mathbf{x}}, \tilde{\mathbf{p}}) &= \hbar \sum_{J=1}^N \sum_{n,m=1}^F \frac{P_J(\tilde{\mathbf{R}}, \tilde{\mathbf{P}}, \tilde{\mathbf{x}}, \tilde{\mathbf{p}})}{M_J} \tilde{x}^{(n)} \tilde{p}^{(m)} \left(\frac{\partial d_{nm}^{(J)}(\tilde{\mathbf{R}})}{\partial \tilde{R}_I} - \frac{\partial d_{nm}^{(I)}(\tilde{\mathbf{R}})}{\partial \tilde{R}_J} \right) \\
&\quad - \sum_{k=1}^F \frac{\partial E_k(\tilde{\mathbf{R}})}{\partial \tilde{R}_I} \left(\frac{1}{2} \left((\tilde{x}^{(k)})^2 + (\tilde{p}^{(k)})^2 \right) - \gamma \right) \\
&\quad + \hbar \sum_{n,m=1}^F \sum_{J=1}^N \sum_{k=1}^F \frac{P_J(\tilde{\mathbf{R}}, \tilde{\mathbf{P}}, \tilde{\mathbf{x}}, \tilde{\mathbf{p}})}{M_J} d_{nk}^{(I)}(\tilde{\mathbf{R}}) d_{km}^{(J)}(\tilde{\mathbf{R}}) (\tilde{x}^{(m)} \tilde{p}^{(n)} - \tilde{x}^{(n)} \tilde{p}^{(m)}) \\
&\quad + \sum_{n,m=1}^F \left(E_n(\tilde{\mathbf{R}}) \tilde{x}^{(n)} \tilde{x}^{(m)} - E_m(\tilde{\mathbf{R}}) \tilde{p}^{(m)} \tilde{p}^{(n)} \right) d_{nm}^{(I)}(\tilde{\mathbf{R}})
\end{aligned} \tag{113}$$

Although $\frac{\partial d_{mn}^{(J)}(\tilde{\mathbf{R}})}{\partial \tilde{R}_I} - \frac{\partial d_{mn}^{(I)}(\tilde{\mathbf{R}})}{\partial \tilde{R}_J} = 0$ holds for $I \neq J$ for two-electronic-state systems as long as the time-

reversal symmetry is satisfied, such an equality is, however, often not valid for $I \neq J$ for general nonadiabatic systems. Note that we have assumed that $\{\mathbf{d}_{mn}^{(I)}(\mathbf{R})\}$ are real, which leads to $\mathbf{d}_{mn}^{(I)}(\mathbf{R}) = -\mathbf{d}_{nm}^{(I)}(\mathbf{R})$. The

third term of the right-hand side (RHS) of eq (113) becomes

$$\begin{aligned}
&\hbar \sum_{n,m=1}^F \sum_{J=1}^N \sum_{k=1}^F \frac{P_J(\tilde{\mathbf{R}}, \tilde{\mathbf{P}}, \tilde{\mathbf{x}}, \tilde{\mathbf{p}})}{M_J} d_{nk}^{(I)}(\tilde{\mathbf{R}}) d_{km}^{(J)}(\tilde{\mathbf{R}}) (\tilde{x}^{(m)} \tilde{p}^{(n)} - \tilde{x}^{(n)} \tilde{p}^{(m)}) \\
&= -\hbar \sum_{n,m=1}^F \sum_{J=1}^N \sum_{k=1}^F \frac{P_J(\tilde{\mathbf{R}}, \tilde{\mathbf{P}}, \tilde{\mathbf{x}}, \tilde{\mathbf{p}})}{M_J} \left(d_{nk}^{(I)}(\tilde{\mathbf{R}}) d_{km}^{(J)}(\tilde{\mathbf{R}}) - d_{mk}^{(I)}(\tilde{\mathbf{R}}) d_{kn}^{(J)}(\tilde{\mathbf{R}}) \right) \tilde{x}^{(n)} \tilde{p}^{(m)} \\
&= -\hbar \sum_{n,m=1}^F \sum_{J=1}^N \sum_{k=1}^F \frac{P_J(\tilde{\mathbf{R}}, \tilde{\mathbf{P}}, \tilde{\mathbf{x}}, \tilde{\mathbf{p}})}{M_J} \left(d_{nk}^{(I)}(\tilde{\mathbf{R}}) d_{km}^{(J)}(\tilde{\mathbf{R}}) - d_{nk}^{(J)}(\tilde{\mathbf{R}}) d_{km}^{(I)}(\tilde{\mathbf{R}}) \right) \tilde{x}^{(n)} \tilde{p}^{(m)}
\end{aligned} \tag{114}$$

Substitution of eq (114) into eq (113) produces

$$\begin{aligned}
\dot{P}_I(\tilde{\mathbf{R}}, \tilde{\mathbf{P}}, \tilde{\mathbf{x}}, \tilde{\mathbf{p}}) = & \hbar \sum_{J=1}^N \sum_{n,m=1}^F \frac{P_J(\tilde{\mathbf{R}}, \tilde{\mathbf{P}}, \tilde{\mathbf{x}}, \tilde{\mathbf{p}})}{M_J} \tilde{x}^{(n)} \tilde{p}^{(m)} \left(\frac{\partial d_{mn}^{(J)}(\tilde{\mathbf{R}})}{\partial \tilde{R}_I} - \frac{\partial d_{mn}^{(I)}(\tilde{\mathbf{R}})}{\partial \tilde{R}_J} \right. \\
& \left. - \sum_{k=1}^F \left(d_{nk}^{(I)}(\tilde{\mathbf{R}}) d_{km}^{(J)}(\tilde{\mathbf{R}}) - d_{nk}^{(J)}(\tilde{\mathbf{R}}) d_{km}^{(I)}(\tilde{\mathbf{R}}) \right) \right) \\
& - \sum_{k=1}^F \frac{\partial E_k(\tilde{\mathbf{R}})}{\partial \tilde{R}_I} \left(\frac{1}{2} \left((\tilde{x}^{(k)})^2 + (\tilde{p}^{(k)})^2 \right) - \gamma \right) \\
& + \sum_{n,m=1}^F \left(E_n(\tilde{\mathbf{R}}) \tilde{x}^{(n)} \tilde{x}^{(m)} - E_m(\tilde{\mathbf{R}}) \tilde{p}^{(m)} \tilde{p}^{(n)} \right) d_{nm}^{(I)}(\tilde{\mathbf{R}})
\end{aligned} \tag{115}$$

The first term of the RHS of eq (115) indicates a relation to the non-abelian gauge theory, as we will demonstrate below.

The derivative of the first-order nonadiabatic coupling is

$$\begin{aligned}
\frac{\partial d_{mn}^{(J)}}{\partial \tilde{R}_I} = & \frac{\partial}{\partial \tilde{R}_I} \left\langle \phi_m \left| \frac{\partial}{\partial \tilde{R}_J} \phi_n \right. \right\rangle = \left\langle \frac{\partial}{\partial \tilde{R}_I} \phi_m \left| \frac{\partial}{\partial \tilde{R}_J} \phi_n \right. \right\rangle + \left\langle \phi_m \left| \frac{\partial^2}{\partial \tilde{R}_I \partial \tilde{R}_J} \phi_n \right. \right\rangle, \\
= & \sum_{k=1}^F d_{kn}^{(I)} d_{km}^{(J)} + D_{mn}^{(IJ)}
\end{aligned} \tag{116}$$

where $D_{mn}^{(IJ)} = \left\langle \phi_m \left| \frac{\partial^2}{\partial \tilde{R}_I \partial \tilde{R}_J} \phi_n \right. \right\rangle$ is a symmetric tensor of nuclear index, i.e., $D_{mn}^{(IJ)} = D_{nm}^{(JI)}$. It is then

straightforward to show

$$\frac{\partial d_{mn}^{(J)}}{\partial \tilde{R}_I} - \frac{\partial d_{mn}^{(I)}}{\partial \tilde{R}_J} = - \sum_{k=1}^F \left(d_{mk}^{(I)} d_{kn}^{(J)} - d_{mk}^{(J)} d_{kn}^{(I)} \right) \tag{117}$$

which leads to the matrix form

$$\frac{\partial \mathbf{d}^{(J)}}{\partial \tilde{R}_I} - \frac{\partial \mathbf{d}^{(I)}}{\partial \tilde{R}_J} + [\mathbf{d}^{(I)}, \mathbf{d}^{(J)}]_{\text{ele}} = \mathbf{0} \tag{118}$$

The LHS of eq (118) is an analogue to the gauge field tensor, a fundamental concept of non-abelian gauge field theory³⁰⁷. Consider vector $-\mathbf{id}(\tilde{\mathbf{R}})$, of which the J -th component, $-\mathbf{id}^{(J)}(\tilde{\mathbf{R}})$, is a Hermitian matrix of the electronic state DOFs (i.e., an $F \times F$ matrix). Vector $-\mathbf{id}(\tilde{\mathbf{R}})$ is the non-abelian gauge potential³⁰⁸, which

is a generalization of the vector potential of the electromagnetic field. That is, each spacial component of the (magnetic) vector potential is generalized by a matrix of the inner DOFs (here the inner DOFs are those of the electronic states) for each nuclear DOF. Different from scalars, matrices often do not commute with each other, which is the origin of the ‘non-abelian’ characteristic. When there exists the diabatic representation of the system, the gauge field tensor,

$$\frac{\partial(-i\mathbf{d}^{(J)})}{\partial\tilde{\mathbf{R}}_I} - \frac{\partial(-i\mathbf{d}^{(I)})}{\partial\tilde{\mathbf{R}}_J} + i[-i\mathbf{d}^{(I)}, -i\mathbf{d}^{(J)}]_{\text{ele}} \quad , \quad (119)$$

is always zero when it is not in the region of conical intersections where some elements of $\{\partial\mathbf{d}^{(J)}/\partial\tilde{\mathbf{R}}_I\}$ are not well-defined. (It is trivial to verify that eq (118) holds even when nonadiabatic coupling terms $\{\mathbf{d}_{mn}^{(I)}(\mathbf{R})\}$ are complex.)

We note that, eq (118) rigorously holds only when infinite electronic levels are considered for the general molecular system (i.e., the electronically diabatic representation is inherently well-defined). The LHS of eq (118) is often effectively zero as long as a finite discrete F -electronic-state description is reasonable for the molecular system.

Substitution of eq (117) into eq (115) yields

$$\begin{aligned} \dot{P}_I(\tilde{\mathbf{R}}, \tilde{\mathbf{P}}, \tilde{\mathbf{x}}, \tilde{\mathbf{p}}) = & -\sum_{k=1}^F \frac{\partial E_k(\tilde{\mathbf{R}})}{\partial \tilde{\mathbf{R}}_I} \left(\frac{1}{2} \left((\tilde{x}^{(k)})^2 + (\tilde{p}^{(k)})^2 \right) - \gamma \right) \\ & - \sum_{n,m=1}^F (E_n(\tilde{\mathbf{R}}) - E_m(\tilde{\mathbf{R}})) d_{mn}^{(I)}(\tilde{\mathbf{R}}) \frac{1}{2} (\tilde{x}^{(n)} \tilde{x}^{(m)} + \tilde{p}^{(n)} \tilde{p}^{(m)}) \end{aligned} \quad , \quad (120)$$

which is equivalent to the second equation of eq 76 of the main text. It indicates that the canonical momentum in the diabatic representation is covariant with *kinematic* momentum \mathbf{P} rather than canonical momentum $\tilde{\mathbf{P}}$ in adiabatic representation unless all nonadiabatic coupling terms vanish. This is consistent with the spirit of the work of Cotton *et. al.* in ref¹⁸⁶. Because the EOMs (eq 70 and eq 76) of the main text are identical to Hamilton’s EOMs generated by eq (107), the mapping Hamiltonian (eq 79 or eq (107)) is conserved during the evolution in the adiabatic representation.

It is straightforward to extend the discussion to the case when nonadiabatic coupling terms $\{\mathbf{d}_{mn}^{(l)}(\mathbf{R})\}$ are complex. The conclusion is similar.

Appendix 3. The relationship between constraint coordinate-momentum phase space and Stratonovich phase space

Stratonovich's original work¹⁰⁰ in 1956 maps a 2-state (spin-1/2) system onto a two-dimensional sphere. We review two kinds of further developments of the Stratonovich-Weyl mapping phase space representations for F -state quantum system: the first one based on the $SU(2)$ structure^{103, 113} and the second one based on the $SU(F)$ structure¹¹⁴. We show the relationship between constrained coordinate-momentum phase space representation that we use in the Focus Article and the two kinds of Stratonovich phase space representations.

In the $SU(2)$ Stratonovich phase space representation, an F -state system is treated as a spin- j system (where $F = 2j + 1$). The basis set consists of $|j, m\rangle$, the eigenstate of the square of total angular momentum \hat{J}^2 and the z -component of angular momentum \hat{J}_z with quantum numbers j and m , respectively. The mapping kernel is

$$\hat{K}_{\text{ele}}^{\text{SU}(2)}(\theta, \varphi, s) = \sqrt{\frac{\pi}{2j+1}} \sum_{l=0}^{2j} (C_{jj,l0}^{jj})^{-s} \sum_{m=-l}^l Y_{lm}^*(\theta, \varphi) \hat{T}_{lm}^j, \quad s \in \mathbb{R} \quad (121)$$

where \hat{T}_{lm}^j is the irreducible tensor operator defined as¹³¹

$$\hat{T}_{lm}^j = \sqrt{\frac{2l+1}{2j+1}} \sum_{m', n=-j}^j C_{jm', lm}^{jm} |j, n\rangle \langle j, m'|. \quad (122)$$

Here $C_{j_1 m_1, j_2 m_2}^{j m}$ is the well-known Clebsch-Gordan coefficient for the angular momentum coupling, and $Y_{lm}(\theta, \varphi)$ is the spherical harmonic function. The inverse kernel of $\hat{K}_{\text{ele}}^{\text{SU}(2)}(\theta, \varphi, s)$ is simply $\hat{K}_{\text{ele}}^{\text{SU}(2)}(\theta, \varphi, -s)$. We note that, although $s = 1, 0$, and -1 are traditionally associated with the Q , Wigner, and P -functions respectively and used in the literature^{111, 128}, parameter s of eq (121) can in principle take any real value.

When $F > 2$, the $SU(2)$ Stratonovich phase space (θ, φ) does *not* have a phase point-to-phase point mapping to constraint coordinate-momentum phase space, although the relation can only be constructed by virtue of the density matrix. Only when $F = 2$ as in the original work of Stratonovich, there exists a phase point-to-phase point mapping to constraint coordinate-momentum phase space. The mapping kernel can be expressed in terms of the spin-coherent state,

$$\hat{K}_{\text{ele}}^{\text{SU}(2)}(\theta, \varphi; s) = 3^{(1+s)/2} |\theta, \varphi\rangle\langle\theta, \varphi| + \frac{\hat{\mathbf{I}}}{2} [1 - 3^{(1+s)/2}] . \quad (123)$$

In eq (123) spin coherent state $|\theta, \varphi\rangle$ is

$$|\theta, \varphi\rangle = \begin{pmatrix} e^{-i\varphi} \sin(\theta/2) \\ \cos(\theta/2) \end{pmatrix} , \quad (124)$$

where (θ, φ) are the spherical coordinate variables on the two-dimensional spherical phase space. The range of θ is $[0, \pi]$ and that for φ is $[0, 2\pi)$. When $F = 2$, the explicit transformation of (θ, φ) to the constrained coordinate-momentum phase space $(x^{(1)}, x^{(2)}, p^{(1)}, p^{(2)})$ is

$$\begin{pmatrix} x^{(1)} \\ p^{(1)} \end{pmatrix} = \sqrt{2(1+2\gamma)} \begin{pmatrix} \cos\psi & -\sin\psi \\ \sin\psi & \cos\psi \end{pmatrix} \begin{pmatrix} \cos\varphi \sin(\theta/2) \\ -\sin\varphi \sin(\theta/2) \end{pmatrix} , \quad (125)$$

$$\begin{pmatrix} x^{(2)} \\ p^{(2)} \end{pmatrix} = \sqrt{2(1+2\gamma)} \begin{pmatrix} \cos\psi & -\sin\psi \\ \sin\psi & \cos\psi \end{pmatrix} \begin{pmatrix} \cos(\theta/2) \\ 0 \end{pmatrix} ,$$

where ψ is an additional global phase.

The second kind of representation is the $SU(F)$ Stratonovich phase space. A kind as described by Tilma *et.al.* in ref ¹¹⁴ is diffeomorphic to the quotient set $SU(F)/U(F-1)$, parameterized by $(2F-2)$ angle variables $(\boldsymbol{\theta}, \boldsymbol{\varphi}) = (\theta_1, \theta_2, \dots, \theta_{F-1}, \varphi_1, \varphi_2, \dots, \varphi_{F-1})$. The range of each angle θ_i is $[0, \pi/2]$ and that for each angle φ_i is $[0, 2\pi)$. The $SU(F)$ Stratonovich phase space of ref ¹¹⁴ has been used to prepare the initial condition for the Meyer-Miller mapping model of non-adiabatic dynamics in ref ¹⁹⁹.

The mapping kernel of the $SU(F)/U(F-1)$ Stratonovich phase space of ref ¹¹⁴ is

$$\hat{K}_{\text{ele}}^{\text{SU}(F)}(\boldsymbol{\theta}, \boldsymbol{\varphi}; s) = (1+F)^{(1+s)/2} |\boldsymbol{\theta}, \boldsymbol{\varphi}\rangle \langle \boldsymbol{\theta}, \boldsymbol{\varphi}| + \frac{\hat{\mathbf{I}}}{F} \left(1 - (1+F)^{(1+s)/2}\right), \quad s \in \mathbb{R} \quad (126)$$

and the inverse kernel is simply $\hat{K}_{\text{ele}}^{\text{SU}(F)}(\boldsymbol{\theta}, \boldsymbol{\varphi}; -s)$. The explicit form of the generalized coherent state $|\boldsymbol{\theta}, \boldsymbol{\varphi}\rangle$

is^{114,242, 243}

$$|\boldsymbol{\theta}, \boldsymbol{\varphi}\rangle = \sum_{n=1}^F c_n |n\rangle, \quad (127)$$

where the coefficients are

$$\begin{pmatrix} c_1 \\ c_2 \\ c_3 \\ \vdots \\ c_{F-3} \\ c_{F-2} \\ c_{F-1} \\ c_F \end{pmatrix} = \begin{pmatrix} e^{i(\varphi_1 + \varphi_2 + \dots + \varphi_{F-1})} \cos(\theta_1) \cos(\theta_2) \dots \cos(\theta_{F-2}) \sin(\theta_{F-1}) \\ -e^{i(-\varphi_1 + \varphi_2 + \dots + \varphi_{F-1})} \sin(\theta_1) \cos(\theta_2) \dots \cos(\theta_{F-2}) \sin(\theta_{F-1}) \\ -e^{i(\varphi_3 + \varphi_4 + \dots + \varphi_{F-1})} \sin(\theta_2) \cos(\theta_3) \dots \cos(\theta_{F-2}) \sin(\theta_{F-1}) \\ \vdots \\ -e^{i(\varphi_{F-3} + \varphi_{F-2} + \varphi_{F-1})} \sin(\theta_{F-4}) \cos(\theta_{F-3}) \cos(\theta_{F-2}) \sin(\theta_{F-1}) \\ -e^{i(\varphi_{F-2} + \varphi_{F-1})} \sin(\theta_{F-3}) \cos(\theta_{F-2}) \sin(\theta_{F-1}) \\ -e^{i(\varphi_{F-1})} \sin(\theta_{F-2}) \sin(\theta_{F-1}) \\ \cos(\theta_{F-1}) \end{pmatrix}. \quad (128)$$

As derived first in Appendix A of ref¹³⁴ in the spirit of ref¹³³ and then in the Supporting Information of ref¹³⁶, the mapping kernel of constraint coordinate-momentum phase space for a set of F states (eq 29 of the main text) is denoted as,

$$\hat{K}_{\text{ele}}(\mathbf{x}, \mathbf{p}; \gamma) = \sum_{m,n=1}^F \left[\frac{(x^{(m)} - ip^{(m)})(x^{(n)} + ip^{(n)})}{2} - \gamma \delta_{mn} \right] |n\rangle \langle m| = |\mathbf{x}, \mathbf{p}\rangle \langle \mathbf{x}, \mathbf{p}| - \gamma \hat{\mathbf{I}}, \quad (129)$$

where the non-normalized state $|\mathbf{x}, \mathbf{p}\rangle$ is

$$\sum_{n=1}^F \frac{x^{(n)} + ip^{(n)}}{\sqrt{2}} |n\rangle. \quad (130)$$

The expression of eq (130) for the amplitudes of being in different states was already used in Appendix B of ref¹³³, while the action-angle version of eq (130) was earlier presented in Meyer and Miller's seminal paper¹⁵⁵. The

$U(F)$ constraint coordinate-momentum phase space is diffeomorphic to $U(F)/U(F-1)$, which is

equivalent to $SU(F)/SU(F-1)$ ³⁰⁹ because both of them lead to the $(2F-1)$ -dimensional sphere in $2F$ dimensional Euclidean space^{310, 311}. Comparison of $\hat{K}_{\text{ele}}^{\text{SU}(F)}(\boldsymbol{\theta}, \boldsymbol{\varphi}; s)$ to $\hat{K}_{\text{ele}}(\mathbf{x}, \mathbf{p}; \gamma)$ implies that the two kernels are closely related. The correspondence between parameters s and γ reads

$$1 + F\gamma = (1 + F)^{(1+s)/2} . \quad (131)$$

It is evident (from eq (131), the relation between constraint coordinate-momentum phase space and the $SU(F)/U(F-1)$ Stratonovich phase space) that parameter s can be any real number in eq (126), *not* limited to $s=1, 0$, or -1 of refs^{114, 115, 117, 199}, where the corresponding value of parameter γ of constraint coordinate-momentum phase space^{133, 134, 136} is $\gamma=1, (\sqrt{1+F}-1)/F$, or 0 . This has been clearly mentioned in refs^{57, 58, 136}.

Any normalized pure state of the F -dimensional Hilbert space uniquely corresponds to a state on constraint coordinate-momentum phase space, $|\mathbf{x}, \mathbf{p}\rangle$, which is equivalent to $\exp[i\psi]|\boldsymbol{\theta}, \boldsymbol{\varphi}\rangle$ with ψ as the global phase. That is, the correspondence between $(\boldsymbol{\theta}, \boldsymbol{\varphi})$ and (\mathbf{x}, \mathbf{p}) is

$$\begin{pmatrix} x^{(n)} \\ p^{(n)} \end{pmatrix} = \sqrt{2(1+F\gamma)} \begin{pmatrix} \cos\psi & -\sin\psi \\ \sin\psi & \cos\psi \end{pmatrix} \begin{pmatrix} \text{Re}\langle n | \boldsymbol{\theta}, \boldsymbol{\varphi} \rangle \\ \text{Im}\langle n | \boldsymbol{\theta}, \boldsymbol{\varphi} \rangle \end{pmatrix} . \quad (132)$$

Under the transformation, eq (132), mapping functions $A_c(\boldsymbol{\theta}, \boldsymbol{\varphi}; s) = \text{Tr} \left[\hat{A} \hat{K}_{\text{ele}}^{\text{SU}(F)}(\boldsymbol{\theta}, \boldsymbol{\varphi}; s) \right]$ and $A_c(\mathbf{x}, \mathbf{p}; \gamma) = \text{Tr} \left[\hat{A} \hat{K}_{\text{ele}}(\mathbf{x}, \mathbf{p}; \gamma) \right]$ of an operator \hat{A} share the same value. The global phase, ψ , which is missing in the $SU(F)/U(F-1)$ Stratonovich phase space¹¹⁴, however, is important for the expression of quantum dynamics as linear equations of motion.

When we consider quantum dynamics in a finite F -dimensional Hilbert space, if the Hamiltonian operator includes linear components beyond the identity operator and generator operators of phase space group, it is impossible to derive trajectory-based exact dynamics. The $SU(2)$ group involves the identity operator and angular momentum operators as generators on \mathbb{S}^2 sphere. It produces trajectory-based exact dynamics only for two-state systems, but fails to do so for all $F > 2$ cases. It is claimed that trajectory-based dynamics is a

good approximation for the large spin limit ($F \rightarrow \infty$) though^{109, 111, 132}. Except for the $F = 2$ case, the expression of quantum dynamics on the $SU(2)$ Stratonovich phase space has no direct relation to the trajectory-based exact dynamics on constrained coordinate-momentum phase space.

The $SU(F)$ Stratonovich phase space, however, produces trajectory-based exact dynamics for the finite F -dimensional Hilbert space. This is because that the evolution generated by any Hamiltonian of the F -dimensional Hilbert space is the action of some group elements of $SU(F)$.³⁰⁴ The inherent symplectic structure of $SU(F)/U(F-1)$ Stratonovich phase space³¹² indicates that the trajectory-based exact dynamics can be produced by the corresponding mapping Hamiltonian function $H_C = \text{Tr}[\hat{H}\hat{K}_{\text{ele}}^{SU(F)}(\boldsymbol{\theta}, \boldsymbol{\varphi}; s)]$, i.e.,

$$\begin{cases} \dot{\theta}_i = -\sum_{j=1}^{F-1} \frac{A_{ji}}{(1+F)^{(1+s)/2}} \frac{\partial H_C}{\partial \varphi_j} \\ \dot{\varphi}_i = +\sum_{j=1}^{F-1} \frac{A_{ij}}{(1+F)^{(1+s)/2}} \frac{\partial H_C}{\partial \theta_j} \end{cases} \quad (133)$$

The elements, $\{A_{ij}\}$, of the $(F-1) \times (F-1)$ matrix, \mathbf{A} , are

$$A_{ij} = \begin{cases} \frac{1}{2} \csc(2\theta_1) \csc^2 \theta_{F-1} \prod_{k=2}^{F-2} \sec^2 \theta_k, & i = j = 1; \\ -\frac{1}{2} \cot(2\theta_1) \csc^2 \theta_{F-1} \prod_{k=2}^{F-2} \sec^2 \theta_k, & (i-1) = j = 1; \\ \csc(2\theta_i) \csc^2 \theta_{F-1} \prod_{k=i+1}^{F-2} \sec^2 \theta_k, & 2 \leq i = j \leq F-2; \\ -\frac{1}{2} \cot(\theta_i) \csc^2 \theta_{F-1} \prod_{k=i+1}^{F-2} \sec^2 \theta_k, & 2 \leq (i-1) = j \leq F-2; \\ -\csc(2\theta_{F-1}), & i = j = (F-1). \end{cases} \quad (134)$$

The explicit expression of the EOMs of eq (133) is, however, much complicated. In addition, because trigonometric functions are involved in eq (134), singularities are inevitable in the EOMs on the $SU(F)/U(F-1)$ Stratonovich phase space for $F > 2$. This makes the expression of quantum dynamics on the $SU(F)/U(F-1)$ Stratonovich phase space numerically unfavorable. In comparison, on (weighted)

constrained coordinate-momentum phase space, Hamilton's EOMs are simply linear in derivatives with coefficients independent of phase variables, as well as exact.

The relation of eq (132) implies the subtle difference between exact trajectory-base dynamics on the $SU(F)/U(F-1)$ Stratonovich phase space and that on constraint coordinate-momentum phase space. The addition of the global phase, ψ , is critical to obtain a one-to-one correspondence between the two approaches. The EOM of ψ reads

$$\dot{\psi} = \left[-\frac{\partial}{\partial \lambda} + \frac{\tan \theta_{F-1}}{2\lambda} \frac{\partial}{\partial \theta_{F-1}} \right] H_C^{(\lambda)}(\boldsymbol{\theta}, \boldsymbol{\varphi}; s) \Big|_{\lambda=(1+F)^{\frac{1+s}{2}}}, \quad (135)$$

where the extended mapping Hamiltonian function is defined by

$$H_C^{(\lambda)}(\boldsymbol{\theta}, \boldsymbol{\varphi}; s) = \text{Tr} \left[\hat{K}_{\text{ele}}^{\text{SU}(F),(\lambda)}(\boldsymbol{\theta}, \boldsymbol{\varphi}; s) \hat{H} \right] \quad (136)$$

for the extended $SU(F)/U(F-1)$ Stratonovich mapping 'kernel'

$$\hat{K}_{\text{ele}}^{\text{SU}(F),(\lambda)}(\boldsymbol{\theta}, \boldsymbol{\varphi}; s) = \lambda |\boldsymbol{\theta}, \boldsymbol{\varphi}\rangle \langle \boldsymbol{\theta}, \boldsymbol{\varphi}| + \frac{\hat{I}}{F} \left(1 - (1+F)^{\frac{1+s}{2}} \right). \quad (137)$$

In eq (137) λ is treated as an 'invariant' variable. The evolution of state $\sqrt{\lambda} e^{i\psi} |\boldsymbol{\theta}, \boldsymbol{\varphi}\rangle \equiv |\mathbf{x}, \mathbf{p}\rangle$ generates

$$\left\{ \begin{array}{l} \dot{\lambda} = \frac{\partial}{\partial \psi} H_C^{(\lambda)}(\boldsymbol{\theta}, \boldsymbol{\varphi}; s) = 0 \\ \dot{\psi} = \left[-\frac{\partial}{\partial \lambda} + \frac{\tan \theta_{F-1}}{2\lambda} \frac{\partial}{\partial \theta_{F-1}} \right] H_C^{(\lambda)}(\boldsymbol{\theta}, \boldsymbol{\varphi}; s) \\ \dot{\theta}_i = -\sum_{j=1}^{F-1} \frac{A_{ji}}{\lambda} \frac{\partial}{\partial \varphi_j} H_C^{(\lambda)}(\boldsymbol{\theta}, \boldsymbol{\varphi}; s) - \delta_{i,F-1} \frac{\tan \theta_{F-1}}{2\lambda} \frac{\partial}{\partial \psi} H_C^{(\lambda)}(\boldsymbol{\theta}, \boldsymbol{\varphi}; s) \\ \dot{\varphi}_i = +\sum_{j=1}^{F-1} \frac{A_{ij}}{\lambda} \frac{\partial}{\partial \theta_j} H_C^{(\lambda)}(\boldsymbol{\theta}, \boldsymbol{\varphi}; s) \end{array} \right. \quad (138)$$

It is straightforward to show that under the bijection,

$$\begin{pmatrix} x^{(n)} \\ p^{(n)} \end{pmatrix} = \sqrt{2\lambda} \begin{pmatrix} \cos \psi & -\sin \psi \\ \sin \psi & \cos \psi \end{pmatrix} \begin{pmatrix} \text{Re} \langle n | \boldsymbol{\theta}, \boldsymbol{\varphi} \rangle \\ \text{Im} \langle n | \boldsymbol{\theta}, \boldsymbol{\varphi} \rangle \end{pmatrix}, \quad (139)$$

between variables $(\lambda, \psi, \boldsymbol{\theta}, \boldsymbol{\varphi})$ and (\mathbf{x}, \mathbf{p}) , eq (138) leads to the EOMs of phase variables of (weighted) constraint phase space

$$\begin{aligned}\dot{x}^{(n)} &= + \frac{\partial H_C}{\partial p^{(n)}} \\ \dot{p}^{(n)} &= - \frac{\partial H_C}{\partial x^{(n)}}\end{aligned}\tag{140}$$

by the chain rules, i.e.,

$$\begin{aligned}\dot{x}^{(n)} &= \sum_{i=1}^{2F} \frac{\partial x^{(n)}}{\partial z_i} \dot{z}_i \\ \dot{p}^{(n)} &= \sum_{i=1}^{2F} \frac{\partial p^{(n)}}{\partial z_i} \dot{z}_i\end{aligned}\tag{141}$$

and

$$\frac{\partial H_C}{\partial z_i} = \sum_{n=1}^F \frac{\partial x^{(n)}}{\partial z_i} \frac{\partial H_C}{\partial x^{(n)}} + \sum_{n=1}^F \frac{\partial p^{(n)}}{\partial z_i} \frac{\partial H_C}{\partial p^{(n)}} ,\tag{142}$$

where $\{z_i\}$ denote variables $\{\lambda, \psi, \boldsymbol{\theta}, \boldsymbol{\varphi}\}$.

The relation has already been clearly pointed out in refs ^{57, 58}. In this Appendix, we demonstrate the subtle difference between the nonlinear EOMs of the mapping Hamiltonian on the $SU(F)/U(F-1)$ Stratonovich phase space and the linear EOMs of the mapping Hamiltonian on the $U(F)/U(F-1)$ constraint coordinate-momentum phase space. Without the definition of the ‘invariant’ variable, λ , in the ‘extended’ $SU(F)/U(F-1)$ Stratonovich mapping kernel and the EOM of the global phase, ψ , (i.e., eq (135) and eq (137)), it is *impossible* to rigorously derive the trajectory-based dynamics generated by the Meyer-Miller mapping Hamiltonian. In comparison, the EOMs of Meyer-Miller mapping Hamiltonian (with $2F$ variables) is naturally derived in constraint coordinate-momentum phase space of refs ^{57, 58, 133, 134, 136} for the discrete F -state system.

Lang *et al.* have recently directly employed $F^2 - 1$ variables of $SU(F)$ in the EOMs of the discrete F -state systems⁶⁰. It is straightforward to show that such an approach can be included in our comprehensive phase space mapping theory with the commutator matrix^{57, 58}, where it is easy to obtain the manifold structure.

Appendix 4. Marginal distribution functions on symmetrically weighted coordinate-momentum phase space

As demonstrated in Figure 5, the marginal distribution functions of a spin-1/2 system on symmetrically weighted constraint coordinate-momentum phase space demonstrate a hollow structure. Equation 50 leads to the marginal functions on symmetrically weighted coordinate-momentum phase space

$$\begin{aligned}
\mathcal{K}_{\uparrow\uparrow}(x^{(1)}, x^{(2)}) &= \frac{1-2\Delta^2+2\Delta}{4\Delta} \frac{1+(x^{(1)})^2/2-(x^{(2)})^2/2}{2\pi(1+2\Delta)} \Big|_{(x^{(1)})^2+(x^{(2)})^2 \leq 2(1+2\Delta)} \\
&\quad - \frac{1-2\Delta^2-2\Delta}{4\Delta} \frac{1+(x^{(1)})^2/2-(x^{(2)})^2/2}{2\pi(1-2\Delta)} \Big|_{(x^{(1)})^2+(x^{(2)})^2 \leq 2(1-2\Delta)} \\
\mathcal{K}_{\uparrow\downarrow}(x^{(1)}, x^{(2)}) &= \mathcal{K}_{\downarrow\uparrow}(x^{(1)}, x^{(2)}) = \frac{1-2\Delta^2+2\Delta}{4\Delta} \frac{x^{(1)}x^{(2)}}{2\pi(1+2\Delta)} \Big|_{(x^{(1)})^2+(x^{(2)})^2 \leq 2(1+2\Delta)} \\
&\quad - \frac{1-2\Delta^2-2\Delta}{4\Delta} \frac{x^{(1)}x^{(2)}}{2\pi(1-2\Delta)} \Big|_{(x^{(1)})^2+(x^{(2)})^2 \leq 2(1-2\Delta)} . \quad (143) \\
\mathcal{K}_{\downarrow\downarrow}(x^{(1)}, x^{(2)}) &= \frac{1-2\Delta^2+2\Delta}{4\Delta} \frac{1-(x^{(1)})^2/2+(x^{(2)})^2/2}{2\pi(1+2\Delta)} \Big|_{(x^{(1)})^2+(x^{(2)})^2 \leq 2(1+2\Delta)} \\
&\quad - \frac{1-2\Delta^2-2\Delta}{4\Delta} \frac{1-(x^{(1)})^2/2+(x^{(2)})^2/2}{2\pi(1-2\Delta)} \Big|_{(x^{(1)})^2+(x^{(2)})^2 \leq 2(1-2\Delta)}
\end{aligned}$$

As $\Delta \rightarrow 0^+$, $\mathcal{K}_{nm}(x^{(1)}, x^{(2)})$ approaches zero in region $(x^{(1)})^2 + (x^{(2)})^2 \leq 2(1-2\Delta)$, yielding the hollow structure. We note that the hollow structure appears only for $F = 2$ but not for $F \geq 3$.

Appendix 5. The Wigner-Moyal equation of composite systems and its semiclassical limit

The quantum Liouville theorem or the von Neumann equation reads

$$\frac{\partial}{\partial t} \hat{\rho} = -\frac{1}{i\hbar} [\hat{\rho}, \hat{H}] . \quad (144)$$

Its expression on quantum phase space leads to the (general) Wigner-Moyal equation,

$$\frac{\partial}{\partial t} \rho(\mathbf{X}) = -\{\{\rho(\mathbf{X}), H(\mathbf{X})\}\} = -\frac{1}{i\hbar} (\rho(\mathbf{X}) \star H(\mathbf{X}) - H(\mathbf{X}) \star \rho(\mathbf{X})). \quad (145)$$

Here \star represents the general Moyal product⁹⁴ operation on phase space functions, and $\{\{A, B\}\} = \frac{1}{i\hbar} (A \star B - B \star A)$ denotes the general Moyal bracket.

In the continuous-variable quantum system, only nuclear mapping DOFs $\mathbf{X} = (\mathbf{R}, \mathbf{P})$ are involved, and the Moyal product^{37, 39, 44, 90, 91, 94} reads

$$\star|_{\text{nuc}} = \exp \left[i \frac{\hbar}{2} (\overleftarrow{\nabla}_{\mathbf{R}} \cdot \overleftarrow{\nabla}_{\mathbf{P}} - \overleftarrow{\nabla}_{\mathbf{P}} \cdot \overleftarrow{\nabla}_{\mathbf{R}}) \right]. \quad (146)$$

When the discrete-variable quantum system is studied, only electronic mapping DOFs $\mathbf{X} = (\mathbf{x}, \mathbf{p})$ are included, because all phase space functions are quadratic in the constraint coordinate-momentum phase space representation, the general Moyal product involves a cut-off formalism,

$$\star|_{\text{ele}} = \hat{\Xi} - \gamma \hat{\Xi} \hat{\Xi}^*, \quad (147)$$

where

$$\begin{aligned} \hat{\Xi} &= \frac{1}{2} (\overleftarrow{\nabla}_{\mathbf{x}} - i \overleftarrow{\nabla}_{\mathbf{p}}) \cdot (\overleftarrow{\nabla}_{\mathbf{x}} + i \overleftarrow{\nabla}_{\mathbf{p}}) \\ &= \sum_{n=1}^F \frac{1}{2} \left(\overleftarrow{\frac{\partial}{\partial x_n}} - i \overleftarrow{\frac{\partial}{\partial p_n}} \right) \left(\overleftarrow{\frac{\partial}{\partial x_n}} + i \overleftarrow{\frac{\partial}{\partial p_n}} \right). \end{aligned} \quad (148)$$

The arrows above the gradient operators in eq (146) or eq (148) indicate the directions in which they act. When we consider the composite system, the total general Moyal product is expressed as the direct product

$$\star = \star|_{\text{nuc}} \otimes \star|_{\text{ele}} \quad (149)$$

for hybrid phase variables $\mathbf{X} = (\mathbf{R}, \mathbf{P}, \mathbf{x}, \mathbf{p})$ in the diabatic representation. When only the terms up to the first-order of \hbar of eq (146) are kept (similar to the mixed quantum-classical approach⁵³), the corresponding Moyal product of eq (149) becomes

$$\star = \left(1 + i \frac{\hbar}{2} (\bar{\nabla}_{\mathbf{R}} \cdot \bar{\nabla}_{\mathbf{P}} - \bar{\nabla}_{\mathbf{P}} \cdot \bar{\nabla}_{\mathbf{R}}) \right) \otimes (\hat{\Xi} - \gamma \hat{\Xi} \hat{\Xi}^*) + O(\hbar^2). \quad (150)$$

and the generalized Wigner-Moyal equation of eq (145) then reads

$$\begin{aligned} \frac{\partial}{\partial t} \rho(\mathbf{X}) &= -\frac{1}{i\hbar} \left(\rho(\mathbf{X}) \hat{\Xi} H(\mathbf{X}) - H(\mathbf{X}) \hat{\Xi} \rho(\mathbf{X}) \right) \\ &\quad - \frac{1}{i\hbar} \left(\rho(\mathbf{X}) \left(i \frac{\hbar}{2} (\bar{\nabla}_{\mathbf{R}} \cdot \bar{\nabla}_{\mathbf{P}} - \bar{\nabla}_{\mathbf{P}} \cdot \bar{\nabla}_{\mathbf{R}}) \right) \otimes (\hat{\Xi} - \gamma \hat{\Xi} \hat{\Xi}^*) H(\mathbf{X}) \right. \\ &\quad \left. - H(\mathbf{X}) \left(i \frac{\hbar}{2} (\bar{\nabla}_{\mathbf{R}} \cdot \bar{\nabla}_{\mathbf{P}} - \bar{\nabla}_{\mathbf{P}} \cdot \bar{\nabla}_{\mathbf{R}}) \right) \otimes (\hat{\Xi} - \gamma \hat{\Xi} \hat{\Xi}^*) \rho(\mathbf{X}) \right) \\ &= -\frac{1}{i\hbar} \left(\rho(\mathbf{X}) \hat{\Xi} H(\mathbf{X}) - H(\mathbf{X}) \hat{\Xi} \rho(\mathbf{X}) \right) \\ &\quad - \frac{1}{2} \left(\nabla_{\mathbf{R}} \rho(\mathbf{X}) (\hat{\Xi} - \gamma \hat{\Xi} \hat{\Xi}^*) \nabla_{\mathbf{P}} H(\mathbf{X}) - \nabla_{\mathbf{P}} \rho(\mathbf{X}) (\hat{\Xi} - \gamma \hat{\Xi} \hat{\Xi}^*) \nabla_{\mathbf{R}} H(\mathbf{X}) \right. \\ &\quad \left. - \nabla_{\mathbf{R}} H(\mathbf{X}) (\hat{\Xi} - \gamma \hat{\Xi} \hat{\Xi}^*) \nabla_{\mathbf{P}} \rho(\mathbf{X}) + \nabla_{\mathbf{P}} H(\mathbf{X}) (\hat{\Xi} - \gamma \hat{\Xi} \hat{\Xi}^*) \nabla_{\mathbf{R}} \rho(\mathbf{X}) \right) \end{aligned} \quad (151)$$

A simplified version of eq (151) reads

$$\begin{aligned} -\frac{\partial}{\partial t} \rho(\mathbf{X}) &= \frac{1}{\hbar} \left(\nabla_{\mathbf{x}} \rho(\mathbf{X}) \cdot \nabla_{\mathbf{p}} H(\mathbf{X}) - \nabla_{\mathbf{x}} H(\mathbf{X}) \cdot \nabla_{\mathbf{p}} \rho(\mathbf{X}) \right) \\ &\quad + \nabla_{\mathbf{R}} \rho(\mathbf{X}) \cdot \nabla_{\mathbf{P}} H(\mathbf{X}) \\ &\quad - \frac{1}{2} \left(\nabla_{\mathbf{P}} \rho(\mathbf{X}) (\hat{\Xi} - \gamma \hat{\Xi} \hat{\Xi}^*) \nabla_{\mathbf{R}} H(\mathbf{X}) + \nabla_{\mathbf{R}} H(\mathbf{X}) (\hat{\Xi} - \gamma \hat{\Xi} \hat{\Xi}^*) \nabla_{\mathbf{P}} \rho(\mathbf{X}) \right) \end{aligned} \quad (152)$$

Equation (152) is the expression of the mixed quantum-classical limit where the limit $\hbar \rightarrow 0$ is taken for only nuclear DOFs.

When dynamics of $\mathbf{X} = (\mathbf{R}, \mathbf{P}, \mathbf{x}, \mathbf{p})$ are approximated by the EOMs generated by the mapping Hamiltonian^{57, 58}, or the linearized semiclassical initial value representation (LSC-IVR) for only nuclear DOFs as first introduced in the constraint coordinate-momentum phase space representation in refs^{134, 136}, the exact generalized Wigner-Moyal equation of eq (149) is replaced by the Poisson bracket

$$\begin{aligned} \{\rho(\mathbf{X}), H(\mathbf{X})\}_{Poisson} &= \frac{1}{\hbar} \left(\nabla_{\mathbf{x}} \rho(\mathbf{X}) \cdot \nabla_{\mathbf{p}} H(\mathbf{X}) - \nabla_{\mathbf{x}} H(\mathbf{X}) \cdot \nabla_{\mathbf{p}} \rho(\mathbf{X}) \right) \\ &\quad + \left(\nabla_{\mathbf{R}} \rho(\mathbf{X}) \cdot \nabla_{\mathbf{P}} H(\mathbf{X}) - \nabla_{\mathbf{P}} \rho(\mathbf{X}) \cdot \nabla_{\mathbf{R}} H(\mathbf{X}) \right) \end{aligned} \quad (153)$$

While the first term of the RHS of eq (152) is equivalent to the first term of eq (153), the Poisson bracket of electronic mapping variables, the sum of the second and third terms of eq (152) are *not* exactly the same as the second term of eq (153), the Poisson bracket of nuclear DOFs. It indicates that the EOMs governed by the mapping Hamiltonian^{57, 58, 134, 136}, are *not* the mixed quantum-classical limit of exact nonadiabatic dynamics, despite that the mapping Hamiltonian generates exact linear EOMs for composite (nonadiabatic) quantum systems in the frozen-nuclei limit (i.e., all terms that involve the derivatives of nuclear DOFs vanish).

References

1. Lee HW, Scully MO. A new approach to molecular collisions: Statistical quasiclassical method. *J Chem Phys* 1980, 73:2238-2242. <https://doi.org/10.1063/1.440419>.
2. Lee HW, Scully MO. The Wigner phase-space description of collision processes. *Found Phys* 1983, 13:61-72. <https://doi.org/10.1007/bf01889411>.
3. Heller EJ. Wigner phase space method: Analysis for semiclassical applications. *J Chem Phys* 1976, 65:1289-1298. <https://doi.org/10.1063/1.433238>.
4. Sun X, Wang H, Miller WH. Semiclassical theory of electronically nonadiabatic dynamics: Results of a linearized approximation to the initial value representation. *J Chem Phys* 1998, 109:7064-7074. <https://doi.org/10.1063/1.477389>.
5. Wang H, Sun X, Miller WH. Semiclassical approximations for the calculation of thermal rate constants for chemical reactions in complex molecular systems. *J Chem Phys* 1998, 108:9726-9736. <https://doi.org/10.1063/1.476447>.
6. Pollak E, Liao J-L. A new quantum transition state theory. *J Chem Phys* 1998, 108:2733-2743. <https://doi.org/10.1063/1.475665>.
7. Shao J, Liao J-L, Pollak E. Quantum transition state theory: Perturbation expansion. *J Chem Phys* 1998, 108:9711-9725. <https://doi.org/10.1063/1.476446>.
8. Hernandez R, Voth GA. Quantum time correlation functions and classical coherence. *Chem Phys* 1998, 233:243-255. [https://doi.org/10.1016/s0301-0104\(98\)00027-5](https://doi.org/10.1016/s0301-0104(98)00027-5).
9. Liu J, Miller WH. Using the thermal Gaussian approximation for the Boltzmann operator in semiclassical initial value time correlation functions. *J Chem Phys* 2006, 125:224104. <https://doi.org/10.1063/1.2395941>.
10. Liu J, Miller WH. Linearized semiclassical initial value time correlation functions using the thermal Gaussian approximation: Applications to condensed phase systems. *J Chem Phys* 2007, 127:114506. <https://doi.org/10.1063/1.2774990>.
11. Liu J, Miller WH. Real time correlation function in a single phase space integral beyond the linearized semiclassical initial value representation. *J Chem Phys* 2007, 126:234110. <https://doi.org/10.1063/1.2743023>.
12. Liu J, Miller WH. Linearized semiclassical initial value time correlation functions with maximum entropy analytic continuation. *J Chem Phys* 2008, 129:124111. <https://doi.org/10.1063/1.2981065>.
13. Liu J, Miller WH. Test of the consistency of various linearized semiclassical initial value time correlation functions in application to inelastic neutron scattering from liquid para-hydrogen. *J Chem Phys* 2008, 128:144511. <https://doi.org/10.1063/1.2889945>.
14. Liu J, Miller WH, Paesani F, Zhang W, Case DA. Quantum dynamical effects in liquid water: A semiclassical study on the diffusion and the infrared absorption spectrum. *J Chem Phys* 2009, 131:164509. <https://doi.org/10.1063/1.3254372>.
15. Liu J, Miller WH. A simple model for the treatment of imaginary frequencies in chemical reaction rates and molecular liquids. *J Chem Phys* 2009, 131:074113. <https://doi.org/10.1063/1.3202438>.
16. Liu J, Alder BJ, Miller WH. A semiclassical study of the thermal conductivity of low temperature liquids. *J Chem Phys* 2011, 135:114105. <https://doi.org/10.1063/1.3639107>.
17. Liu J, Miller WH, Fanourgakis GS, Xantheas SS, Imoto S, Saito S. Insights in quantum dynamical effects in the infrared spectroscopy of liquid water from a semiclassical study with an ab initio-based flexible and polarizable force field. *J Chem Phys* 2011, 135:244503. <https://doi.org/10.1063/1.3670960>.

18. Liu J. Recent advances in the linearized semiclassical initial value representation/classical Wigner model for the thermal correlation function. *Int J Quantum Chem* 2015, 115:657-670. <https://doi.org/10.1002/qua.24872>.
19. Liu X, Liu J. Critical role of quantum dynamical effects in the Raman spectroscopy of liquid water. *Mol Phys* 2018, 116:755-779. <https://doi.org/10.1080/00268976.2018.1434907>.
20. Shi Q, Geva E. Semiclassical theory of vibrational energy relaxation in the condensed phase. *J Phys Chem A* 2003, 107:9059-9069. <https://doi.org/10.1021/jp030497+>.
21. Shi Q, Geva E. A relationship between semiclassical and centroid correlation functions. *J Chem Phys* 2003, 118:8173-8184. <https://doi.org/10.1063/1.1564814>.
22. Ka BJ, Geva E. Vibrational energy relaxation of polyatomic molecules in liquid solution via the linearized semiclassical method. *J Phys Chem A* 2006, 110:9555-9567. <https://doi.org/10.1021/jp062363c>.
23. Poulsen JA, Nyman G, Rossky PJ. Practical evaluation of condensed phase quantum correlation functions: A Feynman-Kleinert variational linearized path integral method. *J Chem Phys* 2003, 119:12179-12193. <https://doi.org/10.1063/1.1626631>.
24. Poulsen JA, Nyman G, Rossky PJ. Feynman-Kleinert linearized path integral (FK-LPI) algorithms for quantum molecular dynamics, with application to water and He(4). *J Chem Theory Comput* 2006, 2:1482-1491. <https://doi.org/10.1021/ct600167s>.
25. Shao J, Makri N. Forward-backward semiclassical dynamics with linear scaling. *J Phys Chem A* 1999, 103:9479-9486. <https://doi.org/10.1021/jp991837n>.
26. Shao J, Makri N. Forward-backward semiclassical dynamics without prefactors. *J Phys Chem A* 1999, 103:7753-7756. <https://doi.org/10.1021/jp991433v>.
27. Liu J, Nakayama A, Makri N. Long-time behaviour of quantized distributions in forward-backward semiclassical dynamics. *Mol Phys* 2006, 104:1267-1274. <https://doi.org/10.1080/00268970500525754>.
28. Liu J, Makri N. Symmetries and detailed balance in forward-backward semiclassical dynamics. *Chem Phys* 2006, 322:23-29. <https://doi.org/https://doi.org/10.1016/j.chemphys.2005.08.010>.
29. Makri N, Nakayama A, Wright NJ. Forward-backward semiclassical simulation of dynamical properties in liquids. *J Theor Comput Chem* 2004, 3:391-417. <https://doi.org/10.1142/s0219633604001112>.
30. Makri N. Quantum-classical path integral: A rigorous approach to condensed phase dynamics. *Int J Quantum Chem* 2015, 115:1209-1214. <https://doi.org/10.1002/qua.24975>.
31. Walters PL, Makri N. Quantum-classical path Integral simulation of ferrocene-ferrocenium charge transfer in liquid hexane. *J Phys Chem Lett* 2015, 6:4959-4965. <https://doi.org/10.1021/acs.jpclett.5b02265>.
32. Kryvohuz M, Cao JS. Quantum-classical correspondence in response theory. *Phys Rev Lett* 2005, 95:180405. <https://doi.org/10.1103/PhysRevLett.95.180405>.
33. Donoso A, Martens CC. Quantum tunneling using entangled classical trajectories. *Phys Rev Lett* 2001, 87:223202. <https://doi.org/10.1103/PhysRevLett.87.223202>.
34. Donoso A, Zheng Y, Martens CC. Simulation of quantum processes using entangled trajectory molecular dynamics. *J Chem Phys* 2003, 119:5010-5020. <https://doi.org/10.1063/1.1597496>.
35. Wang A, Zheng Y, Martens CC, Ren W. Quantum tunneling dynamics using entangled trajectories: General potentials. *Phys Chem Chem Phys* 2009, 11:1588-1594. <https://doi.org/10.1039/b811509e>.
36. Xu F, Martens CC, Zheng Y. Entanglement dynamics with a trajectory-based formulation. *Phys Rev A* 2017, 96:022138. <https://doi.org/10.1103/PhysRevA.96.022138>.
37. Liu J, Miller WH. An approach for generating trajectory-based dynamics which conserves the canonical distribution in the phase space formulation of quantum mechanics. I. Theories. *J Chem Phys* 2011, 134:104101. <https://doi.org/10.1063/1.3555273>.
38. Liu J, Miller WH. An approach for generating trajectory-based dynamics which conserves the canonical distribution in the phase space formulation of quantum mechanics. II. Thermal correlation functions. *J Chem Phys* 2011, 134:104102. <https://doi.org/10.1063/1.3555274>.
39. Liu J. Two more approaches for generating trajectory-based dynamics which conserves the canonical distribution in the phase space formulation of quantum mechanics. *J Chem Phys* 2011, 134:194110. <https://doi.org/10.1063/1.3589406>.
40. Liu J. Path integral Liouville dynamics for thermal equilibrium systems. *J Chem Phys* 2014, 140:224107. <https://doi.org/10.1063/1.4881518>.
41. Liu J, Zhang Z. Path integral Liouville dynamics: Applications to infrared spectra of OH, water, ammonia, and methane. *J Chem Phys* 2016, 144:034307. <https://doi.org/10.1063/1.4939953>.
42. Liu J, Li D, Liu X. Further study of path integral Liouville dynamics. *Sci Sin Chim* 2016, 46:27-37. <https://doi.org/10.1360/N032015-00143>.

43. Zhang Z, Chen Z, Liu J. Path integral Liouville dynamics simulations of vibrational spectra of formaldehyde and hydrogen peroxide. *Chin J Chem Phys* 2020, 33:613-622. <https://doi.org/10.1063/1674-0068/cjcp2006099>.
44. Liu X, Zhang L, Liu J. Machine learning phase space quantum dynamics approaches. *J Chem Phys* 2021, 154:184104. <https://doi.org/10.1063/5.0046689>.
45. Smith KKG, Poulsen JA, Nyman G, Cunsolo A, Rossky PJ. Application of a new ensemble conserving quantum dynamics simulation algorithm to liquid para-hydrogen and ortho-deuterium. *J Chem Phys* 2015, 142:244113. <https://doi.org/10.1063/1.4922888>.
46. Smith KKG, Poulsen JA, Nyman G, Rossky PJ. A new class of ensemble conserving algorithms for approximate quantum dynamics: Theoretical formulation and model problems. *J Chem Phys* 2015, 142:244112. <https://doi.org/10.1063/1.4922887>.
47. Willatt MJ, Ceriotti M, Althorpe SC. Approximating Matsubara dynamics using the planetary model: Tests on liquid water and ice. *J Chem Phys* 2018, 148:102336. <https://doi.org/10.1063/1.5004808>.
48. Orr L, de la Pena LH, Roy P-N. Formulation of state projected centroid molecular dynamics: Microcanonical ensemble and connection to the Wigner distribution. *J Chem Phys* 2017, 146:214116. <https://doi.org/10.1063/1.4984229>.
49. Bonella S, Montemayor D, Coker DF. Linearized path integral approach for calculating nonadiabatic time correlation functions. *Proc Natl Acad Sci USA* 2005, 102:6715-6719. <https://doi.org/10.1073/pnas.0408326102>.
50. Nassimi A, Bonella S, Kapral R. Analysis of the quantum-classical Liouville equation in the mapping basis. *J Chem Phys* 2010, 133:134115. <https://doi.org/10.1063/1.3480018>.
51. Weinbub J, Ferry DK. Recent advances in Wigner function approaches. *Appl Phys Rev* 2018, 5:041104. <https://doi.org/10.1063/1.5046663>.
52. Pie T, Huppert S, Finocchi F, Depondt P, Bonella S. Sampling the thermal Wigner density via a generalized Langevin dynamics. *J Chem Phys* 2019, 151:114114. <https://doi.org/10.1063/1.5099246>.
53. Kapral R, Ciccotti G. Mixed quantum-classical dynamics. *J Chem Phys* 1999, 110:8919-8929. <https://doi.org/10.1063/1.478811>.
54. Kapral R. Quantum dynamics in open quantum-classical systems. *J Phys Condens Matter* 2015, 27:073201. <https://doi.org/10.1088/0953-8984/27/7/073201>.
55. Bai S, Xie W, Zhu L, Shi Q. Calculation of absorption spectra involving multiple excited states: Approximate methods based on the mixed quantum classical Liouville equation. *J Chem Phys* 2014, 140:084105. <https://doi.org/10.1063/1.4866367>.
56. Tao G, Miller WH. Semiclassical description of electronic excitation population transfer in a model photosynthetic system. *J Phys Chem Lett* 2010, 1:891-894. <https://doi.org/10.1021/jz1000825>.
57. He X, Wu B, Gong Z, Liu J. Commutator matrix in phase space mapping models for nonadiabatic quantum dynamics. *J Phys Chem A* 2021, 125:6845-6863. <https://doi.org/10.1021/acs.jpca.1c04429>.
58. Liu J, He X, Wu B. Unified formulation of phase space mapping approaches for nonadiabatic quantum dynamics. *Acc Chem Res* 2021, 54:4215-4228. <https://doi.org/10.1021/acs.accounts.1c00511>.
59. Orioli AP, Safavi-Naini A, Wall ML, Rey AM. Nonequilibrium dynamics of spin-boson models from phase-space methods. *Phys Rev A* 2017, 96:033607. <https://doi.org/10.1103/PhysRevA.96.033607>.
60. Lang H, Vendrell O, Hauke P. Generalized discrete truncated Wigner approximation for nonadiabatic quantum-classical dynamics. *J Chem Phys* 2021, 155:024111. <https://doi.org/10.1063/5.0054696>.
61. Glauber RJ. Coherent and incoherent states of radiation field. *Phys Rev* 1963, 131:2766. <https://doi.org/10.1103/PhysRev.131.2766>.
62. Sudarshan ECG. Equivalence of semiclassical and quantum mechanical descriptions of statistical light beams. *Phys Rev Lett* 1963, 10:277. <https://doi.org/10.1103/PhysRevLett.10.277>.
63. Cahill KE, Glauber RJ. Ordered expansions in boson amplitude operators. *Phys Rev* 1969, 177:1857. <https://doi.org/10.1103/PhysRev.177.1857>.
64. Cahill KE, Glauber RJ. Density operators and quasiprobability distributions. *Phys Rev* 1969, 177:1882. <https://doi.org/10.1103/PhysRev.177.1882>.
65. Arecchi FT, Courtens E, Gilmore R, Thomas H. Atomic coherent states in quantum optics. *Phys Rev A* 1972, 6:2211. <https://doi.org/10.1103/PhysRevA.6.2211>.
66. Drummond PD, Gardiner CW. Generalized P-representations in quantum optics. *J Phys A Math Gen* 1980, 13:2353-2368. <https://doi.org/10.1088/0305-4470/13/7/018>.
67. Walls DF, Millburn GJ. *Quantum Optics*. Berlin: Springer-Verlag; 1994.
68. Gardiner C, Zoller P. *Quantum Noise: A Handbook of Markovian and Non-Markovian Quantum Stochastic Methods with Applications to Quantum Optics*. 3rd ed. 3rd edition ed. Berlin Heidelberg: Springer-Verlag; 2004.
69. Schleich WP. *Quantum Optics in Phase Space*. Berlin: WILEY-VCH Verlag Berlin GmbH; 2001.

70. Deléglise S, Dotsenko I, Sayrin C, Bernu J, Brune M, Raimond J-M, Haroche S. Reconstruction of non-classical cavity field states with snapshots of their decoherence. *Nature* 2008, 455:510-514. <https://doi.org/10.1038/nature07288>.
71. Steel MJ, Olsen MK, Plimak LI, Drummond PD, Tan SM, Collett MJ, Walls DF, Graham R. Dynamical quantum noise in trapped Bose-Einstein condensates. *Phys Rev A* 1998, 58:4824-4835. <https://doi.org/10.1103/PhysRevA.58.4824>.
72. Sinatra A, Lobo C, Castin Y. The truncated Wigner method for Bose-condensed gases: Limits of validity and applications. *J Phys B Atomic Mol Opt Phys* 2002, 35:3599-3631. <https://doi.org/10.1088/0953-4075/35/17/301>.
73. Blakie PB, Bradley AS, Davis MJ, Ballagh RJ, Gardiner CW. Dynamics and statistical mechanics of ultra-cold Bose gases using c-field techniques. *Adv Phys* 2008, 57:363-455. <https://doi.org/10.1080/00018730802564254>.
74. Polkovnikov A. Phase space representation of quantum dynamics. *Ann Phys* 2010, 325:1790-1852. <https://doi.org/10.1016/j.aop.2010.02.006>.
75. Mukherjee R, Mirasola AE, Hollingsworth J, White IG, Hazzard KRA. Geometric representation of spin correlations and applications to ultracold systems. *Phys Rev A* 2018, 97:043606. <https://doi.org/10.1103/physreva.97.043606>.
76. Zurek WH. Sub-Planck structure in phase space and its relevance for quantum decoherence. *Nature* 2001, 412:712-717. <https://doi.org/10.1038/35089017>.
77. Miquel C, Paz JP, Saraceno M. Quantum computers in phase space. *Phys Rev A* 2002, 65:062309. <https://doi.org/10.1103/PhysRevA.65.062309>.
78. Wootters WK. Picturing qubits in phase space. *IBM J Res Dev* 2004, 48:99-110. <https://doi.org/10.1147/rd.481.0099>.
79. Paz JP, Roncaglia AJ, Saraceno M. Qubits in phase space: Wigner-function approach to quantum-error correction and the mean-king problem. *Phys Rev A* 2005, 72:012309. <https://doi.org/10.1103/PhysRevA.72.012309>.
80. Braunstein SL, van Loock P. Quantum information with continuous variables. *Rev Mod Phys* 2005, 77:513-577. <https://doi.org/10.1103/RevModPhys.77.513>.
81. Delfosse N, Guerin PA, Bian J, Raussendorf R. Wigner function negativity and contextuality in quantum computation on rebits. *Phys Rev X* 2015, 5:021003. <https://doi.org/10.1103/PhysRevX.5.021003>.
82. Schachenmayer J, Pikovski A, Rey AM. Many-body quantum spin dynamics with Monte-Carlo trajectories on a discrete phase space. *Phys Rev X* 2015, 5:011022. <https://doi.org/10.1103/PhysRevX.5.011022>.
83. Schachenmayer J, Pikovski A, Rey AM. Dynamics of correlations in two-dimensional quantum spin models with long-range interactions: A phase-space Monte-Carlo study. *New J Phys* 2015, 17:065009. <https://doi.org/10.1088/1367-2630/17/6/065009>.
84. Bermejo-Vega J, Delfosse N, Browne DE, Okay C, Raussendorf R. Contextuality as a resource for models of quantum computation with qubits. *Phys Rev Lett* 2017, 119:120505. <https://doi.org/10.1103/PhysRevLett.119.120505>.
85. Rundle RP, Mills PW, Tilma T, Samson JH, Everitt MJ. Simple procedure for phase-space measurement and entanglement validation. *Phys Rev A* 2017, 96:022117. <https://doi.org/10.1103/physreva.96.022117>.
86. Zhu B, Rey AM, Schachenmayer J. A generalized phase space approach for solving quantum spin dynamics. *New J Phys* 2019, 21:082001. <https://doi.org/10.1088/1367-2630/ab354d>.
87. Rundle RP, Everitt MJ. Overview of the phase space formulation of quantum mechanics with application to quantum technologies. *Adv Quantum Technol* 2021, 4:2100016. <https://doi.org/10.1002/qute.202100016>.
88. Weyl H. Quantum mechanics and group theory. *Z Phys* 1927, 46:1-46. <https://doi.org/10.1007/bf02055756>.
89. Wigner EP. On the quantum correction for thermodynamic equilibrium. *Phys Rev* 1932, 40:749-759. <https://doi.org/10.1103/physrev.40.749>.
90. Hillery M, Oconnell RF, Scully MO, Wigner EP. Distribution-functions in physics: Fundamentals. *Phys Rep* 1984, 106:121-167. [https://doi.org/10.1016/0370-1573\(84\)90160-1](https://doi.org/10.1016/0370-1573(84)90160-1).
91. Lee HW. Theory and application of the quantum phase-space distribution functions. *Phys Rep* 1995, 259:147-211. [https://doi.org/10.1016/0370-1573\(95\)00007-4](https://doi.org/10.1016/0370-1573(95)00007-4).
92. Cohen L. Generalized phase-space distribution functions. *J Math Phys* 1966, 7:781-786. <https://doi.org/10.1063/1.1931206>.
93. Groenewold HJ. On the Principles of Elementary Quantum Mechanics. *Physica* 1946, 12:405-460. [https://doi.org/10.1016/s0031-8914\(46\)80059-4](https://doi.org/10.1016/s0031-8914(46)80059-4).
94. Moyal JE. Quantum mechanics as a statistical theory. *Math Proc Cambridge Phil Soc* 1949, 45:99-124. <https://doi.org/10.1017/s0305004100000487>.

95. Bopp F. *Werner Heisenberg und die Physik unserer Zeit*. Braunschweig: Vieweg; 1961.
96. Miller WH. Quantum dynamics of complex molecular systems. *Proc Natl Acad Sci USA* 2005, 102:6660-6664. <https://doi.org/10.1073/pnas.0408043102>.
97. Miller WH. Including quantum effects in the dynamics of complex (i.e., large) molecular systems. *J Chem Phys* 2006, 125:132305. <https://doi.org/10.1063/1.2211608>.
98. Miller WH. Classical-limit quantum mechanics and the theory of molecular collisions. *Adv Chem Phys* 1974, 25:69-177. <https://doi.org/10.1002/9780470143773.ch2>.
99. Miller WH. The classical S-matrix in molecular collisions. *Adv Chem Phys* 1975, 30:77. <https://doi.org/10.1002/9780470143827.ch3>.
100. Stratonovich RL. On distributions in representation space. *Zh Eksp Teor Fiz* 1956, 31:1012.
101. Feynman RP. Negative probability. In: Hiley BJ, Peat D, eds. *Quantum Implications: Essays in Honour of David Bohm*. New York: Routledge; 1987, 235-248.
102. Wootters WK. A Wigner-function formulation of finite-state quantum mechanics. *Ann Phys* 1987, 176:1-21. [https://doi.org/10.1016/0003-4916\(87\)90176-x](https://doi.org/10.1016/0003-4916(87)90176-x).
103. Várilly JC, Gracia-Bonda J. The Moyal representation for spin. *Ann Phys* 1989, 190:107-148. [https://doi.org/10.1016/0003-4916\(89\)90262-5](https://doi.org/10.1016/0003-4916(89)90262-5).
104. Amiet JP, Cibils MB. Description of quantum spin using functions on the sphere S². *J Phys A Math Gen* 1991, 24:1515-1535. <https://doi.org/10.1088/0305-4470/24/7/023>.
105. Amiet JP, Weigert S. Discrete Q- and P-symbols for spin s. *J Opt B Quantum Semiclassical Opt* 2000, 2:118-121. <https://doi.org/10.1088/1464-4266/2/2/309>.
106. Dowling JP, Agarwal GS, Schleich WP. Wigner distribution of a general angular-momentum state: Applications to a collection of 2-level atoms. *Phys Rev A* 1994, 49:4101-4109. <https://doi.org/10.1103/PhysRevA.49.4101>.
107. Brif C, Mann A. Phase-space formulation of quantum mechanics and quantum-state reconstruction for physical systems with Lie-group symmetries. *Phys Rev A* 1999, 59:971-987. <https://doi.org/10.1103/physreva.59.971>.
108. Cunha MOT, Man'ko VI, Scully MO. Quasiprobability and probability distributions for spin-1/2 states. *Found Phys Lett* 2001, 14:103-117. <https://doi.org/10.1023/a:1012373419313>.
109. Klimov AB, Espinoza P. Moyal-like form of the star product for generalized SU(2) Stratonovich-Weyl symbols. *J Phys A Math Gen* 2002, 35:8435-8447. <https://doi.org/10.1088/0305-4470/35/40/305>.
110. Klimov AB, Romero JL. A generalized Wigner function for quantum systems with the SU(2) dynamical symmetry group. *J Phys A Math Theor* 2008, 41:055303. <https://doi.org/10.1088/1751-8113/41/5/055303>.
111. Klimov AB, Romero JL, de Guise H. Generalized SU(2) covariant Wigner functions and some of their applications. *J Phys A Math Theor* 2017, 50:323001. <https://doi.org/10.1088/1751-8121/50/32/323001>.
112. Adam P, Andreev VA, Man'ko MA, Man'ko VI, Mechler M. SU(2) symmetry of qubit states and Heisenberg-Weyl symmetry of systems with continuous variables in the probability representation of quantum mechanics. *Symmetry* 2020, 12:23. <https://doi.org/10.3390/sym12071099>.
113. Koczor B, Zeier R, Glaser SJ. Continuous phase-space representations for finite-dimensional quantum states and their tomography. *Phys Rev A* 2020, 101:022318. <https://doi.org/10.1103/physreva.101.022318>.
114. Tilma T, Nemoto K. SU(N)-symmetric quasi-probability distribution functions. *J Phys A Math Theor* 2012, 45:015302. <https://doi.org/10.1088/1751-8113/45/1/015302>.
115. Tilma T, Everitt MJ, Samson JH, Munro WJ, Nemoto K. Wigner functions for arbitrary quantum systems. *Phys Rev Lett* 2016, 117:180401. <https://doi.org/10.1103/physrevlett.117.180401>.
116. Marchioli MA, Galetti D. On the discrete Wigner function for SU(N). *J Phys A Math Theor* 2019, 52:405305. <https://doi.org/10.1088/1751-8121/ab3bab>.
117. Rundle RP, Tilma T, Samson JH, Dwyer VM, Bishop RF, Everitt MJ. General approach to quantum mechanics as a statistical theory. *Phys Rev A* 2019, 99:012115. <https://doi.org/10.1103/physreva.99.012115>.
118. Cohendet O, Combe P, Sirugue M, Sirugue-Collin M. A stochastic treatment of the dynamics of an integer spin. *J Phys A Math Gen* 1988, 21:2875-2883. <https://doi.org/10.1088/0305-4470/21/13/012>.
119. Leonhardt U. Quantum-state tomography and discrete Wigner function. *Phys Rev Lett* 1995, 74:4101-4105. <https://doi.org/10.1103/PhysRevLett.74.4101>.
120. Leonhardt U. Discrete Wigner function and quantum-state tomography. *Phys Rev A* 1996, 53:2998-3013. <https://doi.org/10.1103/PhysRevA.53.2998>.
121. Gibbons KS, Hoffman MJ, Wootters WK. Discrete phase space based on finite fields. *Phys Rev A* 2004, 70:062101. <https://doi.org/10.1103/physreva.70.062101>.
122. Wootters WK. Quantum measurements and finite geometry. *Found Phys* 2006, 36:112-126. <https://doi.org/10.1007/s10701-005-9008-x>.

123. Ruzzi M, Marchioli MA, Galetti D. Extended Cahill-Glauber formalism for finite-dimensional spaces: I. Fundamentals. *J Phys A Math Gen* 2005, 38:6239-6251. <https://doi.org/10.1088/0305-4470/38/27/010>.
124. Chaturvedi S, Ercolessi E, Marmo G, Morandi G, Mukunda N, Simon R. Wigner distributions for finite dimensional quantum systems: An algebraic approach. *Pramana* 2005, 65:981-993. <https://doi.org/10.1007/bf02705275>.
125. Chaturvedi S, Ercolessi E, Marmo G, Morandi G, Mukunda N, Simon R. Wigner-Weyl correspondence in quantum mechanics for continuous and discrete systems-a Dirac-inspired view. *J Phys A Math Gen* 2006, 39:1405-1423. <https://doi.org/10.1088/0305-4470/39/6/014>.
126. Gross D. Hudson's theorem for finite-dimensional quantum systems. *J Math Phys* 2006, 47:25. <https://doi.org/10.1063/1.2393152>.
127. Valtierra IF, Romero JL, Klimov AB. TWA versus semiclassical unitary approximation for spin-like systems. *Ann Phys* 2017, 383:620-634. <https://doi.org/10.1016/j.aop.2017.06.006>.
128. Valtierra IF, Klimov AB, Leuchs G, Sánchez-Soto LL. Quasiprobability currents on the sphere. *Phys Rev A* 2020, 101:033803. <https://doi.org/10.1103/PhysRevA.101.033803>.
129. Czischek S. Discrete Truncated Wigner Approximation. In: *Springer Theses*: Springer International Publishing; 2020, 85-109.
130. Morales-Hernández GE, Castellanos JC, Romero JL, Klimov AB. Semi-classical discretization and long-time evolution of variable spin systems. *Entropy* 2021, 23:684. <https://doi.org/10.3390/e23060684>.
131. Fano U. Geometrical characterization of nuclear states and the theory of angular correlations. *Phys Rev* 1953, 90:577-579. <https://doi.org/10.1103/PhysRev.90.577>.
132. Klimov AB. Exact evolution equations for SU(2) quasidistribution functions. *J Math Phys* 2002, 43:2202-2213. <https://doi.org/10.1063/1.1463711>.
133. Liu J. A unified theoretical framework for mapping models for the multi-state Hamiltonian. *J Chem Phys* 2016, 145:204105. <https://doi.org/10.1063/1.4967815>.
134. He X, Liu J. A new perspective for nonadiabatic dynamics with phase space mapping models. *J Chem Phys* 2019, 151:024105. <https://doi.org/10.1063/1.5108736>.
135. Liu J. Isomorphism between the multi-state Hamiltonian and the second-quantized many-electron Hamiltonian with only 1-electron interactions. *J Chem Phys* 2017, 146:024110. <https://doi.org/10.1063/1.4973708>.
136. He X, Gong Z, Wu B, Liu J. Negative zero-point-energy parameter in the Meyer-Miller mapping model for nonadiabatic dynamics. *J Phys Chem Lett* 2021, 12:2496-2501. <https://doi.org/10.1021/acs.jpcclett.1c00232>.
137. Domcke W, Yarkony DR, Köppel H. *Conical Intersections: Theory, Computation and Experiment*. Singapore: World Scientific; 2011.
138. Yonehara T, Hanasaki K, Takatsuka K. Fundamental approaches to nonadiabaticity: Toward a chemical theory beyond the Born-Oppenheimer paradigm. *Chem Rev* 2011, 112:499-542. <https://doi.org/10.1021/cr200096s>.
139. Tully JC. Perspective: Nonadiabatic dynamics theory. *J Chem Phys* 2012, 137:22A301. <https://doi.org/10.1063/1.4757762>.
140. Miller WH, Cotton SJ. Classical molecular dynamics simulation of electronically non-adiabatic processes. *Faraday Discuss* 2016, 195:9-30. <https://doi.org/10.1039/c6fd00181e>.
141. Levine BG, Martínez TJ. Isomerization through conical intersections. *Annu Rev Phys Chem* 2007, 58:613-634. <https://doi.org/10.1146/annurev.physchem.57.032905.104612>.
142. Martínez TJ. Seaming is believing. *Nature* 2010, 467:412-413. <https://doi.org/10.1038/467412a>.
143. Sisto A, Glowacki DR, Martínez TJ. Ab Initio nonadiabatic dynamics of multichromophore complexes: A scalable graphical-processing-unit-accelerated exciton framework. *Acc Chem Res* 2014, 47:2857-2866. <https://doi.org/10.1021/ar500229p>.
144. Makhov DV, Glover WJ, Martínez TJ, Shalashilin DV. Ab initio multiple cloning algorithm for quantum nonadiabatic molecular dynamics. *J Chem Phys* 2014, 141:054110. <https://doi.org/10.1063/1.4891530>.
145. Mai S, Marquetand P, González L. Nonadiabatic dynamics: The SHARC approach. *WIREs Comput Mol Sci* 2018, 8:e1370. <https://doi.org/10.1002/wcms.1370>.
146. Mai S, González L. Molecular photochemistry: Recent developments in theory. *Angew Chem Int Ed* 2020, 59:16832-16846. <https://doi.org/10.1002/anie.201916381>.
147. Subotnik JE, Jain A, Landry B, Petit A, Ouyang W, Bellonzi N. Understanding the surface hopping view of electronic transitions and decoherence. *Annu Rev Phys Chem* 2016, 67:387-417. <https://doi.org/10.1146/annurev-physchem-040215-112245>.
148. Fang W-H. Ab Initio determination of dark structures in radiationless transitions for aromatic carbonyl compounds. *Acc Chem Res* 2008, 41:452-457. <https://doi.org/10.1021/ar700205f>.
149. Long R, Prezhdo OV, Fang W-H. Nonadiabatic charge dynamics in novel solar cell materials. *WIREs Comput Mol Sci* 2017, 7:e1305. <https://doi.org/10.1002/wcms.1305>.

150. Feng W, Xu L, Li X-Q, Fang W-H, Yan Y. Nonadiabatic molecular dynamics simulation: An approach based on quantum measurement picture. *AIP Advances* 2014, 4:077131. <https://doi.org/10.1063/1.4891821>.
151. Lan Z, Shao J. Approximate theoretical methods for nonadiabatic dynamics of polyatomic molecules. *Prog Chem* 2012, 24:1105-1119.
152. Wang Y-C, Ke Y, Zhao Y. The hierarchical and perturbative forms of stochastic Schrodinger equations and their applications to carrier dynamics in organic materials. *WIREs Comput Mol Sci* 2019, 9:e1375. <https://doi.org/10.1002/wcms.1375>.
153. Nelson T, Fernandez-Alberti S, Roitberg AE, Tretiak S. Nonadiabatic excited-state molecular dynamics: Modeling photophysics in organic conjugated materials. *Acc Chem Res* 2014, 47:1155-1164. <https://doi.org/10.1021/ar400263p>.
154. Crespo-Otero R, Barbatti M. Recent advances and perspectives on nonadiabatic mixed quantum-classical dynamics. *Chem Rev* 2018, 118:7026-7068. <https://doi.org/10.1021/acs.chemrev.7b00577>.
155. Meyer H-D, Miller WH. A classical analog for electronic degrees of freedom in nonadiabatic collision processes. *J Chem Phys* 1979, 70:3214-3223. <https://doi.org/10.1063/1.437910>.
156. Stock G, Thoss M. Semiclassical description of nonadiabatic quantum dynamics. *Phys Rev Lett* 1997, 78:578-581. <https://doi.org/10.1103/PhysRevLett.78.578>.
157. Wigner EP. *Perspectives in Quantum Theory*. Cambridge: MIT; 1971.
158. Husimi K. Some formal properties of the density matrix. *Proc Physico-Math Soc Jpn* 1940, 22:264-314. https://doi.org/10.11429/ppmsj1919.22.4_264.
159. Glauber RJ. Optical coherence and photon statistics. In: deWitt C, Blandin A, C. C-T, eds. *Quantum Optics and Electronics*. New York: Gordon and Breach; 1965.
160. Kirkwood JG. Quantum statistics of almost classical assemblies. *Phys Rev* 1933, 44:31. <https://doi.org/10.1103/PhysRev.44.31>.
161. Rihaczek AW. Signal energy distribution in time and frequency. *IEEE Trans Inform Theory* 1968, 14:369-374. <https://doi.org/10.1109/TIT.1968.1054157>.
162. Mehta CL. Phase-space formulation of the dynamics of canonical variables. *J Math Phys* 1964, 5:677-686. <https://doi.org/10.1063/1.1704163>.
163. Rivier DC. On a one-to-one correspondence between infinitesimal canonical transformations and infinitesimal unitary transformations. *Phys Rev* 1951, 83:862. <https://doi.org/10.1103/PhysRev.83.862>.
164. Margenau H, Hill RN. Correlation between measurements in quantum theory. *Prog Theor Phys* 1961, 26:722-738. <https://doi.org/10.1143/PTP.26.722>.
165. Born M, Jordan P. On quantum mechanics. *Z Phys* 1925, 34:858-888. <https://doi.org/10.1007/BF01328531>.
166. Meyer H-D, Miller WH. Classical-models for electronic degrees of freedom: Derivation via spin analogy and application to $F^*+H_2 \rightarrow F+H_2$. *J Chem Phys* 1979, 71:2156-2169. <https://doi.org/10.1063/1.438598>.
167. Gray SK, Miller WH. Classical model for electronic degrees of freedom: Charge transfer in $Na + I$ collisions. *Chem Phys Lett* 1982, 93:341-344. [https://doi.org/10.1016/0009-2614\(82\)83705-6](https://doi.org/10.1016/0009-2614(82)83705-6).
168. Ali DP, Miller WH. Effect of electronic transition dynamics on iodine atom recombination in liquids. *J Chem Phys* 1983, 78:6640-6645. <https://doi.org/10.1063/1.444662>.
169. Ali DP, Miller WH. Classical models for electronic degrees of freedom: Quenching of $Br^*(2P_{1/2})$ by collision with H_2 in three dimensions. *Chem Phys Lett* 1984, 103:470-474. [https://doi.org/10.1016/0009-2614\(84\)85279-3](https://doi.org/10.1016/0009-2614(84)85279-3).
170. Stock G, Miller WH. A classical model for time- and frequency-resolved spectroscopy of nonadiabatic excited-state dynamics. *Chem Phys Lett* 1992, 197:396-404. [https://doi.org/10.1016/0009-2614\(92\)85791-8](https://doi.org/10.1016/0009-2614(92)85791-8).
171. Stock G, Miller WH. Classical formulation of the spectroscopy of nonadiabatic excited-state dynamics. *J Chem Phys* 1993, 99:1545-1555. <https://doi.org/10.1063/1.465323>.
172. Sun X, Miller WH. Semiclassical initial value representation for electronically nonadiabatic molecular dynamics. *J Chem Phys* 1997, 106:6346-6353. <https://doi.org/10.1063/1.473624>.
173. Coronado EA, Batista VS, Miller WH. Nonadiabatic photodissociation dynamics of ICN in the \tilde{A} continuum: A semiclassical initial value representation study. *J Chem Phys* 2000, 112:5566-5575. <https://doi.org/10.1063/1.481130>.
174. Coronado EA, Xing J, Miller WH. Ultrafast non-adiabatic dynamics of systems with multiple surface crossings: A test of the Meyer-Miller Hamiltonian with semiclassical initial value representation methods. *Chem Phys Lett* 2001, 349:521-529. [https://doi.org/10.1016/s0009-2614\(01\)01242-8](https://doi.org/10.1016/s0009-2614(01)01242-8).
175. Ananth N, Venkataraman C, Miller WH. Semiclassical description of electronically nonadiabatic dynamics via the initial value representation. *J Chem Phys* 2007, 127:084114. <https://doi.org/10.1063/1.2759932>.

176. Miller WH. Electronically nonadiabatic dynamics via semiclassical initial value methods. *J Phys Chem A* 2009, 113:1405-1415. <https://doi.org/10.1021/jp809907p>.
177. Ananth N, Miller TF. Exact quantum statistics for electronically nonadiabatic systems using continuous path variables. *J Chem Phys* 2010, 133:234103. <https://doi.org/10.1063/1.3511700>.
178. Cotton SJ, Miller WH. Symmetrical windowing for quantum states in quasi-classical trajectory simulations. *J Phys Chem A* 2013, 117:7190-7194. <https://doi.org/10.1021/jp401078u>.
179. Cotton SJ, Miller WH. Symmetrical windowing for quantum states in quasi-classical trajectory simulations: Application to electronically non-adiabatic processes. *J Chem Phys* 2013, 139:234112. <https://doi.org/10.1063/1.4845235>.
180. Cotton SJ, Igumenshchev K, Miller WH. Symmetrical windowing for quantum states in quasi-classical trajectory simulations: Application to electron transfer. *J Chem Phys* 2014, 141:084104. <https://doi.org/10.1063/1.4893345>.
181. Cotton SJ, Miller WH. A symmetrical quasi-classical spin-mapping model for the electronic degrees of freedom in non-adiabatic processes. *J Phys Chem A* 2015, 119:12138-12145. <https://doi.org/10.1021/acs.jpca.5b05906>.
182. Miller WH, Cotton SJ. Communication: Note on detailed balance in symmetrical quasi-classical models for electronically non-adiabatic dynamics. *J Chem Phys* 2015, 142:131103. <https://doi.org/10.1063/1.4916945>.
183. Cotton SJ, Miller WH. A new symmetrical quasi-classical model for electronically non-adiabatic processes: Application to the case of weak non-adiabatic coupling. *J Chem Phys* 2016, 145:144108. <https://doi.org/10.1063/1.4963914>.
184. Cotton SJ, Miller WH. The symmetrical quasi-classical model for electronically non-adiabatic processes applied to energy transfer dynamics in site-exciton models of light-harvesting complexes. *J Chem Theory Comput* 2016, 12:983-991. <https://doi.org/10.1021/acs.jctc.5b01178>.
185. Miller WH, Cotton SJ. Communication: Wigner functions in action-angle variables, Bohr-Sommerfeld quantization, the Heisenberg correspondence principle, and a symmetrical quasi-classical approach to the full electronic density matrix. *J Chem Phys* 2016, 145:081102. <https://doi.org/10.1063/1.4961551>.
186. Cotton SJ, Liang R, Miller WH. On the adiabatic representation of Meyer-Miller electronic-nuclear dynamics. *J Chem Phys* 2017, 147:064112. <https://doi.org/10.1063/1.4995301>.
187. Liang R, Cotton SJ, Binder R, Hegger R, Burghardt I, Miller WH. The symmetrical quasi-classical approach to electronically nonadiabatic dynamics applied to ultrafast exciton migration processes in semiconducting polymers. *J Chem Phys* 2018, 149:044101. <https://doi.org/10.1063/1.5037815>.
188. Cotton SJ, Miller WH. A symmetrical quasi-classical windowing model for the molecular dynamics treatment of non-adiabatic processes involving many electronic states. *J Chem Phys* 2019, 150:104101. <https://doi.org/10.1063/1.5087160>.
189. Cotton SJ, Miller WH. Trajectory-adjusted electronic zero point energy in classical Meyer-Miller vibronic dynamics: Symmetrical quasiclassical application to photodissociation. *J Chem Phys* 2019, 150:194110. <https://doi.org/10.1063/1.5094458>.
190. Müller U, Stock G. Flow of zero-point energy and exploration of phase space in classical simulations of quantum relaxation dynamics. II. Application to nonadiabatic processes. *J Chem Phys* 1999, 111:77-88. <https://doi.org/10.1063/1.479255>.
191. Stock G, Müller U. Flow of zero-point energy and exploration of phase space in classical simulations of quantum relaxation dynamics. *J Chem Phys* 1999, 111:65-76. <https://doi.org/10.1063/1.479254>.
192. Müller U, Stock G. Consistent treatment of quantum-mechanical and classical degrees of freedom in mixed quantum-classical simulations. *J Chem Phys* 1998, 108:7516-7526. <https://doi.org/10.1063/1.476184>.
193. Stock G, Thoss M. Classical description of nonadiabatic quantum dynamics. *Adv Chem Phys* 2005, 131:243-375. <https://doi.org/10.1002/0471739464.ch5>.
194. Thoss M, Miller WH, Stock G. Semiclassical description of nonadiabatic quantum dynamics: Application to the S1-S2 conical intersection in pyrazine. *J Chem Phys* 2000, 112:10282-10292. <https://doi.org/10.1063/1.481668>.
195. Thoss M, Stock G. Mapping approach to the semiclassical description of nonadiabatic quantum dynamics. *Phys Rev A* 1999, 59:64-79. <https://doi.org/10.1103/PhysRevA.59.64>.
196. Golosov AA, Reichman DR. Classical mapping approaches for nonadiabatic dynamics: Short time analysis. *J Chem Phys* 2001, 114:1065-1074. <https://doi.org/10.1063/1.1332812>.
197. Saller MAC, Kelly A, Richardson JO. On the identity of the identity operator in nonadiabatic linearized semiclassical dynamics. *J Chem Phys* 2019, 150:071101. <https://doi.org/10.1063/1.5082596>.
198. Saller MAC, Kelly A, Richardson JO. Improved population operators for multi-state nonadiabatic dynamics with the mixed quantum-classical mapping approach. *Faraday Discuss* 2020, 221:150-167. <https://doi.org/10.1039/c9fd00050j>.

199. Runeson JE, Richardson JO. Generalized spin mapping for quantum-classical dynamics. *J Chem Phys* 2020, 152:084110. <https://doi.org/10.1063/1.5143412>.
200. Kananenka AA, Hsieh CY, Cao JS, Geva E. Nonadiabatic dynamics via the symmetrical quasi-classical method in the presence of anharmonicity. *J Phys Chem Lett* 2018, 9:319-326. <https://doi.org/10.1021/acs.jpcclett.7b03002>.
201. Mulvihill E, Gao X, Liu Y, Schubert A, Dunietz BD, Geva E. Combining the mapping Hamiltonian linearized semiclassical approach with the generalized quantum master equation to simulate electronically nonadiabatic molecular dynamics. *J Chem Phys* 2019, 151:074103. <https://doi.org/10.1063/1.5110891>.
202. Gao X, Geva E. Improving the accuracy of quasiclassical mapping Hamiltonian methods by treating the window function width as an adjustable parameter. *J Phys Chem A* 2020, 124:11006-11016. <https://doi.org/10.1021/acs.jpca.0c09750>.
203. Gao X, Lai Y, Geva E. Simulating absorption spectra of multiexcitonic systems via quasiclassical mapping Hamiltonian methods. *J Chem Theory Comput* 2020, 16:6465-6480. <https://doi.org/10.1021/acs.jctc.0c00709>.
204. Gao X, Sailer MAC, Liu Y, Kelly A, Richardson JO, Geva E. Benchmarking quasiclassical mapping Hamiltonian methods for simulating electronically nonadiabatic molecular dynamics. *J Chem Theory Comput* 2020, 16:2883-2895. <https://doi.org/10.1021/acs.jctc.9b01267>.
205. Liu Y, Gao X, Lai Y, Mulvihill E, Geva E. Electronic dynamics through conical intersections via quasiclassical mapping Hamiltonian methods. *J Chem Theory Comput* 2020, 16:4479-4488. <https://doi.org/10.1021/acs.jctc.0c00177>.
206. Saller MAC, Kelly A, Geva E. Benchmarking quasiclassical mapping Hamiltonian methods for simulating cavity-modified molecular dynamics. *J Phys Chem Lett* 2021, 12:3163-3170. <https://doi.org/10.1021/acs.jpcclett.1c00158>.
207. Bonella S, Coker DF. A semiclassical limit for the mapping Hamiltonian approach to electronically nonadiabatic dynamics. *J Chem Phys* 2001, 114:7778-7789. <https://doi.org/10.1063/1.1366331>.
208. Bonella S, Coker DF. Semiclassical implementation of the mapping Hamiltonian approach for nonadiabatic dynamics using focused initial distribution sampling. *J Chem Phys* 2003, 118:4370-4385. <https://doi.org/10.1063/1.1542883>.
209. Bonella S, Coker DF. LAND-map, a linearized approach to nonadiabatic dynamics using the mapping formalism. *J Chem Phys* 2005, 122:194102. <https://doi.org/10.1063/1.1896948>.
210. Huo PF, Coker DF. Semi-classical path integral non-adiabatic dynamics: A partial linearized classical mapping Hamiltonian approach. *Mol Phys* 2012, 110:1035-1052. <https://doi.org/10.1080/00268976.2012.684896>.
211. Tang D, Fang W-H, Shen L, Cui G. Combining Meyer-Miller Hamiltonian with electronic structure methods for on-the-fly nonadiabatic dynamics simulations: Implementation and application. *Phys Chem Chem Phys* 2019, 21:17109-17117. <https://doi.org/10.1039/c9cp02682g>.
212. Zheng J, Xie Y, Jiang S, Long Y, Ning X, Lan Z. Ultrafast electron transfer with symmetrical quasi-classical dynamics based on mapping Hamiltonian and quantum dynamics based on ML-MCTDH. *Chin J Chem Phys* 2017, 30:800-810. <https://doi.org/10.1063/1.674-0068/30/cjcp1711210>.
213. Xie Y, Zheng J, Lan Z. Performance evaluation of the symmetrical quasi-classical dynamics method based on Meyer-Miller mapping Hamiltonian in the treatment of site-exciton models. *J Chem Phys* 2018, 149:174105. <https://doi.org/10.1063/1.5047002>.
214. Zheng J, Xie Y, Jiang S, Long Y, Ning X, Lan Z. Initial sampling in symmetrical quasiclassical dynamics based on Li-Miller mapping Hamiltonian. *Phys Chem Chem Phys* 2019, 21:26502-26514. <https://doi.org/10.1039/c9cp03975a>.
215. Zheng J, Peng J, Xie Y, Long Y, Ning X, Lan Z. Study of the exciton dynamics in perylene bisimide (PBI) aggregates with symmetrical quasiclassical dynamics based on the Meyer-Miller mapping Hamiltonian. *Phys Chem Chem Phys* 2020, 22:18192-18204. <https://doi.org/10.1039/d0cp00648c>.
216. Peng J, Xie Y, Hu D, Lan Z. Analysis of bath motion in MM-SQC dynamics via dimensionality reduction approach: Principal component analysis. *J Chem Phys* 2021, 154:094122. <https://doi.org/10.1063/5.0039743>.
217. Hu D, Xie Y, Peng J, Lan Z. On-the-fly symmetrical quasi-classical dynamics with Meyer-Miller mapping Hamiltonian for the treatment of nonadiabatic dynamics at conical intersections. *J Chem Theory Comput* 2021, 17:3267-3279. <https://doi.org/10.1021/acs.jctc.0c01249>.
218. Tao G. A multi-state trajectory method for non-adiabatic dynamics simulations. *J Chem Phys* 2016, 144:094108. <https://doi.org/10.1063/1.4943006>.
219. Tao G. Coherence-controlled nonadiabatic dynamics via state-space decomposition: A consistent way to incorporate Ehrenfest and Born-Oppenheimer-like treatments of nuclear motion. *J Phys Chem Lett* 2016, 7:4335-4339. <https://doi.org/10.1021/acs.jpcclett.6b01857>.

220. Tao G. Multi-state trajectory approach to non-adiabatic dynamics: General formalism and the active state trajectory approximation. *J Chem Phys* 2017, 147:044107. <https://doi.org/10.1063/1.4985898>.
221. Schwinger J. In: Biedenharn LC, VanDam H, eds. *Quantum Theory of Angular Momentum*. New York: Academic; 1965.
222. Sakurai JJ. *Modern Quantum Mechanics*. New York: Addison-Wesley; 1994.
223. Flammia ST, Liu Y-K. Direct fidelity estimation from few Pauli measurements. *Phys Rev Lett* 2011, 106:230501. <https://doi.org/10.1103/PhysRevLett.106.230501>.
224. Sperling J, Walmsley IA. Quasiprobability representation of quantum coherence. *Phys Rev A* 2018, 97:062327. <https://doi.org/10.1103/PhysRevA.97.062327>.
225. Bohmann M, Agudelo E, Sperling J. Probing nonclassicality with matrices of phase-space distributions. *Quantum* 2020, 4:16. <https://doi.org/10.22331/q-2020-10-15-343>.
226. Bohmann M, Agudelo E. Phase-space inequalities beyond negativities. *Phys Rev Lett* 2020, 124:133601. <https://doi.org/10.1103/PhysRevLett.124.133601>.
227. Lutterbach LG, Davidovich L. Method for direct measurement of the Wigner function in cavity QED and ion traps. *Phys Rev Lett* 1997, 78:2547-2550. <https://doi.org/10.1103/PhysRevLett.78.2547>.
228. Signoles A, Facon A, Grosso D, Dotsenko I, Haroche S, Raimond J-M, Brune M, Gleyzes S. Confined quantum Zeno dynamics of a watched atomic arrow. *Nat Phys* 2014, 10:715-719. <https://doi.org/10.1038/nphys3076>.
229. Leiner D, Glaser SJ. Wigner process tomography: Visualization of spin propagators and their spinor properties. *Phys Rev A* 2018, 98:012112. <https://doi.org/10.1103/PhysRevA.98.012112>.
230. Tian Y, Wang Z, Zhang P, Li G, Li J, Zhang T. Measurement of complete and continuous Wigner functions for discrete atomic systems. *Phys Rev A* 2018, 97:013840. <https://doi.org/10.1103/PhysRevA.97.013840>.
231. Chen B, Geng J, Zhou F, Song L, Shen H, Xu N. Quantum state tomography of a single electron spin in diamond with Wigner function reconstruction. *Appl Phys Lett* 2019, 114:041102. <https://doi.org/10.1063/1.5082878>.
232. Jing Y, Fadel M, Ivannikov V, Byrnes T. Split spin-squeezed Bose-Einstein condensates. *New J Phys* 2019, 21:093038. <https://doi.org/10.1088/1367-2630/ab3fcf>.
233. Song C, Xu K, Li H, Zhang Y-R, Zhang X, Liu W, Guo Q, Wang Z, Ren W, Hao J, et al. Generation of multicomponent atomic Schrodinger cat states of up to 20 qubits. *Science* 2019, 365:574-577. <https://doi.org/10.1126/science.aay0600>.
234. Eichler C, Lang C, Fink JM, Govenius J, Filipp S, Wallraff A. Observation of entanglement between itinerant microwave photons and a superconducting qubit. *Phys Rev Lett* 2012, 109:240501. <https://doi.org/10.1103/PhysRevLett.109.240501>.
235. Morin O, Huang K, Liu J, Le Jeannic H, Fabre C, Laurat J. Remote creation of hybrid entanglement between particle-like and wave-like optical qubits. *Nat Photon* 2014, 8:570-574. <https://doi.org/10.1038/nphoton.2014.137>.
236. Agudelo E, Sperling J, Costanzo LS, Bellini M, Zavatta A, Vogel W. Conditional hybrid nonclassicality. *Phys Rev Lett* 2017, 119:120403. <https://doi.org/10.1103/PhysRevLett.119.120403>.
237. Banaszek K, Radzewicz C, Wódkiewicz K, Krasiński JS. Direct measurement of the Wigner function by photon counting. *Phys Rev A* 1999, 60:674-677. <https://doi.org/10.1103/PhysRevA.60.674>.
238. Garon A, Zeier R, Glaser SJ. Visualizing operators of coupled spin systems. *Phys Rev A* 2015, 91:042122. <https://doi.org/10.1103/PhysRevA.91.042122>.
239. Koczor B, Zeier R, Glaser SJ. Time evolution of coupled spin systems in a generalized Wigner representation. *Ann Phys* 2019, 408:1-50. <https://doi.org/10.1016/j.aop.2018.11.020>.
240. Davies BI, Rundle RP, Dwyer VM, Samson JH, Tilma T, Everitt MJ. Visualizing spin degrees of freedom in atoms and molecules. *Phys Rev A* 2019, 100:042102. <https://doi.org/10.1103/PhysRevA.100.042102>.
241. Rundle RP, Davies BI, Dwyer VM, Tilma T, Everitt MJ. Visualization of correlations in hybrid discrete-continuous variable quantum systems. *J Phys Commun* 2020, 4:025002. <https://doi.org/10.1088/2399-6528/ab6fb6>.
242. Tilma T, Sudarshan ECG. Generalized Euler angle parameterization for U(N) with applications to SU(N) coset volume measures. *J Geometry Phys* 2004, 52:263-283. <https://doi.org/10.1016/j.geomphys.2004.03.003>.
243. Tilma T, Sudarshan ECG. Generalized Euler angle parametrization for SU(N). *J Phys A Math Gen* 2002, 35:10467-10501. <https://doi.org/10.1088/0305-4470/35/48/316>.
244. Isserlis L. On a formula for the product-moment coefficient of any order of a normal frequency distribution in any number of variables. *Biometrika* 1918, 12:134-139. <https://doi.org/10.1093/biomet/12.1-2.134>.
245. Wang MC, Uhlenbeck GE. On the theory of the Brownian motion II. *Rev Mod Phys* 1945, 17:323-342. <https://doi.org/10.1103/revmodphys.17.323>.

246. Ehrenfest P. Bemerkung über die angenäherte gültigkeit der klassischen mechanik innerhalb der quantenmechanik. *Z Phys* 1927, 45:455-457. <https://doi.org/10.1007/BF01329203>.
247. Li X, Tully JC, Schlegel HB, Frisch MJ. Ab initio Ehrenfest dynamics. *J Chem Phys* 2005, 123:084106. <https://doi.org/10.1063/1.2008258>.
248. Tully JC. Molecular dynamics with electronic transitions. *J Chem Phys* 1990, 93:1061-1071. <https://doi.org/10.1063/1.459170>.
249. Wang L, Akimov A, Prezhdo OV. Recent progress in surface hopping: 2011-2015. *J Phys Chem Lett* 2016, 7:2100-2112. <https://doi.org/10.1021/acs.jpcclett.6b00710>.
250. Peng J, Xie Y, Hu D, Du L, Lan Z. Treatment of nonadiabatic dynamics by on-the-fly trajectory surface hopping dynamics. *Acta Physico-Chim Sin* 2019, 35:28-48. <https://doi.org/10.3866/PKU.WHXB201801042>.
251. Meyer KR, Hall GR. *Introduction to Hamiltonian Dynamical Systems and the N-Body Problem*. New York: Springer New York; 1992.
252. Yarkony DR. Conical intersections: Diaboloical and often misunderstood. *Acc Chem Res* 1998, 31:511-518. <https://doi.org/10.1021/ar970113w>.
253. Paterson MJ, Bearpark MJ, Robb MA, Blancafort L, Worth GA. Conical intersections: A perspective on the computation of spectroscopic Jahn-Teller parameters and the degenerate 'intersection space'. *Phys Chem Chem Phys* 2005, 7:2100-2115. <https://doi.org/10.1039/b416538a>.
254. Matsika S, Krause P. Nonadiabatic Events and Conical Intersections. *Annu Rev Phys Chem* 2011, 62:621-643. <https://doi.org/10.1146/annurev-physchem-032210-103450>.
255. Makarov DE, Makri N. Path integrals for dissipative systems by tensor multiplication: Condensed phase quantum dynamics for arbitrarily long time. *Chem Phys Lett* 1994, 221:482-491. [https://doi.org/10.1016/0009-2614\(94\)00275-4](https://doi.org/10.1016/0009-2614(94)00275-4).
256. Makri N, Makarov DE. Tensor propagator for iterative quantum time evolution of reduced density matrices. I. Theory. *J Chem Phys* 1995, 102:4600-4610. <https://doi.org/10.1063/1.469508>.
257. Makri N, Makarov DE. Tensor propagator for iterative quantum time evolution of reduced density matrices. II. Numerical methodology. *J Chem Phys* 1995, 102:4611-4618. <https://doi.org/10.1063/1.469509>.
258. Topaler M, Makri N. Path integral calculation of quantum nonadiabatic rates in model condensed phase reactions. *J Phys Chem* 1996, 100:4430-4436. <https://doi.org/10.1021/jp951673k>.
259. Makri N. Small matrix disentanglement of the path integral: Overcoming the exponential tensor scaling with memory length. *J Chem Phys* 2020, 152:041104. <https://doi.org/10.1063/1.5139473>.
260. Makri N. Small matrix path integral for system-bath dynamics. *J Chem Theory Comput* 2020, 16:4038-4049. <https://doi.org/10.1021/acs.jctc.0c00039>.
261. Tanimura Y, Kubo R. Time evolution of a quantum system in contact with a nearly Gaussian-Markoffian noise bath. *J Phys Soc Jpn* 1989, 58:101-114. <https://doi.org/10.1143/JPSJ.58.101>.
262. Yan Y-A, Yang F, Liu Y, Shao J. Hierarchical approach based on stochastic decoupling to dissipative systems. *Chem Phys Lett* 2004, 395:216-221. <https://doi.org/10.1016/j.cplett.2004.07.036>.
263. Xu R-X, Cui P, Li X-Q, Mo Y, Yan Y. Exact quantum master equation via the calculus on path integrals. *J Chem Phys* 2005, 122:041103. <https://doi.org/10.1063/1.1850899>.
264. Shao J. Stochastic description of quantum open systems: Formal solution and strong dissipation limit. *Chem Phys* 2006, 322:187-192. <https://doi.org/10.1016/j.chemphys.2005.08.007>.
265. Moix JM, Cao J. A hybrid stochastic hierarchy equations of motion approach to treat the low temperature dynamics of non-Markovian open quantum systems. *J Chem Phys* 2013, 139:134106. <https://doi.org/10.1063/1.4822043>.
266. Tanimura Y. Reduced hierarchical equations of motion in real and imaginary time: Correlated initial states and thermodynamic quantities. *J Chem Phys* 2014, 141:044114. <https://doi.org/10.1063/1.4890441>.
267. Yan Y. Theory of open quantum systems with bath of electrons and phonons and spins: Many-dissipaton density matrixes approach. *J Chem Phys* 2014, 140:054105. <https://doi.org/10.1063/1.4863379>.
268. Tang Z, Ouyang X, Gong Z, Wang H, Wu J. Extended hierarchy equation of motion for the spin-boson model. *J Chem Phys* 2015, 143:224112. <https://doi.org/10.1063/1.4936924>.
269. Tanimura Y. Real-time and imaginary-time quantum hierarchal Fokker-Planck equations. *J Chem Phys* 2015, 142:144110. <https://doi.org/10.1063/1.4916647>.
270. Meyer H-D, Manthe U, Cederbaum LS. The multi-configurational time-dependent Hartree approach. *Chem Phys Lett* 1990, 165:73-78. [https://doi.org/10.1016/0009-2614\(90\)87014-i](https://doi.org/10.1016/0009-2614(90)87014-i).
271. Thoss M, Wang H, Miller WH. Self-consistent hybrid approach for complex systems: Application to the spin-boson model with Debye spectral density. *J Chem Phys* 2001, 115:2991-3005. <https://doi.org/10.1063/1.1385562>.

272. Wang H, Thoss M, Miller WH. Systematic convergence in the dynamical hybrid approach for complex systems: A numerically exact methodology. *J Chem Phys* 2001, 115:2979-2990. <https://doi.org/10.1063/1.1385561>.
273. Wang H, Thoss M. Multilayer formulation of the multiconfiguration time-dependent Hartree theory. *J Chem Phys* 2003, 119:1289-1299. <https://doi.org/10.1063/1.1580111>.
274. Wang H, Thoss M. From coherent motion to localization: Dynamics of the spin-boson model at zero temperature. *New J Phys* 2008, 10:115005. <https://doi.org/10.1088/1367-2630/10/11/115005>.
275. Worth GA, Meyer H-D, Köppel H, Cederbaum LS, Burghardt I. Using the MCTDH wavepacket propagation method to describe multimode non-adiabatic dynamics. *Int Rev Phys Chem* 2008, 27:569-606. <https://doi.org/10.1080/01442350802137656>.
276. Wang H, Thoss M. From coherent motion to localization: II. Dynamics of the spin-boson model with sub-Ohmic spectral density at zero temperature. *Chem Phys* 2010, 370:78-86. <https://doi.org/10.1016/j.chemphys.2010.02.027>.
277. Craig IR, Thoss M, Wang H. Proton transfer reactions in model condensed-phase environments: Accurate quantum dynamics using the multilayer multiconfiguration time-dependent Hartree approach. *J Chem Phys* 2007, 127:144503. <https://doi.org/10.1063/1.2772265>.
278. Wang H. Iterative calculation of energy eigenstates employing the multilayer multiconfiguration time-dependent Hartree theory. *J Phys Chem A* 2014, 118:9253-9261. <https://doi.org/10.1021/jp503351t>.
279. Makri N. The linear response approximation and its lowest order corrections: An influence functional approach. *J Phys Chem B* 1999, 103:2823-2829. <https://doi.org/10.1021/jp9847540>.
280. Purcell EM. Spontaneous Emission Probabilities at Radio Frequencies. In: Burstein E, Weisbuch C, eds. *Confined Electrons and Photons: New Physics and Applications*. Boston, MA: Springer US; 1995.
281. Krasnok AE, Slobozhanyuk AP, Simovski CR, Tretyakov SA, Poddubny AN, Miroshnichenko AE, Kivshar YS, Belov PA. An antenna model for the Purcell effect. *Sci Rep* 2015, 5:12956. <https://doi.org/10.1038/srep12956>.
282. Rybin MV, Mingaleev SF, Limonov MF, Kivshar YS. Purcell effect and Lamb shift as interference phenomena. *Sci Rep* 2016, 6:20599. <https://doi.org/10.1038/srep20599>.
283. Holsteen AL, Raza S, Fan P, Kik PG, Brongersma ML. Purcell effect for active tuning of light scattering from semiconductor optical antennas. *Science* 2017, 358:1407-1410. <https://doi.org/10.1126/science.aao5371>.
284. Alagappan G, Krivitsky LA, Png CE. Diamond in a nanopocket: A new route to a strong Purcell effect. *ACS Omega* 2018, 3:4733-4742. <https://doi.org/10.1021/acsomega.8b00139>.
285. Gallego J, Alt W, Macha T, Martinez-Dorantes M, Pandey D, Meschede D. Strong Purcell effect on a neutral atom trapped in an open fiber cavity. *Phys Rev Lett* 2018, 121:173603. <https://doi.org/10.1103/PhysRevLett.121.173603>.
286. Ren T, Dong Y, Xu S, Gong X. Strong Purcell effect in deep subwavelength coaxial cavity with GeSn active medium. *Opt Lett* 2021, 46:3889-3892. <https://doi.org/10.1364/OL.432164>.
287. Carmichael HJ, Brecha RJ, Raizen MG, Kimble HJ, Rice PR. Subnatural linewidth averaging for coupled atomic and cavity-mode oscillators. *Phys Rev A* 1989, 40:5516-5519. <https://doi.org/10.1103/physreva.40.5516>.
288. Zhu Y, Gauthier DJ, Morin SE, Wu Q, Carmichael HJ, Mossberg TW. Vacuum Rabi splitting as a feature of linear-dispersion theory: Analysis and experimental observations. *Phys Rev Lett* 1990, 64:2499-2502. <https://doi.org/10.1103/PhysRevLett.64.2499>.
289. Field JE. Vacuum-Rabi-splitting-induced transparency. *Phys Rev A* 1993, 47:5064-5067. <https://doi.org/10.1103/physreva.47.5064>.
290. Abram I, Oudar JL. Spontaneous emission in planar semiconductor microcavities displaying vacuum Rabi splitting. *Phys Rev A* 1995, 51:4116-4122. <https://doi.org/10.1103/physreva.51.4116>.
291. Li K, Wang W, Chen Z, Gao N, Yang W, Li W, Chen H, Li S, Li H, Jin P, et al. Vacuum Rabi splitting of exciton-polariton emission in an AlN film. *Sci Rep* 2013, 3:3551. <https://doi.org/10.1038/srep03551>.
292. Toida H, Nakajima T, Komiyama S. Vacuum Rabi splitting in a semiconductor circuit QED system. *Phys Rev Lett* 2013, 110:066802. <https://doi.org/10.1103/PhysRevLett.110.066802>.
293. Guerin W, Santo T, Weiss P, Cipris A, Schachenmayer J, Kaiser R, Bachelard R. Collective multimode vacuum Rabi splitting. *Phys Rev Lett* 2019, 123:243401. <https://doi.org/10.1103/PhysRevLett.123.243401>.
294. Yan Y, Ergogo TT, Lü Z, Chen L, Luo J, Zhao Y. Lamb shift and the vacuum Rabi splitting in a strongly dissipative environment. *J Phys Chem Lett* 2021, 12:9919-9925. <https://doi.org/10.1021/acs.jpclett.1c02791>.
295. Meystre P. *Elements of Quantum Optics*. Berlin New York: Springer; 2007.

296. Hoffmann NM, Schafer C, Rubio A, Kelly A, Appel H. Capturing vacuum fluctuations and photon correlations in cavity quantum electrodynamics with multitrajectory Ehrenfest dynamics. *Phys Rev A* 2019, 99:063819. <https://doi.org/10.1103/PhysRevA.99.063819>.
297. Hoffmann NM, Schäfer C, Säkkinen N, Rubio A, Appel H, Kelly A. Benchmarking semiclassical and perturbative methods for real-time simulations of cavity-bound emission and interference. *J Chem Phys* 2019, 151:244113. <https://doi.org/10.1063/1.5128076>.
298. Li TE, Chen HT, Nitzan A, Subotnik JE. Quasiclassical modeling of cavity quantum electrodynamics. *Phys Rev A* 2020, 101:033831. <https://doi.org/10.1103/PhysRevA.101.033831>.
299. Levine BG, Ko C, Quenneville J, Martínez TJ. Conical intersections and double excitations in time-dependent density functional theory. *Mol Phys* 2006, 104:1039-1051. <https://doi.org/10.1080/00268970500417762>.
300. Halcrow MA. Jahn-Teller distortions in transition metal compounds, and their importance in functional molecular and inorganic materials. *Chem Soc Rev* 2013, 42:1784-1795. <https://doi.org/10.1039/c2cs35253b>.
301. Bersuker IB. The Jahn-Teller and pseudo-Jahn-Teller Effects: A unique and only source of spontaneous symmetry breaking in atomic matter. *Symmetry* 2021, 13:1577. <https://doi.org/10.3390/sym13091577>.
302. Qin A, Lam JWY, Tang BZ. Luminogenic polymers with aggregation-induced emission characteristics. *Prog Polym Sci* 2012, 37:182-209. <https://doi.org/10.1016/j.progpolymsci.2011.08.002>.
303. Schneider R, Domcke W. S1-S2 Conical intersection and ultrafast S2->S1 Internal conversion in pyrazine. *Chem Phys Lett* 1988, 150:235-242. [https://doi.org/10.1016/0009-2614\(88\)80034-4](https://doi.org/10.1016/0009-2614(88)80034-4).
304. Bóna P. *Classical Systems in Quantum Mechanics*. Cham: Springer; 2020.
305. Hacker B, Welte S, Daiss S, Shaukat A, Ritter S, Li L, Rempe G. Deterministic creation of entangled atom-light Schrodinger-cat states. *Nat Photon* 2019, 13:110-115. <https://doi.org/10.1038/s41566-018-0339-5>.
306. Vlastakis B, Petrenko A, Ofek N, Sun L, Leghtas Z, Sliwa K, Liu Y, Hatridge M, Blumoff J, Frunzio L, et al. Characterizing entanglement of an artificial atom and a cavity cat state with Bell's inequality. *Nat Commun* 2015, 6:8970. <https://doi.org/10.1038/ncomms9970>.
307. Pacher T, Cederbaum LS, Köppel H. Adiabatic and quasidiabatic states in a gauge theoretical framework. *Adv Chem Phys* 1993, 84:293-391. <https://doi.org/10.1002/9780470141427.ch4>.
308. Das A. *Field Theory*. Singapore: World Scientific; 2019.
309. Nemoto K. Generalized coherent states for SU(n) systems. *J Phys A Math Gen* 2000, 33:3493-3506. <https://doi.org/10.1088/0305-4470/33/17/307>.
310. Atiyah MF, Todd JA. On complex Stiefel manifolds. *Math Proc Cambridge Phil Soc* 1960, 56:342 - 353. <https://doi.org/10.1017/S0305004100034642>.
311. Fomenko A, Fuchs D. *Homotopical Topology*. Switzerland: Springer; 2016.
312. Provost JP, Vallee G. Riemannian structure on manifolds of quantum states. *Commun Math Phys* 1980, 76:289-301. <https://doi.org/10.1007/BF02193559>.